ROLE OF INTERMITTENT DYNAMICS IN THE ONSET OF COMBUSTION INSTABILITY

A THESIS

submitted by

VINEETH NAIR V

for the award of the degree

of

DOCTOR OF PHILOSOPHY

DEPARTMENT OF AEROSPACE ENGINEERING
INDIAN INSTITUTE OF TECHNOLOGY MADRAS.

APRIL 2014

THESIS CERTIFICATE

This is to certify that the thesis titled **ROLE OF INTERMITTENT DYNAMICS IN THE ONSET OF COMBUSTION INSTABILITY**, submitted by **Vineeth Nair V**, to the Indian Institute of Technology, Madras, for the award of the degree of **Doctor of Philosophy**, is a bona fide record of the research work done by him under our supervision. The contents of this thesis, in full or in parts, have not been submitted to any other Institute or University for the award of any degree or diploma.

Prof. R.I. Sujith
Research Guide
Professor
Dept. of Aerospace Engineering
IIT-Madras, 600 036

Place: Chennai

Date: 15th April 2014

ACKNOWLEDGEMENTS

I wish to thank my advisor Prof. Sujith for his indomitable spirit towards research which has been a huge motivation in leading my work to fruition. I also wish to thank my doctoral committee, for the continued support and valuable insights. I wish to thank my labmates for their support and cooperation.

ABSTRACT

KEYWORDS: Turbulent reacting flows; Combustion noise; Combustion instability; Intermittency; Multifractals; Homoclinic orbits; Flame dynamics; Bluff-body stabilized combustor.

Unsteady combustion in a confined, compressible flow-field can lead to the spontaneous excitation of self-sustained periodic oscillations, provided the heat release rate fluctuations are in phase with the pressure fluctuations inside the confinement. These periodic oscillations termed 'combustion instability' or 'thermoacoustic instability' remain a major cause of concern in industrial applications as diverse as household burners which are used for cooking and heating, gas turbine engines used for propulsion and power generation, as well as rocket engines used for space exploration and defense applications. A description of the mechanism underlying the inception of such self-sustained oscillations in combustors remain difficult even after decades of active research as the dynamics involves a complex nonlinear interplay amongst the hydrodynamic, acoustic and combustion processes.

The present thesis aims to identify the route through which combustion instability is established from stable operating conditions, when the underlying flow field inside the combustion chamber is turbulent. The work focuses on the dynamic transitions observed in a bluff-body stabilized backward facing step combustor, when the air flow rate (Reynolds number) is gradually increased keeping the fuel flow rate fixed. The operating conditions were varied from near unity equivalence ratios towards the lean blowout limit. As a first step, the dynamics of unsteady pressure fluctuations acquired during stable conditions is characterized. These fluctuations—which are termed as 'combustion noise' in the literature—are often modelled as a stochastic process. Our results indicate that combustion noise is in fact deterministic chaos with weak correlations (finite memory) and does not display properties one would expect from a typical random process. Increasing the Reynolds number towards combustion instability leads to a loss of this chaotic behaviour.

It was observed that combustion instability is presaged by an intermittent regime characterized by bursts of high-amplitude periodic oscillations that appear in a near random manner from a background of low-amplitude chaotic fluctuations. Interaction amongst the hydrodynamic and the acoustic subsystems results in the formation of homoclinic orbits which can be identified in the reconstructed phase space of the pressure time series. Such orbits result in occasional excursions of the dynamics away from the low-amplitude regimes, leading to the formation of intermittent bursts in measurements. Since combustion instability is an undesirable state in combustors, early warning signals to an impending instability can be obtained by quantifying these intermittent states.

High speed images at instability reveal periodic vortex formation at the backward facing step and impingement on the bluff-body and the spectrum of the flame intensity reveals a strong peak at the subharmonic close to the acoustic mode. Based on these experimental insights, a mechanism was proposed which necessitates that when the underlying flow-field to be turbulent, the transition to combustion instability must happen via the intermittency route. A phenomenological model is introduced based on the mechanism that describes the onset of combustion instability as a lock-in between hydrodynamics and the acoustic field. The model qualitatively reproduces the intermittent behaviour observed in experiments and also provides early warning signals to an impending transition.

Due to the inherent complexity of the dynamics, a fractal description was sought to understand the scaling of pressure fluctuations observed prior to combustion instability. It was found that these irregular pressure fluctuations are amenable to a multifractal description; in other words, fluctuations of different amplitudes grow at different rates within a short time range. The transition to combustion instability results in a collapse of the number of relevant time scales in the problem, which leads to a loss of multifractality. This reduction in complexity can be quantified to act as yet another early warning signal to combustion instability.

Intermittent burst oscillations were also observed as Reynolds number is increased beyond regimes of combustion instability, as operating conditions near lean blowout. High speed imaging of the flame in this intermittent regime reveals an aperiodic detachment and reattachment of the flame from the lip of the bluff-body. These intermittent regimes are thus seen to act a precursor to lean blowout as well.

Such an intermittent regime was also observed in systems without combustion. Increasing the Reynolds number in a system comprising a duct terminated by an orifice results in the onset of self-sustained pipe tone oscillations (whistling). It was observed that the onset of whistling in such systems is also preceded by a regime of intermittent burst oscillations, just as in combustors, provided the transition to whistling happens at high Reynolds numbers. When whistling is established, the boundary condition at the orifice is modified, which can be captured using a 1D linear acoustic model. The change in boundary condition can also be used to explain the merging of vortices downstream of the orifice as has been observed previously.

These observations reinforce the idea that intermittency is a universal feature observed in systems with turbulent flow-sound interaction prior to a regime of periodic oscillations. Further, the nature of the problem requires that the effects of flow turbulence be incorporated appropriately in the models and not just ignored as background perturbations to the underlying dynamics, as is currently often done.

TABLE OF CONTENTS

LIST OF FIGURES

ABBREVIATIONS

LPG	Liquified Petroleum Gas
FNN	False Nearest Neighbor
RR	Recurrence Rate
DFA	Detrended Fluctuation Analysis
SLPM	Standard Litres Per Minute

NOTATION

Re	Reynolds number
ϕ	Equivalence ratio
$\dot{m}$	Mass flow rate
D_1	Characteristic dimension for the computations of Re
D_0	Diameter of the burner
$p'(t)$	Unsteady pressure measurement
μ	Dynamic viscosity
T	Dominant time period during combustion instability
τ_{opt}	Optimum time delay for embedding
I_τ	Average mutual information
d_0	Optimum embedding dimension
$E_1(d)$	Measure used to compute optimum embedding dimension
$E_2(d)$	Measure used to check for determinism in Cao's method
N	Length of the time signal
H	Translation horizon
Λ	A measure of determinism
q_c, r_c	Translation variables
M_c	Mean square displacement
D_c	Modified mean square displacement
ξ	Vector of time steps
Δ	Vector of mean square displacements
K_c	Correlation of ξ and Δ
K	Median of K_c

CHAPTER 1

Introduction

Combustion instability refers to the self-sustained, large amplitude oscillations of the unsteady pressure and velocity components in combustors. It arises primarily through an interaction of the acoustic waves in a confined space with the unsteady rate of heat release through combustion. The pressure waves are amplified by fluctuations in heat release rate. These wave in turn modulate the rate of heat release after reflection from the walls and boundaries of the combustion chamber.

When the rate of change of heat release by the flame responds in phase with the unsteady pressure pulsations, a positive feedback loop is established (Rayleigh, 1878), with the flame acting as an acoustic actuator and the combustion chamber as an acoustic resonator. The positive feedback amplifies an initial perturbation as the addition and abstraction of heat occur during the compression and rarefaction phases of the pressure oscillation, respectively. The fluctuations can thus grow exponentially until nonlinearity takes over, resulting in a saturation of pressure amplitude when the total energy losses from the chamber balances the energy input through combustion. Predicting and controlling the onset of such oscillations, therefore, require an intimate understanding of the interaction between the the acoustic pressure field and the processes that lead to a fluctuating heat release.

Despite decades of active research, the appearance of combustion instability has remained a serious problem in the design and development of combustors for rockets, ramjets and gas turbines (McManus *et al.*, 1993). When pulsations start spontaneously at an operating condition, the combustor is said to be linearly unstable at that condition; i.e., the combustor is prone to instability for arbitrarily small pressure disturbances that may arise at that operating condition. By modelling the combustor as a series of network elements with specified boundary conditions and performing a linear stability analysis, conditions of linear instability have been successfully investigated for various design configurations. In a network model, the analysis is performed in the frequency domain wherein each element is described using a linear transfer function (Huber and Polifke,

2009*a*,*b*). These transfer functions describe the variation of acoustic pressure and velocity within the elements and also provide the necessary boundary conditions across the element interfaces. The stability of the combustor can then be easily determined by examining the eigenvalues of a matrix composed of its transfer functions.

However, in many cases, a combustor that is linearly stable can be 'triggered' into pulsating operation by introducing a pressure disturbance of finite amplitude. Such disturbances may arise, for instance, during spark plug ignition or small explosions in the combustion chamber. In such a scenario, the dynamics inside combustors is stable only if the amplitude of initial disturbances falls below a certain threshold value, which in general depends on the geometry of the combustor, fuel composition and the flow rates inside the chamber. A qualitative change in the behaviour of the combustor from stable operation to unstable operation is termed as a bifurcation. A transition to periodic oscillations due to a change in the initial disturbances is characteristic of systems that exhibit a subcritical Hopf bifurcation (Strogatz, 2001). For systems exhibiting subcritical Hopf bifurcations, there exists a range of operating conditions in a control parameter (like the air flow rate) for which two stable solutions are possible in the asymptotic state; the solution which is manifested depends on the magnitude of the initial perturbation. The techniques of classical linear stability does not include the effects of initial conditions in the analysis and hence cannot explain triggering.

Although much progress has been made over the last 50 years in assessing the stability margins of combustors, it has mostly been in the framework of classical linear stability analysis. A comprehensive prediction of the conditions under which combustion instability is established remains a difficult task, which has not yet been mastered. In particular, prediction of the amplitude or the frequency of oscillations at the onset of instability remains a key challenge as surprisingly little is known—even in a qualitative sense—about the key parameters controlling nonlinear flame dynamics (Zinn and Lieuwen, 2005). Therefore, to describe the onset of combustion instability, estimate the amplitude and frequency of the periodic oscillations and to describe features such as triggering, a nonlinear theory of combustion instability is necessary.

1.1 The role of nonlinearities

In the 70's and 80's, much work was focused on identifying the role of nonlinear gas dynamic processes in establishing combustion instability. The work was primarily motivated by instabilities in both solid and liquid rocket motors where the resultant amplitude of pressure oscillations can reach a significant proportion of the mean pressure value; typical values correspond to $p'/\overline{p} \approx 20 - 50\%$. The nonlinearity of acoustic waves in the combustion chamber of a rocket motor were studied by Culick using one-dimensional wave equations (Culick, 1970, 1976a,b, 1988). The response of combustion to the pressure fluctuations were considered linear. The work paved the first steps in tackling the general problem of analyzing the nonlinear growth and saturation of the amplitude of acoustic waves in a combustion chamber. The limit-cycle amplitude was determined numerically by solving a set of coupled nonlinear wave equations.

In contrast to the model proposed by Culick, Sterling (Sterling, 1993) reasoned that the only nonlinearities of significance in a combustion chamber originated from the combustion process itself and that the acoustic dynamics could be treated as essentially linear. His idea was '*motivated by experimental results from a laboratory combustor that demonstrated that the heat-addition and fluctuations are dominated by the Rayleigh mechanism.*' He concluded that in order to adequately represent the flame dynamics, a nonlinear expression for heat release rate is necessary. It has also been subsequently shown that the combustion response needs to be nonlinear to be able to trigger spontaneous pulsations in a combustor (Culick, 1994; Wicker *et al.*, 1996). It should however be mentioned that the nonlinear models adopted in these studies are 'ad hoc', and are not derived from first principles.

Nonlinear gas dynamical processes are even less significant in premixed gas turbine combustors, where reported pressure amplitudes are typically around $1 - 5\%$ of the mean pressure value (Lieuwen, 2002; Dowling, 1997; Peracchio and Proscia, 1999). Therefore, the acoustic (i.e., gas dynamic) processes remain in the linear regime, even during combustion instability. These studies also highlight the fact that the dominant nonlinear contribution arises from the relationship between flow and heat release oscillations, which in the frequency domain is represented as a flame transfer function or a flame describing function. Since the typical flow Mach numbers in a premix combustor are low, the amplitude of pressure fluctuations tend to be quite small compared to

the mean pressure, which allows a linear analysis of the acoustic processes, even if the combustion response turns out to be nonlinear.

Later studies have confirmed that the heat release response in premixed combustors is nonlinear (Hosseini and Lawn, 2005; Lieuwen, 2004; Preetham and Lieuwen, 2004, 2005). Typically, one needs to worry about nonlinear effects only when the amplitude of the velocity fluctuations is comparable to the mean flow velocity. The response of bluff-body stabilized lean premixed flames to acoustic forcing was investigated by Balachandran (2005) to understand the combustion response during limit cycle operation. They found that that nonlinearity in heat release response becomes significant only when the amplitude of inlet velocity fluctuations reaches around 15% of the mean value, a value that depends on the forcing frequency and the equivalence ratio. Tyagi *et al.* (2007) have shown that the combustion response of non-premixed flames also becomes nonlinear, even for very low amplitudes of acoustic excitation.

For the type of flow-fields that exist in a combustor, hydrodynamic instabilities play an important role in the determining its overall stability. A large class of combustion instabilities are driven by the interaction of vortices with flames and the acoustic field. Such interactions also—to a great extent—dictate the structure of turbulent flames and the corresponding rates of reaction inside the combustion chamber (Renard *et al.*, 2000). These interactions are inevitably, highly nonlinear.

1.2 Dynamical systems theory

A major share of the literature on the nonlinear analysis of combustion instabilities has been restricted to obtaining nonlinear describing functions either experimentally or theoretically (Noiray *et al.*, 2008). The procedure involves decoupling the flame from the acoustic field, and forcing the flame over all the possible ranges of frequencies and amplitudes. The nonlinear flame describing function (or the nonlinear flame transfer function) thus obtained is a function of both the amplitude and frequency which is then substituted in the wave equation (transformed to the frequency domain) to model the acoustic driving. The dispersion relation (relation connecting the frequency and the wavenumber) is then solved for its eigenvalues at different levels of acoustic velocity amplitude. These eigenvalues indicate the growth or decay in the system at any ampli-

tude. The point of zero growth or decay rate is interpreted as a limit cycle. The stability of a limit cycle is determined by the change in sign in the growth rate. A change in sign of the growth rate to a negative value from a positive value with increasing amplitude indicates that the limit cycle is stable. This is because perturbations with an amplitude smaller than the limit cycle amplitude grow with time, whereas perturbations with amplitude larger than that at limit cycle decay to the limit cycle amplitude. Conversely, a change in the growth rate from negative to positive with increasing amplitude indicates that the limit cycle is unstable.

Although a large body of recent literature exists on this topic, it is not established if the describing function technique can make accurate predictions. First, at its core, the technique still relies on a linear analysis using eigenvalues to infer stability. More importantly, the dynamics of a forced system is different from that of a self-evolving system especially as regards the phase of the resulting oscillations (Pikovsky *et al.*, 2003) and the transient envelope of the growing oscillations (Burnley and Culick, 2000; Culick, 2006). Recent studies have further shown that the stability margins obtained using describing functions do not match with numerical simulations (Kashinath, 2013).

Time evolution of a typical pressure measurement made from the combustor can give information about its stability and the nature of the resulting asymptotic state. However, this information is highly dependent on the system parameters, operating conditions and often times the type of initial condition (the levels of flow noise, ignition of a spark plug or an explosion) that exists inside the combustor. Hence, trying to assess the stability of a combustor by following the evolution in time of pressure oscillations individually for all the possible ranges of parameter values and initial conditions is not only expensive, but also impractical. Tools from dynamical systems theory can provide a systematic and efficient framework to investigate both the linear (Trefethen and Embree, 2005) and nonlinear (Burnley, 1996) behaviour of the system.

Jahnke and Culick (Jahnke and Culick, 1993) discussed the operating conditions under which stable limit cycles can exist in a system which is linearly unstable, and conditions under which bifurcations to a limit cycle can occur. Although Culick and co-workers have applied some concepts from dynamical systems theory such as continuation methods (Burnley, 1996; Ananthkrishnan *et al.*, 2005), they have not posed the problem of combustion instability in the framework of dynamical systems theory.

The technique saw its revival in recent years wherein the onset and triggering of combustion instability was successfully investigated in a number of scenarios by Sujith and coworkers (Balasubramanian and Sujith, 2008*a,b*; Mariappan *et al.*, 2010, May 17-21, 2010; Mariappan and Sujith, 2010; Subramanian, 2011)

1.3 Secondary bifurcations

Pressure oscillations more complex than a limit cycle have also been reported previously in the context of combustion instability, by a few authors. Jahnke and Culick (1994) reported the possibility of quasiperiodic oscillations (oscillations characterized by two incommensurate dominant frequencies and their multiples) using numerical continuation in their model of a solid rocket motor. Using a numerical bifurcation analysis, Sterling (1993) and later Lei and Turan (2009) reported the presence of chaotic oscillations in models of premixed combustors. In experiments, Fichera *et al.* (2001) reported chaotic dynamics in a lean gas turbine combustor through an analysis of heat release rate fluctuations.

Kabiraj *et al.* (Kabiraj *et al.*, 2010; Kabiraj and Sujith, 2011) performed bifurcation analysis on pressure and CH^* chemiluminescence time traces obtained from a simple setup comprising of ducted, laminar premixed conical flames to investigate the features of nonlinear thermoacoustic oscillations. It was observed that as the bifurcation parameter is varied, the system undergoes a series of bifurcations leading to characteristically different states of nonlinear oscillations. Through the application of techniques from nonlinear time series analysis, these oscillations were characterized as periodic, aperiodic or chaotic oscillations and subsequently, the nature of the obtained bifurcations was explained based on dynamical systems theory. Their recent findings indicate that limit cycle is just one of the possible end states in a combustor. A thermoacoustic system can undergo further bifurcations and attain states characterized by quasiperiodicity, period doubling, frequency locking and chaos. They have observed both the Ruelle-Takens and the frequency locking quasi-periodic route to chaos in their experiments. Using high speed flame images acquired simultaneously with the pressure time trace, it was shown that the source of nonlinearity is in the interaction between the flame and the acoustic field. These finding were later confirmed numerically by Kashinath (2013).

1.4 Transition to combustion instability

The topics of combustion noise and combustion instability both figure fairly prominently in the combustion literature (see for example (Strahle, 1978; McManus *et al.*, 1993; Candel, 2002; Culick, 2006; Candel *et al.*, 2009; Schwarz and Janicka, 2009) for extensive reviews on the topics). Lieuwen (2002) showed that inherent noise in a thermoacoustic system can strongly affect the limit cycles, and under certain operating conditions may even be responsible for causing the combustor to become stable under linearly stable conditions. He also investigated the characteristics of the fluctuating pressure in an unstable combustor (Lieuwen, 2001) and concluded that the phase drift characteristics are caused mainly by random processes (noise) and do not reflect the underlying low-dimensional dynamics of the instability. The statistical characteristics of self-excited and noise driven pressure oscillations in a premixed combustor were investigated by Lieuwen (2003). Using experimental data, he showed that the probability density function of the amplitude of these oscillations transitions from Gaussian to a Rayleigh-type distribution as the combustor moves from stable to unstable operation. Lieuwen and Banaszuk (2005) considered the effect of background turbulent fluctuations on the stability boundaries of a combustor. They show that additive noise sources change only quantitative aspects of the combustor oscillations. However, parametric noise sources can affect the dynamics qualitatively as well; in particular, parametric noise can destabilize a system that is stable in the absence of these noise sources.

However, most studies individually assess and contrast stable and unstable operation in combustors; studies that perform a smooth variation of operating parameters starting from stable operation, leading towards instability remain few. Thus, although various physical mechanisms responsible for combustion instability have been identified from earlier studies, the exact nature of transition, or the pathways (routes) through which instability is established is still not well understood. Chakravarthy and coworkers (Chakravarthy *et al.*, 2007*b*,*a*) performed a systematic variation of operating conditions in bluff-body and backward-facing step combustors from stable to unstable operation in a single set of continuous experiments. They reported that the non-lock-on regime (where vortex shedding and duct acoustics do not lock-on) is characterized by low-amplitude broadband noise generation. However, at the onset of lock-on (between

vortex shedding and duct acoustics), the broad band noise generation gives way to the excitation of high-amplitude discrete tones, which could be limit cycle oscillations. Recently, Gotoda *et al.* (2011) have presented results from an experimental investigation on the onset of thermoacoustic oscillations for decreases in the fuel equivalence ratio. The study employed novel methods of nonlinear time series analysis and reported the possibility of encountering low dimensional chaotic oscillations in combustors.

1.5 Interim summary and motivation

Unsteady combustion in a turbulent, convecting air-fuel mixture tends to be noisy, even more so when the heat release happens in a confined space (Strahle, 1978). These fluctuations get amplified, when localized hydrodynamic perturbations augmented by the heat release gets coupled to the acoustics of the chamber—resulting in self-sustained, large amplitude pressure oscillations termed combustion instability (McManus *et al.*, 1993). Such oscillations are often detrimental and cause losses in billions of dollars of annual revenue to the gas-turbine manufacturers. For instance, the repair and replacement costs of hot section components due to combustion instability alone exceeds $\$1$ billion annually and amounts to about 70% of the non-fuel costs of F-class gas turbines (ed: T. C. Lieuwen and Yang, 2005). Designers of high-energy propulsion and power generation systems have hence resorted to conservative stability margins as a preventive measure. Setting such conservative and often experience-based operational boundaries results in increased levels of NO_x emissions, which makes it difficult for gas-turbine manufacturers to meet the stringent emission norms. In propulsion devices such as rockets and ramjets, one may not even have the flexibility of choosing such a conservative, stable operational boundary. Despite decades of active research, an understanding of the mechanisms underlying this transition is far from complete and finding robust precursors that can forewarn impending combustion instability remains an important practical problem.

1.6 Objective of the thesis

The objective of the present thesis is aimed at filling the lacunae as regards understanding, modelling and predicting the transition from stable operation in combustors to detrimental large amplitude combustion instability. The outstanding questions raised in the thesis may be summarized as follows:

1. Is combustion noise deterministic or stochastic?
2. How does low amplitude combustion noise transition to large amplitude combustion instability?
3. Are there precursors to combustion instability?

1.6.1 Is combustion noise deterministic or stochastic?

The sources of combustion noise should be deterministic, as they derive from fluid dynamic and combustion processes: flame roll-up, vortex coalescence or impingement, fluid dilatation etc. (Coats, 1996), which are governed by a deterministic set of equations. The use of the term 'noise' to describe the phenomena, therefore, creates a lot of confusion. However, combustion noise is typically modelled as an acoustic problem by decoupling the hydrodynamics from the analysis. In a review by Candel *et al.* (2009), the authors clearly describe the formulation and its drawbacks as follows: *'Studies of combustion noise generally focus on situations where the flow dynamics can be considered to be independent of the radiated sound. It is implicitly assumed that the flow dynamics is decoupled from the induced wave motion and the sound emission from unstable flames is generally not considered when dealing with combustion noise.'* As they further note, such a decoupling—although could ease computations—cannot be justified because practical systems are confined and boundaries reflect sound towards the reactive region. In summary, there exists a gap between the ways in which combustion noise is understood and theoretically modelled. Identifying whether combustion noise is deterministic or not, therefore, forms the first major objective of the thesis.

1.6.2 How does low amplitude combustion noise transition to large amplitude combustion instability?

Combustion instability is also fundamentally treated as an acoustic problem and the effects of turbulence are often times decoupled or neglected (Lieuwen, 2001, 2002, 2003; Noiray and Schuermans, 2013). The traditional approach in dealing with unsteady measurements acquired from combustors is to treat these measurements as signals modulated by random perturbations. In models, turbulence is introduced as an external perturbation to the wave equation—as random inputs or inputs with the properties determined by the measured power spectrum (Clavin *et al.* (1994); Burnley and Culick (2000); Lieuwen and Banaszuk (2005) to mention a few). In such a mean-field description, the spectrum of dynamics under consideration is restricted to fixed points and limit cycle oscillations, wherein the observed amplitude modulations in the measured data are described as the effects of background noise. The strategy then is to identify conditions of linear instability of the system, the boundaries of which form the margins of operability.

In turbulent combustors, the transition to self-sustained oscillations from regimes of stable operation can often be triggered due to the unsteadiness in the flow and combustion. The distributions of the pressure measurements acquired from combustors well before conditions of instability have a characteristic Gaussian distribution (Lieuwen, 2002) suggestive of dynamics dictated by random processes in these regimes. However, bursts of pressure oscillations have been reported close to critical transition to instability in liquid-propellant rocket engines (Clavin *et al.*, 1994). This erratic behaviour of pressure fluctuations was then incorporated as a multiplicative noise term in the wave equation. For an unchoked fuel flow at the injector in a swirl combustor, Hong *et al.* (2008) reported the presence of pressure oscillations that alternated between a *'noisy period of 200 Hz fluctuation and a silent period with a small pressure fluctuation.'* Arndt *et al.* (2010) have observed a transition in the flame dynamics between a state of stable combustion and self-excited oscillations in a premixed gas turbine model combustor using simultaneous OH^* chemiluminescence, OH^* PLIF and stereoscopic measurements.

Predicting the amplitude or frequency of such triggered oscillations, or even the stability margins of combustors remain yet a challenge for researchers in the field due to

the complicated nature of the dynamics in combustors amongst the flow, heat release and the chamber acoustics (Zinn and Lieuwen, 2005). An understanding of the universal features of such transitions is limited and operators often rely on heuristic measures to prevent instability in fielded combustors. This limitation is possibly a consequence of the traditional 'signal plus noise' paradigm assumed in the analysis of such oscillations. Since it is possible that the irregular fluctuations seen in measurements are a direct result of the inherent complexity of turbulent combustion dynamics, it is unclear whether a separation of the measurements into a signal and noise is justified. Understanding and characterizing these transition states forms another major objective of the thesis.

1.6.3 Are there precursors to combustion instability?

From a more practical viewpoint, an important additional question is to know whether we can extract information about an impending instability, from the irregular states observed prior to instability. The methodologies available in the literature to prevent large-amplitude oscillations in combustors mostly focus on suppression of an incipient instability, i.e., an instability that has already begun. The operational parameters are modified based on a feedback signal acquired from the combustor, in order to suppress the incipient instability. At other times, modifications are made at the design stage based on operational experience as a passive control strategy. Poinsot *et al.* (1992) proposed a technique for the active monitoring of combustion instability through modulations of the pressure in the fuel line to suppress instabilities. This requires external actuators and/or modification of combustor configuration and knowledge of frequency response for an arbitrary input which limits its applicability to fielded systems. Further, the detection and control strategy requires the system to reach instability before control can take over. Hence, it would be more desirable to look for early warning signals to an impending instability—through active monitoring—so that instability is avoided in combustors altogether.

Hobson *et al.* (2000) analyzed combustor stability in terms of the bandwidth of combustor casing vibration and dynamic pressure measurements in combustion chambers. They observed that bandwidth which is indicative of the damping decreases towards zero as the combustors approach their stability limits. However, the presence of noise in the combustion chamber could make the technique untenable in practice as it relies

on a frequency domain analysis. Johnson *et al.* (2000) presented a technique to determine the stability margin using exhaust flow and fuel injection rate modulation. The technique is again limited in its scope as its applicability to practical combustors is restricted by the need for acoustic drivers and pulsed fuel injectors.

Lieuwen (2005) used the autocorrelation of the acquired signal to characterize the damping of the system and tracked the stability margin as the operating parameter value at which the damping goes to zero. This method again has the disadvantage that the dynamics of the system prior to onset cannot adequately be described using linear data processing techniques. The method, for instance, may not be effective for combustors exhibiting pulsed instabilities or a noise-induced transition to instability. Also, the presence of multiple frequencies often seen in the frequency spectrum at the onset makes the estimation of damping unclear.

The current solution adopted by combustion designers is thus to incorporate sufficient stability margin into the design to prevent instabilities from occurring even in the worst possible scenario. Setting such conservative estimates on operational regimes leads to increased levels of NO_x emissions making it more difficult to meet the demanding emission norms. It is desirable to have measures that predict the instability well before it happens because after the onset it may often be too late to take adequate control action to save the combustor from wear and tear or fatigue failure. There is thus a need for precursors to an impending instability so that appropriate stability margins may be devised to prevent the combustors from entering a regime of instability. Also, in order that these early warning signals are sensitive to operating conditions, such as ambient temperature or fuel composition, online stability monitoring seems like the optimal solution as a prevention methodology.

To resolve this question on precursors, we propose a formalism which involves searching for precursors to instability in data acquired from turbulent combustion environments, for conditions ranging from low amplitude combustion noise to high amplitude combustion-driven oscillations. That the formalism is data driven should be seen as an advantage, because models or simulations often contain many inherent assumptions themselves. Further, suitable models can be appropriately devised once the underlying mechanisms are well understood. The existence of precursors would imply that it is possible at least in principle, to reconstruct the dynamics that generates low amplitude

combustion noise. Identifying precursors—at the very least—should provide operators of combustors with sufficient warning of impending oscillations.

1.7 Identifying precursors to combustion instability: Proposed methodology

Early warning signals to combustion instability may also be obtained if measures can be devised that quantify the irregular states in a measured signal observed in a combustor prior to combustion instability. This requires that these irregular states be persistent features of the dynamics and not merely transients that decay down to low-amplitude fluctuations or large-amplitude periodic oscillations. This involves studying the dynamic characteristics of these states by identifying repeating patterns in such signals. Also, since typical measures such as the amplitude of oscillations cannot serve as measures of bifurcation in such systems with varying amplitudes, one must also seek to identify suitable bifurcation measures to study intermittent transitions to instability in turbulent combustors.

Yet another way to obtain early warning measures is to force the system under consideration with broadband noise (Wiesenfeld, 1985; Surovyatkina, 2005). The noise gets selectively amplified at the instability frequencies when the operating conditions are sufficiently close to instability. The width of the peak frequency in the amplitude spectrum then informs of the proximity of the system to instability (Wiesenfeld, 1985). Further, it has also been observed that there is a reduction in the bistable regime for systems exhibiting subcritical bifurcation, when the levels of noise used to force the system are increased (Surovyatkina, 2005). However, it should be noted that this procedure involves external stochastic forcing of a deterministic system; our interests lie in describing the deterministic features of the system itself. Moreover, the dynamics of a forced system is different from that of a self-evolving system especially with regards to the phase of the resulting oscillations (Pikovsky *et al.*, 2003) and the transient envelope of the growing oscillations (Burnley, 1996; Culick, 2006). Also, introducing noise can lead to noise-induced transitions (Jegadeesan and Sujtih, 2013), with dynamics different from that of the original system. Furthermore, it is well-known that a system chaotic dynamics can result in signals that appear noisy.

A chaotic time signal can be identified through its self-similar structure resulting in patterns that fill non-integer dimensions called fractals. A fractal time series has sections that resemble the whole and hence can be distinguished from stochastic signals which are—by definition—devoid of any patterns. The non-integer dimension of occupation of a fractal is termed the fractal dimension. A multifractal time series differs from a fractal series in that it is composed of interwoven subsets with different fractal dimensions (Frisch and Parisi, 1985). Gouldin was the first to recognize the utility of applying fractal geometry concepts to combustion problems in both turbulent premixed and diffusion flames (Gouldin, 1987; Gouldin *et al.*, 1989*b*,*a*). However, most of these and several subsequent studies focused on the geometrical aspects of open flames. Using hot film anemometry of the cold flow and Rayleigh scattering density measurements, multifractality in the time series data of turbulent premixed open flames was illustrated by Strahle and Jagoda (1989). However, the utility of the fractal description to measurements made in confined combusting environments has not been explored save for a recent study on the pressure fluctuations acquired prior to lean blowout (Gotoda *et al.*, 2012).

Since a multifractal process entails multiple time scales, it must necessarily display a broad spectrum in the frequency domain, such as one would observe in turbulent velocity measurements. It is now well-known that turbulent velocity measures are multifractal (Meneveau and Sreenivasan (1987, 1989, 1991); Sreenivasan and Meneveau (1986, 1988); Prasad *et al.* (1988) to name a few pioneering studies; see Sreenivasan (1991) for an excellent review on the subject). Energy injected into a turbulent flow at large scales cascade down multiplicatively through the inertial subrange down to Kolmogorov scales, where it is finally dissipated. The multifractal formalism is necessary to understand and explain the reason for the intermittency observed in the measurements of this energy dissipation rates in the inertial range.

The amplitude spectrum of ducted combustion noise is also known have a broad profile in the frequency domain with shallow peaks in the vicinity of acoustic modes of the duct (Chakravarthy *et al.*, 2007*a*). It would therefore be interesting to examine, whether measured pressure fluctuations acquired during such stable operating conditions in combustors are amenable to a multifractal description. We know that the transition to combustion instability results in a transition of the spectrum, from a broad one with shallow peaks, to one with sharp, discrete peaks. Provided combustion noise

is multifractal, we should therefore expect deviations from this multifractality, when the operating conditions are varied systematically towards combustion instability. Such deviations—if they exist—are of prognostic value, since they presage an impending instability.

1.8 Overview of the thesis

To achieve these objectives, experiments were performed on a laboratory scale combustor operating in a turbulent flow-field combustor to acquire unsteady pressure measurements and high speed flame images for a variety of operating conditions from stable operation towards combustion instability. Then, techniques from nonlinear time series analysis such as phase space reconstruction, recurrence quantification and fractal analysis are applied to the measured time signals to characterize the various dynamical states in order to identify the routes (pathways) underlying such undesirable transitions in combustors. Finally, precursor measures are sought for to provide an operator of fielded combustion systems with early warning signals of an impending combustion instability so that such regimes are avoided altogether.

The remainder of the thesis is organized as follows. Schematics of the experimental setup and details of data acquisition and post-processing are provided in **Chapter 2**. The study principally focusses on a bluff-body stabilized backward facing step combustor burning LPG as fuel. The results presented in the study also hold true for a swirl stabilized combustor the results of which have been presented elsewhere (see list of publications).

In **Chapter 3**, the nature of the dynamics of pressure fluctuations acquired during stable operating conditions at operating conditions far away from the stability margin are investigated. The technique of phase space reconstruction in introduced and the methods to investigate determinism in a time series are illustrated. Finally, a test for chaos is described to understand whether the irregularity in the pressure fluctuations signify chaotic dynamics.

The irregular burst states reported in the literature and observed prior to combustion instability are explored in **Chapter 4**. Methods to construct bifurcations diagrams for signals with varying amplitudes are introduced. Repeating patterns in the dynamics are

tracked using recurrence plots and the transition in the patterns at various dynamical states are highlighted. A mechanism is proposed to describe the onset of combustion instability in a turbulent flow-field.

Chapter 5 discusses a phenomenological model for the intermittent burst states which is derived from first principles based on the proposed mechanism. The model incorporates the hydrodynamic contributions to the combustion instability problem both due to turbulence and due to periodic vortex formation and impingement in the combustion chamber. The possibility of devising model-based early warning measures are also explored.

The fractal scaling of combustion noise is explored in **Chapter 6**. The methods to determine the generalized scaling behaviour of normalized moments of a measured pressure time signal are introduced and the possibility of a multifractal description of combustion noise is explored.

In **Chapter 7**, the possibility of intermittent burst oscillations close to lean blowout is investigated. A description of the intermittent dynamics as arising through the formation of homoclinic orbits with subsystems operating over different time/length scales is introduced. The flame dynamics of the states observed prior to lean blowout are also presented and contrasted with the flame dynamics observed during combustion instability.

Chapter 8 asks the question whether unsteady combustion and heat release are necessary to obtain intermittency and the precursors discussed previously. Using a simple setup consisting of a ducted unsteady flow across an orifice, the transition to self-sustained oscillations (whistling) is investigated by measuring the pressure fluctuations just outside the lip of the orifice. A mechanism is proposed to explain the onset of whistling and the presence of precursors to whistling is explored.

Finally, the conclusions derived from the study are summarized in **Chapter 9** along with an outlook for future investigations.

CHAPTER 2

Experiments

This chapter describes the experimental setup and the instrumentation used to obtain the measurements reported in the study.

2.1 Setup

Experiments were conducted on a backward-facing step combustor geometry with the flame stabilized using a circular bluff-body operating at high Reynolds number ($Re > 18000$). Schematics of the setup for the measurements reported in the current study is shown in Fig. 2.1. It consists of an upstream plenum, a burner of $40mm$ diameter and a combustion chamber of cross-section $90 \times 90mm^2$ with extension ducts. The length of the combustion chamber along with the extension ducts was $700mm$. A support mechanism that hinges on the plenum was used to traverse a shaft of $16mm$ diameter into the burner. The bluff-body—a circular disk of diameter $47mm$ and thickness $10mm$—was then attached to this shaft and was positioned $50mm$ from the rearward facing step using a rack and pinion traverse of least count $1mm$. The central shaft was used to deliver fuel (LPG) into the chamber through four radial injection holes of diameter $1.7mm$ and spark-ignited in the recirculation zone at the dump plane using an $11kV$ ignition transformer. The fuel injection location was $160mm$ upstream from the bluff-body. A circular disk of $2mm$ thickness and $40mm$ diameter with 300 holes of diameter $1.7mm$ was inserted $30mm$ downstream of the fuel-injection location to prevent flashback. It also served to reduce the influence of pressure perturbations in the plenum on the dynamics happening inside the combustion chamber. A blow-down mechanism was used to supply air from high pressure tanks which then passed through a moisture separator before finally entering the plenum chamber.

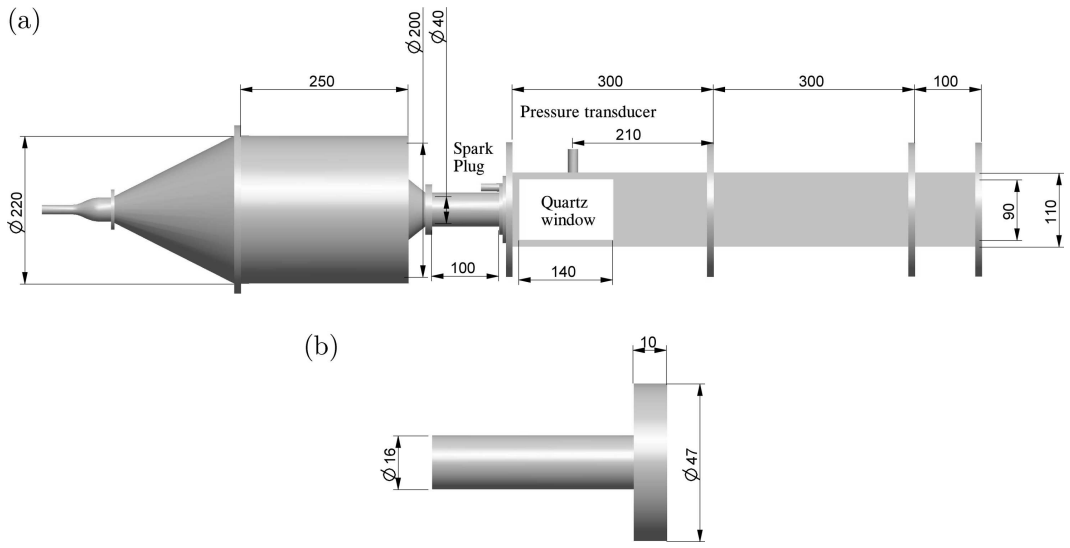

Figure 2.1: (a) The experimental setup used in the current study. The length of the combustion chamber is $700mm$ with three extension ducts, two of length $300mm$ and one of length $100mm$. The measurements reported in this study were acquired using a piezoelectric transducer located $90mm$ from the backward facing step. The design of the combustor was adapted from Komarek and Polifke (2012).

2.2 Measurements

Unsteady pressure measurements (p') were acquired for $3s$ at $10kHz$ using piezoelectric transducers with a sensitivity of $72.5mV/kPa$, $0.48Pa$ resolution and $\pm 0.64\%$ uncertainty. The voltage signals from the transducers were acquired using a 16-bit A-D conversion card (NI-643) that had a resolution of $\pm 0.15mV$ and an input voltage range of $\pm 5V$. The transducers were mounted on specially made pressure ports with Teflon adapters which were flush mounted on the combustor wall. Semi-infinite tubes were provided to the pressure ports to prevent acoustic resonance within the mount. The configuration helps prevent the transducers from excess heating and also ensured that the phase correction required was less than 2^0.

Mass flow controllers (Alicat Scientific, MCR Series) with digital logging and monitoring capabilities were used to measure and control the supply fuel and air into the combustion chamber and had a measurement uncertainty of $\pm(0.8\%$ of reading $+0.2\%$ of full scale). Liquified Petroleum Gas (LPG) was used as the fuel which is 60% C_4H_{10} and 40% C_3H_8 by volume. The fuel flow rate ($\dot{m}_f$) is held fixed and the air flow rate ($\dot{m}_a$) is gradually increased leading to progressively increasing values of Reynolds number (decreasing equivalence ratio ϕ). At each flow condition, the flow was allowed to

settle for $10s$ before acquiring the pressure data to remove transients associated with the change in mass flow rate. The Reynolds number was computed using the expression $Re = 4\dot{m}D_1/\pi\mu D_0^2$, where $\dot{m}$ ($= \dot{m}_a + \dot{m}_f$) is the mass flow rate of the fuel-air mixture, D_0 is the diameter of the burner, D_1 is diameter of the circular bluff-body and μ is the dynamic viscosity of the fuel-air at the experiment conditions. Corrections to Reynolds number due to the change in viscosity for the varying fuel-air ratios were performed, the procedure for which can be found in Wilke (1950).

For selected operating conditions, high speed images with CH^* filter (transmission peaks around a wave length of $431nm$ and bandwidth of $10nm$) were also acquired simultaneously with the pressure measurements at a frame rate of $1kHz$ using a Phantom v12.1 high speed camera (resolution 1280×800 pixels.

CHAPTER 3

What is combustion noise?

Combustion noise has been traditionally treated as stochastic fluctuations present in the background of the dynamics in combustors amongst the flow, heat release and the chamber acoustics. The aim of the current chapter is to study whether the pressure signals acquired from the combustor during stable operating conditions (termed 'combustion noise') show signs of determinism. The presence of determinism would imply predictability in the underlying dynamics and allows for the possibility of devising precursor measures that can forewarn the onset of an impending combustion instability. Precursors to such a transition from chaos to dynamics dominated by periodic oscillations are of interest to designers and operators of combustors in estimating the boundaries of operability. Techniques from nonlinear time series are used to embed the pressure signals into its underlying mathematical phase space. Then separate tests for determinism (Kaplan-Glass test) and chaos (0-1 test for chaos) are utilized to probe the dynamic features of the measured pressure fluctuations.

3.1 Reconstructing the phase space

The amount of experimental data available at the disposal of an experimental researcher is often just a few variables and in extreme cases just one measurement. The dynamics of a combustor at different operating conditions can be visualized by reconstructing the mathematical phase space of evolution of the time series data of unsteady pressure measurements acquired at those conditions. In such a reconstructed phase space (Takens, 1985), limit cycle oscillations would correspond to a closed loop around a fixed point.

Such a reconstruction, also known as delay-embedding, involves converting the measured time series into a set of delay vectors each of which has a one-to-one correspondence with one of the dynamic variables involved in the combustor dynamics. That is, we construct the vectors $[p'(t), p'(t+\tau), p'(t+2\tau), ..., p'(t+d-1)\tau]$ from the measured pressure data $p'(t)$ such that these vectors in combination provide us with

maximum information on the combustor dynamics. The elements of these vectors are the coordinates in the d-dimensional phase space of evolution of the time signal. For instance, $\boldsymbol{p'_i}(d) = [p'(t_i), p'(t_i + \tau), p'(t_i + 2\tau), ..., p'(t_i + d - 1)\tau]$ is the point in the d-dimensional phase space at time instant t_i. To accomplish an appropriate reconstruction, we need to obtain the optimum time lag (τ_{opt}) amongst the delay vectors and the least embedding dimension (d_0) for the phase space composed of these delay vectors such that the dynamics is faithfully captured.

3.1.1 Obtaining the optimum time delay

The optimum delay τ_{opt} may be estimated as that value of τ for which the average mutual information (Abarbanel *et al.*, 1993) between the delay vectors reaches its first minimum. The average mutual information of a signal $p'(t)$ is given by the expression:

$$I(\tau) = \sum_{i=1}^{N} P(p'(t), p'(t+\tau)) \log_2 \left[\frac{P(p'(t), p(t+\tau)}{P(p'(t))P(p'(t+\tau))} \right] \tag{3.1}$$

where, $P(S)$ represents the probability of the event S.

To compute the average mutual information for various time lags τ, we first normalize the time signal $p'(t)$ to lie between 0 and 1 and then sort the data in bins. The probability distributions $p'(t)$ and $p'(t + \tau)$ are then obtained by normalizing the histograms on these bins. Similarly, the joint probability distribution $P(p'(t), p'(t + \tau))$ is obtained by normalizing a two dimensional histogram obtained on a two dimensional bin in $p'(t)$ and $p'(t + \tau)$.

Average mutual information, which is a function of the time distance between the data points of a time series, is an indicator of the amount of information shared by two sets of data. The location of the minimum would, therefore, correspond to a set of vectors that would provide more information about the system than either of them in isolation. Shown in Fig. 3.1(a) is the measured pressure fluctuations during stable operation of the combustor ($\phi = 1.1$, $Re = 1.83 \times 10^4$). The amplitude of the fluctuations vary wildly and give the appearance of an aperiodic noisy signal. The corresponding average mutual information for data has its first minimum $\tau_{opt} = 1.1ms$ (Fig. 3.1(b)). This values corresponds approximately to $T/4$ where T is the time period of oscillation

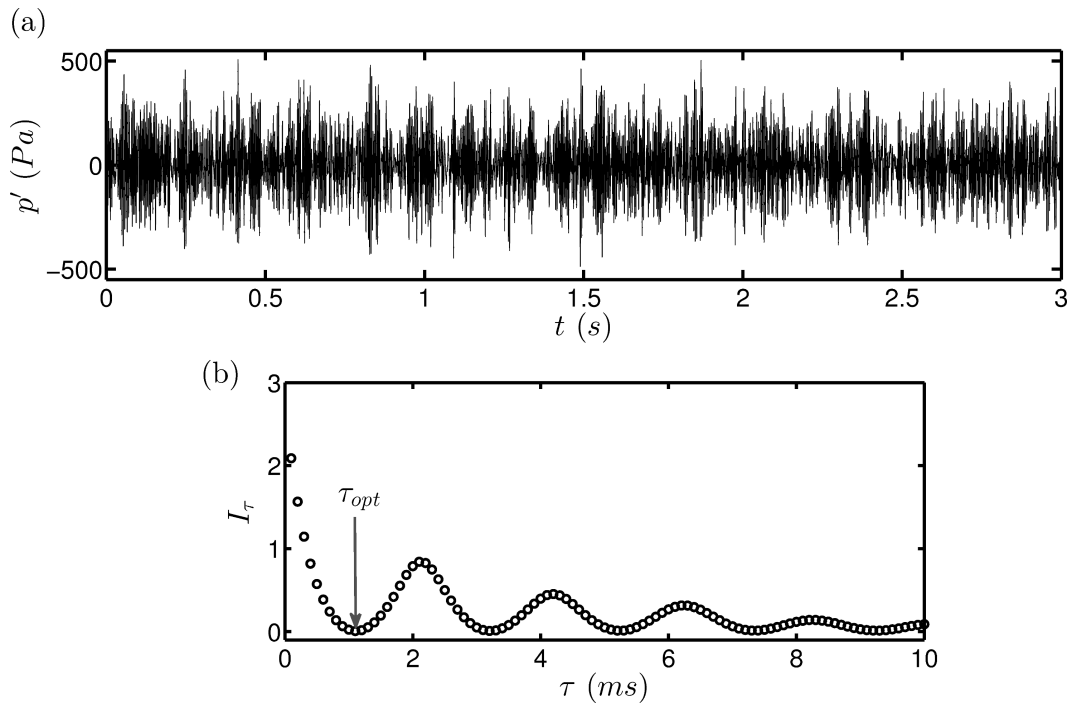

Figure 3.1: (a) The pressure signal obtained at stable operating regime from the combustor with the bluff-body stabilized flame ($\phi = 1.1$, $Re = 1.8 \times 10^4$). (b) The average mutual information for the signal. The optimal delay is $\tau_{opt} = 1.1ms$.

at combustion instability. This time period was discerned from the FFT of the pressure signal at combustion instability. The delay vector $p'(t_i + \tau_{opt})$ can thus alternately be seen to be related to the acoustic velocity in a one-to-one fashion since the acoustic pressure and velocity differ in phase by 90^0 for a standing wave pattern in the duct. The small deviation from 90^0 is due to damping.

The plot of I_τ further shows that the signal displays correlations that decay very fast. This rapid decay of average mutual information implies that the signal has a finite memory of the past and hence indicates the possibility of determinism.

3.1.2 Optimum embedding dimension

To obtain a suitable dimension d_0 in which the attractor dynamics unfold, we use the technique developed by Cao (1997). This is an optimized version of the False Nearest Neighbors (FNNs) method (Abarbanel *et al.*, 1993) wherein one tracks the number of false neighbours to each point in the phase space as the embedding dimension is progressively increased. A false neighbour to a point in phase space is one that moves away from it once the embedding dimension is increased. Mathematically, once the

optimum time lag has been obtained, we can construct a measure $a(i,d)$ of the form:

$$a(i,d) = \frac{||\boldsymbol{p'_i}(d+1) - \boldsymbol{p'_{n(i,d)}}(d+1)||}{||\boldsymbol{p'_i}(d) - \boldsymbol{p'_{n(i,d)}}(d)||} \tag{3.2}$$

where $i = 1, 2, \ldots, (N - d\tau)$ and $n(i,d)$ is the index of the nearest neighbouring point in phase space to the point $\boldsymbol{p'_i}$. $||\ldots||$ represents the Euclidean distance between two points. The dependency on the index i is removed by taking the average $a(i,d)$ obtained at different values of i as:

$$E(d) = \frac{1}{N - d\tau_{opt}} \sum_{i=1}^{N-d\tau_{opt}} a(i,d) \tag{3.3}$$

Here, $E(d)$ is a function only of the dimension d and the optimum time lag τ_{opt}. The variation of $E(d)$ on increasing the dimension from d to $d+1$ is determined by defining $E_1(d)$ as:

$$E_1(d) = \frac{E(d+1)}{E(d)} \tag{3.4}$$

If $E_1(d)$ stops changing when the value of d is greater than d_0, then d_0 is chosen as the minimum embedding dimension for the time series. Since the acquired time signal is limited, it is often difficult to distinguish a stochastic signal from a deterministic signal merely by observing the variation of $E_1(d)$ for various values of d. Whereas $E_1(d)$ saturates beyond a value of d for a deterministic signal, it always increases with increasing d for random signals. To clearly distinguish deterministic signals from stochastic signals, we define an additional measure $E_2(d)$ from the time series $p'(t)$ as:

$$E_2(d) = \frac{E^*(d+1)}{E^*(d)} \tag{3.5}$$

where

$$E^*(d) = \frac{1}{N - d\tau_{opt}} \sum_{i=1}^{N-d\tau_{opt}} |p(i + d\tau_{opt} - p(n(i,d) + d\tau_{opt})| \tag{3.6}$$

Since future values are independent of past values for random signals, $E_2(d)$ equals

one for all values of d (Cao, 1997). That is, $E_2(d)$ is independent of d. For deterministic signals on the other hand, $E_2(d)$ is dependent on d, because of which there must exist some values of d for which $E_2(d)$ is not equal to one. The validation of the computational procedure on a simple system comprising three coupled nonlinear differential equations is provided in Appendix A.

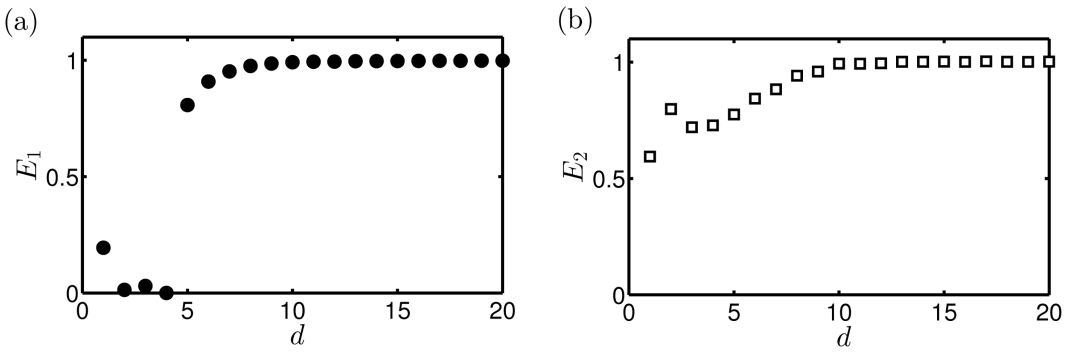

Figure 3.2: The measures $E_1(d)$ and $E_2(d)$ for the combustion noise data on applying Cao's method ($\phi = 1.1$, $Re = 1.83 \times 10^4$). The plot of $E_1(d)$ saturates after $d = 10$. Also, the values of $E_2(d)$ do not equal 1 for all values of d. This indicates that combustion noise is deterministic with moderately high dimensions.

The variation of E_1 and E_2 for the combustion noise data are shown in Fig. 3.2. The least embedding dimension for the combustion noise data can be taken to be $d_0 = 10$ as the measure E_1 does not vary significantly after $d = 10$. Also, the value of the measure $E_2(d)$ is not equal to 1 for all values of d. Hence, we see that combustion noise is deterministic with a moderately high dimensional attractor. Although, average mutual information and Cao's method to determine the least embedding dimension provides us with information as to whether the signal is deterministic or not, additional tests are often performed to confirm the determinism in measured signals. One of such methods is described in what follows.

3.2 Kaplan-Glass test for determinism

The local flow test for determinism is a discrete adaptation (Kaplan, 1993) of a technique devised by Kaplan and Glass (1992) for continuous dynamical systems. After delay-embedding the time series, one selects points in the phase space that are close to each other. These points are then evolved in time for a short duration known as the translation horizon. Points in the phase space that are close to each other tend to move

in the same direction for deterministic signals and in random directions for stochastic signals. Hence, for a given translation horizon, we construct vectors that connect the initial and final points, which are then normalized and averaged. These averaged vectors would then be larger for deterministic signals. The process is then repeated for various translation horizons. For deterministic signals, although the deterministic structure is preserved for short horizons, it is lost once the translation horizon is made too large. Hence, the average vector lengths will be small once the translation horizon is made large.

3.2.1 Computational procedure

To construct a measure of determinism, we first cover the phase space with a grid of non-overlapping hypercubes (cubes in d_0 dimensions). The number of points in each cube is n_j with time indices $t_{(j,1)}, t_{(j,2)}, ..., t_{(j,n_j)}$. If H is the translation horizon, the change in state from time $t_{(j,k)}$ to $t_{(j,k)} + H$ for each of the n_j points in the cube j is given by:

$$\Delta \boldsymbol{p_{j,k}} = \boldsymbol{p}(t_{j,k} + H) - \boldsymbol{p}(t_{j,k}) \tag{3.7}$$

where $k = 1, 2, ..., n_j$. Note that here we have explicitly written out the index in terms of time to distinguish different points within the same hypercube. Points near the edge of a cloud of points will have a directional bias towards the middle of the cloud (Kaplan, 1993). To correct for this, $\Delta \boldsymbol{p'_{j,k}}$ is mapped onto a sine function as:

$$\begin{aligned} \Delta \boldsymbol{p'_{j,k}} = \Bigg[& \sin\left(2\pi \frac{p'(t_{j,k} + H) - p'(t_{j,k})}{\lambda}\right), \\ & \sin\left(2\pi \frac{p'(t_{j,k} + H + \tau) - p'(t_{j,k} + \tau)}{\lambda}\right), ..., \\ & \sin\left(2\pi \frac{p'(t_{j,k} + H + (d-1)\tau) - p'(t_{j,k} + (d-1)\tau)}{\lambda}\right)\Bigg] \end{aligned} \tag{3.8}$$

where λ is the characteristic length of the embedded attractor in phase space. Summing up all vectors through hypercube of index j, we obtain the resultant vector V_j normalized by the number of vectors passing through the cube n_j in the following fashion:

$$\boldsymbol{V_j} = \frac{1}{n_j} \sum_k \frac{\Delta \boldsymbol{p'_{j,k}}}{||\Delta \boldsymbol{p'_{j,k}}||} \tag{3.9}$$

We can then define a measure Λ that quantifies local flow in phase space by averaging over the vectors $\boldsymbol{V_j}$ based on the number of vectors present in the hypercube (say, l), as:

$$\Lambda = \left\langle \frac{V_l^2 - c_{d_0}^2/l}{1 - c_{d_0}^2/l} \right\rangle \tag{3.10}$$

Here, V_l represents the norm of $\boldsymbol{V_l}$ (the replaced index in the subscript indicative of the new ordering) and c_E is a constant defined as (Kaplan and Glass, 1992):

$$c_{d_0} = \sqrt{\frac{2}{d_0}} \frac{\Gamma\left(\frac{d_0+1}{2}\right)}{\Gamma\left(\frac{d_0}{2}\right)} \tag{3.11}$$

with Γ being the standard gamma function. The measure Λ retains values close to 1 for deterministic signals and has values close to zero for stochastic signals (Kaplan and Glass, 1992).

Although Λ quantifies local flow, it is insensitive to false positives that may arise due to a directional preference in the time series. The method of surrogate data helps to circumvent this uncertainty.

3.2.2 Surrogate data analysis

Interpretation of results from experimentally acquired data can sometimes pose problems because filtered noise data can occasionally give the impression of chaos and low-dimensional dynamics. The technique of surrogate data analysis provides an efficient method to avoid such misinterpretations. One starts the analysis with a null hypothesis (the default position in the absence of evidence to the contrary) that the experimental data can be described by a linear stochastic model. Surrogate data sets are generated from a measured signal such that they retain certain characteristics of the original data (such as number of data points, mean and standard deviation) while ensuring that the

data is sufficiently randomized so that any deterministic structure that may be present in the original data is destroyed (Theiler *et al.*, 1992). Techniques like the determinism tests are then applied to both the original data and the surrogate data. If the results are similar for the experimental and surrogate data sets; i.e., if the predictions of the tests are equally good or bad, then one cannot reject the null hypothesis that a linear stochastic model is sufficient to describe the experimental data.

One of the techniques of surrogate generation involves randomly shuffling the data values in the signal, without adding or subtracting data (West, 2006). Such a random shuffling destroys any correlation originally present among the data points. This produces a random time signal that has the same mean and standard deviation as the original time series.

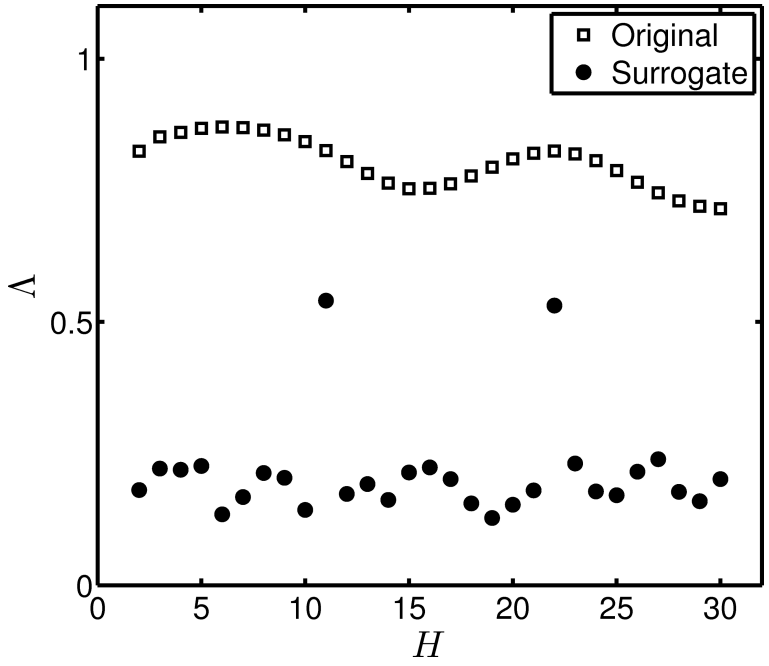

Figure 3.3: Results on applying the local flow method of determinism on the combustion noise data ($\phi = 1.1$, $Re = 1.83 \times 10^4$,$\tau_{opt} = 1.1ms$). Whereas the original data shows high levels of determinism, it is lost when the data values are randomly shuffled. The embedding dimension was kept as $d_0 = 10$ for all the data sets. τ_{opt} for the surrogate sets was kept the same as that for original data for the sake of comparison. The spikes in the surrogate data correspond to those values of translation horizon H that are multiples of the optimum time delay τ_{opt} non-dimensionalized by the sampling time ($0.1ms$).

3.2.3 Determinism in combustion noise

Surrogate data sets were constructed from unsteady pressure measurements acquired during combustion noise with the same mean, standard deviation and power spectrum as the original data. Then the local flow test for determinism was applied on both the original and surrogate data sets and the results are shown in Fig. 3.3. Whereas the measure Λ remains fairly close to one for the original data over a range of translation horizons, they remain at a lower value close to zero for the surrogate data sets. The occasional spikes correspond to those values of translation horizon which are multiples of τ_{opt} (normalized by the sampling time). This happens because the delay vectors partially overlap after moving over a distance τ_{opt} which also happens to be the optimum delay chosen for embedding. Hence, we have convincing evidence that combustion noise is deterministic. Thus, the traditional signal plus noise paradigm often implicitly assumed in models and analysis of experimental data sets (Clavin *et al.*, 1994; Burnley and Culick, 2000; Lieuwen, 2001, 2002, 2003; Lieuwen and Banaszuk, 2005) needs to be reexamined if one wishes to capture the onset of instabilities in combustors because these irregular fluctuations may contain useful information of prognostic value.

3.3 The 0-1 test for chaos

The motivation behind the 0-1 test (Gottwald and Melbourne, 2004) is that when the combustor encounters limit cycle oscillations, the dynamics transitions from chaotic to regular. The signal $p'(t)$ is measured ensuring that the acquired value at each instant provides essentially little information about future values at stable operation. This can be done by sampling at a time interval corresponding to the minimum of the average mutual information. Typically, this would correspond to a sampling time of $\tau_{opt} = T/4$ where T is the period of oscillations in the combustion chamber during instability. Typically, the time period of oscillations at instability is itself an unknown. However, the detector is robust for various values of sampling interval as long as the consecutive values are poorly correlated. For example, comparable results can be obtained for values of τ_{opt} corresponding to the first zero crossing of the autocorrelation of $p'(t)$. The time period corresponding to the dominant frequency in the FFT during stable operation of the combustor can also be utilized as a suitable measure of T to obtain the sampling time.

From the measured signal $p'(t)$ for $t = (1, 2, ..., N)$ and $t_{(i+1)} - t_i = \tau_{opt}$, translation variables q_c and r_c can be created as follows:

$$q_c(n) = \sum_{t=1}^{n} p'(t)cos(ct) \tag{3.12a}$$

$$r_c(n) = \sum_{t=1}^{n} p'(t)sin(ct) \tag{3.12b}$$

where $c \in (\pi/5, 4\pi/5)$. The mean square displacement of these translation variables may then be computed for different values of c as following:

$$M_c(n) = \lim_{N\to\infty} \sum_{t=1}^{N} \left([q_c(t+n) - q_c(t)]^2 + [r_c(t+n) - r_c(t)]^2 \right) \tag{3.13}$$

with $n \ll N$. It is seen that $n \leq n_{cut}$ where $n_{cut} = N/10$ yields good results.

The mean square displacement is indicative of the diffusive nature of the translation variables. If the dynamics is regular, then the mean square displacement is a bounded function in time and for chaotic dynamics, it scales linearly with time.

A modified mean square displacement D_c may be defined to ensure better convergence properties but with the same asymptotic growth rate as:

$$D_c(n) = M_c(n) - V_{osc}(c, n) \tag{3.14}$$

where

$$V_{osc}(c, n) = \langle p'(t) \rangle^2 \frac{1 - \cos nc}{1 - \cos c} \tag{3.15}$$

and

$$\langle p'(t) \rangle = \lim_{N\to\infty} \frac{1}{N} \sum_{t=1}^{N} p'(t) \tag{3.16}$$

Hence by defining vectors $\xi = (1, 2, n_{cut})$ and $\Delta = (D_c(1), D_c(2), ..., D_c(n_{cut}))$,

the correlation K_c given by:

$$K_c = \mathrm{corr}(\xi, \Delta) \tag{3.17}$$

which essentially allows one to distinguish between the two types of behaviour possible in such systems.

To ensure robustness of the measure to outliers and spurious resonances, the median value of K_c (say K) may be taken which is obtained for different random values of c. This value of K would lie close to one for chaotic signals and close to zero for regular dynamics. If the system is inherently turbulent, the transition to instability would be associated with a decrease in the value of K from one to a value depending on the turbulent intensity, i.e., higher the intensity of turbulence at instability higher the departure of K from zero at instability.

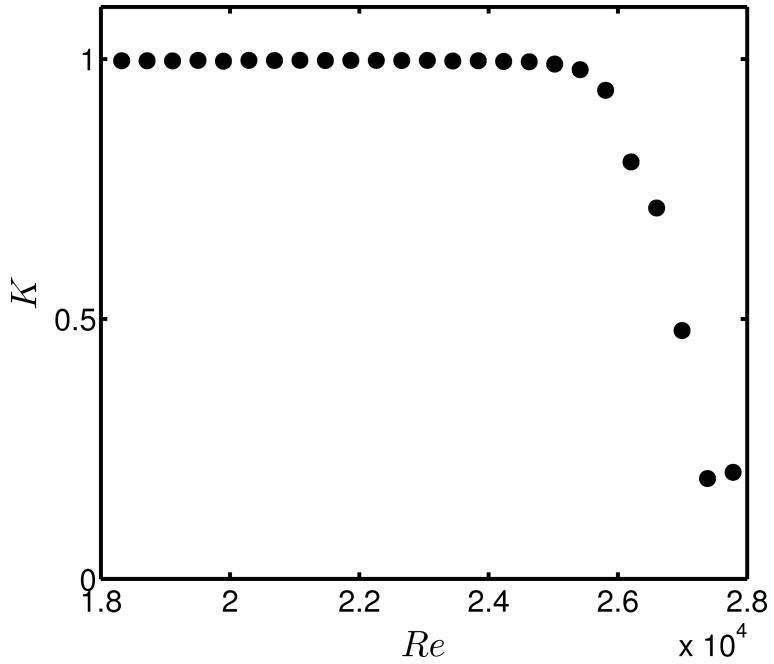

Figure 3.4: The results on applying the 0-1 test for chaos on the bluff-body stabilized backward facing step combustor for signals acquired at various Reynolds numbers. Whereas the values lie fairly close to one for chaotic combustion which is stable, departure from one indicates the onset of impending combustion instability which happens as the Reynolds number is increased. The results presented are for the entire $3s$ data which brings in some graininess due to amplitude modulations. By setting threshold at a value of say 0.9 for K, operators can be informed of an impending instability so that appropriate control measures can be taken.

3.3.1 Chaos in combustion noise

The 0-1 test for chaos was applied on the pressure measurements acquired sequentially at various Reynolds numbers starting from low amplitude combustion noise to high amplitude combustion instability. The measure K remains fairly close to one during the initial stages which indicates that combustion noise is chaotic. The value of K gradually starts decreasing as the flow Reynolds numbers are increased eventually reaching values close to zero at the onset of instabilities. Since this loss of chaos happens in a smooth manner, we can use the measure K as a precursor to impending instability. By choosing a threshold value of K that corresponds to the initial stages of loss of chaos (say, 0.9), operators get to know well in advance of an impending instability so that appropriate control action may be taken through modification of control parameters to prevent the onset. Further, the precursor is an objective measure of proximity of the combustor to unstable operating regimes since it is independent of the details of geometry, fuel composition and flame stabilization.

A controller was devised succesfully that determines the proximity of combustors to instability that utilizes the 0-1 test for chaos. Although we used the entire $3s$ data in the analysis results presented in Fig. 3.4, the test performs robustly even with a sampling rate as poor as $1kHz$ with 500 samples of data (data acquisition for $500ms$) for an instability frequency around $250Hz$.

Since the measure falls smoothly as the operating conditions approach onset, suitable control action may be taken by modifying operational parameters to prevent high amplitude oscillations. Thus, the stability margins of practical fielded systems can safely be estimated without encountering instabilities.

3.4 Concluding remarks

Combustion noise was shown to be deterministic by performing the Kaplan-Glass test for determinism on unsteady pressure data acquired from the bluff-body combustor different combustors operating at turbulent Reynolds numbers. The embedding dimension for combustion noise was seen to be much lower ($d_0 < 10$) than turbulence which is high dimensional. This difference can be attributed to the interaction of the acoustic

field with the turbulent flow-field. Using the 0-1 test for chaos, combustion noise was further shown to be chaotic, which is in stark contrast with the current description of the phenomenon where it is often treated as a stochastic background to the dynamics. In the next chapter, attention will be focused on the intermediate regimes prior to combustion instability—where the measure for chaos (K) displayed a smooth decrease in value from 1 towards 0—in order that the transition route to combustion instability is identified. These states lie in between the chaotic regime termed combustion noise and ordered oscillations termed combustion instability.

CHAPTER 4

What happens in between chaos and order?

In this chapter, we show that the onset of combustion instability is presaged by operating conditions that display intermittent bursts of high amplitude periodic oscillations in pressure, that appear in a near random manner amidst chaotic fluctuations. A mechanism is proposed that describes the onset of low frequency combustion instabilities via the intermittency route, which requires the flow-field to be at least locally turbulent in the vicinity of the flame. The repeating patterns in the dynamics are then extracted using a visualization technique known as a recurrence plot. Using the statistics of the recurrent states, various measures are constructed that can forewarn an impending instability well before the amplitudes start rising in the combustor. Also, since typical measures such as the amplitude of oscillations cannot serve as measures of bifurcation in such systems with varying amplitudes, we also seek to identify suitable bifurcation measures to study intermittent transitions to instability in turbulent combustors. The performance of these measures are then compared with the existing measures available in the literature such as the damping rate of the autocorrelation measure of the pressure signal.

4.1 Intermittency route to combustion instability

In turbulent combustors, the transition to self-sustained oscillations from regimes of stable operation can often be triggered due to the unsteadiness in the flow and combustion. Predicting the amplitude or frequency of such triggered oscillations, or even the stability margins of combustors remain yet a challenge for researchers in the field due to the complicated nature of the dynamics in combustors amongst the flow, heat release and the chamber acoustics (Zinn and Lieuwen, 2005). An understanding of the universal features of such transitions is limited and operators often rely on heuristic measures to prevent instability in fielded combustors.

The distributions of the pressure measurements acquired from combustors well before conditions of instability have a characteristic Gaussian distribution (Lieuwen, 2002) suggestive of dynamics dictated by random processes in these regimes. In chapter 3, it was shown that combustion noise is deterministic chaos and therefore is not noise in the traditional sense of the word. Pressure signals acquired during combustion noise were subjected to determinism tests and were shown to be chaotic. Further, it was also shown that a loss of chaos which happens as a result of triggering happens in a smooth fashion. An objective measure K was defined to capture this loss of chaos independent of the details of geometry, fuel composition, or flow parameters. However, the reason for the smooth variation of the precursor was not explained in the study and requires further elaboration.

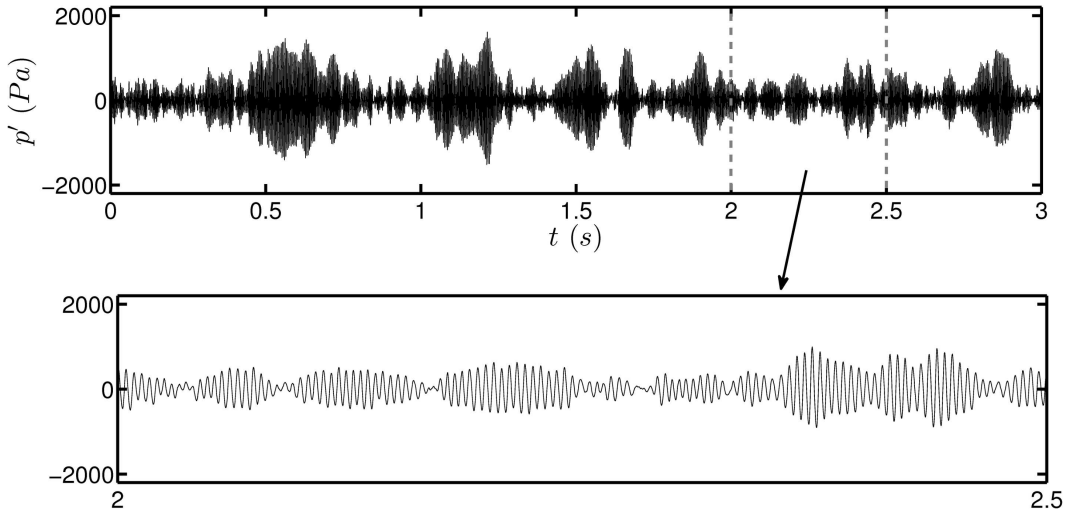

Figure 4.1: Intermittent signal obtained from the the bluff-body stabilized backward facing step combustor ($Re = 2.58 \times 10^4$, $\phi = 0.77$). The signal is composed of high amplitude oscillations interspersed amidst low amplitude aperiodic fluctuations as seen in the zoomed regions of the signals. Such intermittent burst oscillations were always observed prior to the onset of instabilities.

The smooth variation of the measure for chaos hinted at the existence of a dynamic regime different from chaos and limit cycle oscillations. Shown in Fig. 4.1 is a signal obtained from the combustor at these intermediate conditions between regimes of unsteady chaotic fluctuations and large amplitude periodic oscillations. The signal displays bursts of high amplitude oscillations amidst regions of low amplitude fluctuations. Such an intermediate regime of intermittent oscillations was observed in all the experiments we performed prior to the transition to combustion instability. Also, such states were seen to persist in time; they are not transients that eventually transform to periodic oscillations or combustion noise.

The present study focusses on establishing that intermittency is a stable dynamical state in combustors distinct from the regimes classified as stable (chaotic) or unstable (periodic). Although reports of such possibly intermittent burst states are present in the literature, their dynamics have not been investigated or characterized in detail. For an unchoked fuel flow at the injector in a swirl combustor, Hong *et al.* (2008) reported the presence of pressure oscillations that alternated between a *'noisy period of 200 Hz fluctuation and a silent period with a small pressure fluctuation'*. Arndt *et al.* (2010) have observed a transition in the flame dynamics between a state of stable combustion and self-excited oscillations in a premixed gas turbine model combustor using simultaneous OH^* chemiluminescence, OH^* PLIF and stereoscopic measurements. Bursts of pressure oscillations have also been reported close to critical transition to instability in liquid-propellant rocket engines (Clavin *et al.*, 1994).

An explanation for the burst oscillations was provided in the study by Clavin *et al.* (1994) where the erratic behaviour of pressure fluctuations was incorporated as a multiplicative noise term in the wave equation. The effect of such a noise term, which was used to model the effects of turbulence, in the vicinity of a sub- and supercritical Hopf bifurcation was then explored, and the corresponding probability distribution of pressure fluctuations were obtained after deriving the amplitude equations for the underlying acoustic system close to criticality. The proposed model highlights the need for a nonlinear approach in describing the nature of transition. However, it is known that in addition to modulating the pressure fluctuations, turbulence also brings with it its own dynamics such as vortex shedding that can have contributions over time scales close to combustion instability. To bring in the effects of turbulence as a parametric (multiplicative) noise term is to concede that it is not possible to describe or quantify the dynamics brought about by phenomena such as the formation, roll-up, coalescence and impingement of vortices. Hence, appropriately modelling these deterministic aspects of the hydrodynamics remains a continuing challenge in the field.

The dynamics of fluctuations in turbulent combustors may be better understood as a complex interplay amongst two subsystems operating over different length and time scales. Acoustics operates over time scales determined by the passage time of sound through the combustion chamber. Interaction due to hydrodynamics on the other hand, can be spread over multiple orders of temporal magnitude due to the broad-band nature of the underlying turbulence. At the same time, unsteady flow phenomena such as

vortex shedding, roll-up, coalescence, or impingement can give rise to dynamics over a narrow frequency band, some of which could lie close to the natural acoustic modes of the confining combustion chamber. Hydrodynamics thus operates over a broad range of time scales associated with convection and unsteadiness due to turbulence.

The major contribution to the driving received by the acoustics through combustion—other than those due to direct hydrodynamic or acoustic modulation of the flame—comes from fuel unmixedness through equivalence ratio perturbations. These equivalence ratio perturbations, which again arise due to acoustic modulation of the feed system and flow unsteadiness, are seen to influence only the magnitude of heat release rate fluctuations. Lieuwen *et al.* (1998) have shown that chemical time scales, being typically much smaller than flow/acoustic time scales, are unlikely to provide the necessary phase delay needed for an acoustic –chemical kinetic coupling to sustain low-frequency instabilities. Hence, it is reasonable to assume fast chemistry and essentially incorporate the effects of combustion as part of the hydrodynamic and acoustic subsystems. It should further be noted that such a description does not decouple the dynamics of acoustics and hydrodynamics; rather it emphasizes a mutual nonlinear coupling of the two subsystems. A model based on this mechanism will be introduced in Chapter 5.

In modelling these effects, if one were to discount the effects of turbulence or average out the equations (a mean field description), the bifurcation of the acoustic system will be seen as a transition from a fixed point solution to a periodic final state—a transition termed Hopf bifurcation. Such a description which decouples the two subsystems leaves no room for phenomena such as the intermittent bursts states observed in the experiments. The intermittent oscillations can arise if the acoustic subsystem is modulated by the hydrodynamics over slower time scales (turbulent velocity fluctuations typically have an increased energy content at lower frequencies), essentially shifting the dynamics of the acoustic subsystem back and forth across the Hopf point. If the mechanism proposed above is correct, combustion instability in turbulent combustors must necessarily happen via a regime of intermittent burst oscillations. Further, the mechanism also requires that such intermittent periodic bursts be absent when the underlying flow-field is laminar, as there are no possible mechanisms to allow for the required low frequency, near-random modulation. Such a situation can arise, for instance, in ducted laminar flames, as long as the flame itself doesn't become turbulent; or in an electrical Rijke tube as long as the mean flow is laminar. For such laminar transitions, the r.m.s.

levels of pressure in the system form a convenient measure that characterizes the onset of instability. In what follows, we shall describe ways to characterize intermittent burst oscillations observed in turbulent combustors.

4.1.1 Bifurcation diagrams

Typically, bifurcation diagrams of experimental data are drawn by tracking the peaks in a measured signal and plotting them as a function of the control parameter. However, the presence of turbulence shifts the peak amplitude across a range of values even during combustion instability. One simple way to bypass this issue would be to count the number of peaks (N) in the signal $\phi(j)$ for a time duration t above a fixed threshold ϵ which would correspond to acceptable levels of amplitude for the system. If N_{tot} is the total number of peaks that happen within that time one can then assign a probability of the system to attain instability as:

$$f = N/N_{tot} \tag{4.1}$$

The value of f is a measure of the proximity of the system to instability. The measure also makes sense from a dynamical systems perspective as an order parameter; i.e., a parameter that measures the amount of order (order in the sense of ordered oscillations or organized behaviour) in the system (Haken, 1985).

Figure 4.2 shows the value of f at various Re starting from low amplitude combustion noise to instability and back to stable operating regimes at two different fuel flow rates. The threshold was set at $500Pa$ that corresponds to the levels of pressure fluctuations in the system during stable regimes of operation. The values of f vary smoothly as the control parameter (Re) traverses regimes of stable operation towards combustion instability. This is because of the presence of an intermediate intermittent regime in which the pressure signals occasionally cross the threshold and leads to increased values of f. These intermittent excursions last longer in time as flow conditions approach combustion instability and finally saturates to 1 as instability is reached, when the dynamics becomes dominantly periodic. These values of f thus serve as an appropriate measure—a measure of the order in the signal—to draw the bifurcation diagram in systems exhibiting widely varying amplitudes in the signals.

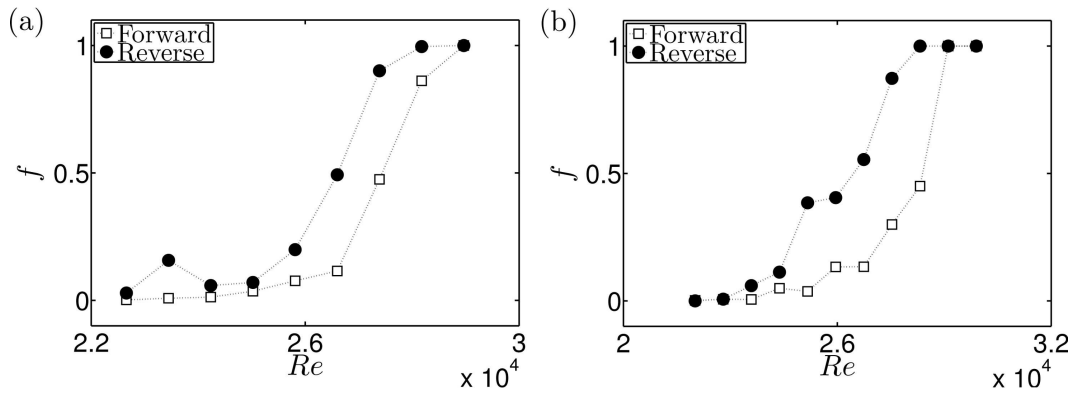

Figure 4.2: Bifurcation diagram obtained through normalized burst count (f) for the transition from chaotic combustion noise to high amplitude combustion instability (a) $\dot{m}_f = 0.55g/s$, (b) $\dot{m}_f = 0.59g/s$. The shape of the forward and return trajectories resembles a sigmoid (S-shaped) curve. The threshold was set at $500Pa$.

The bifurcation diagrams further enable us to infer the nature of criticality of the bifurcation of the acoustic subsystem that leads to combustion instability in both the configurations. A hysteresis is clearly visible in this new bifurcation diagram (Fig. 4.2). The nature of the graphs were found to be qualitatively similar on shifting the threshold a few tens of Pascals on either side although there is an associated quantitative change in the probability measure f. Hence, it is to be concluded that the bifurcation diagram is useful only to infer the qualitative nature of the transitions at the onset of instability. The bifurcation diagrams show that the presence of the bluff-body causes the bifurcation of the acoustic subsystem to be subcritical.

4.1.2 Precursors to combustion instability

Although bifurcation diagrams can be drawn by computing the probability that the peaks in a measured signal exceed the levels of noise in the combustor, they cannot be used to determine the proximity of the system to an impending instability sufficiently in advance. This is because the measure f starts growing only when the amplitude levels in the combustor grow, which can in turn be conveniently be measured by computing the r.m.s. levels of pressure fluctuations in the combustor.

Lieuwen (2005) has used the damping rate of the autocorrelation to predetermine the stability margin of combustors. The transition point was identified as that operating condition at which the damping of the autocorrelation of measured signals become zero.

After computing the autocorrelation of the pressure signal, a Hilbert transform was applied on the autocorrelation to obtain the variation of the amplitude and phase of the autocorrelation. The effective damping rate was then obtained as the slope of the logarithmic decrement of the amplitude of the autocorrelation.

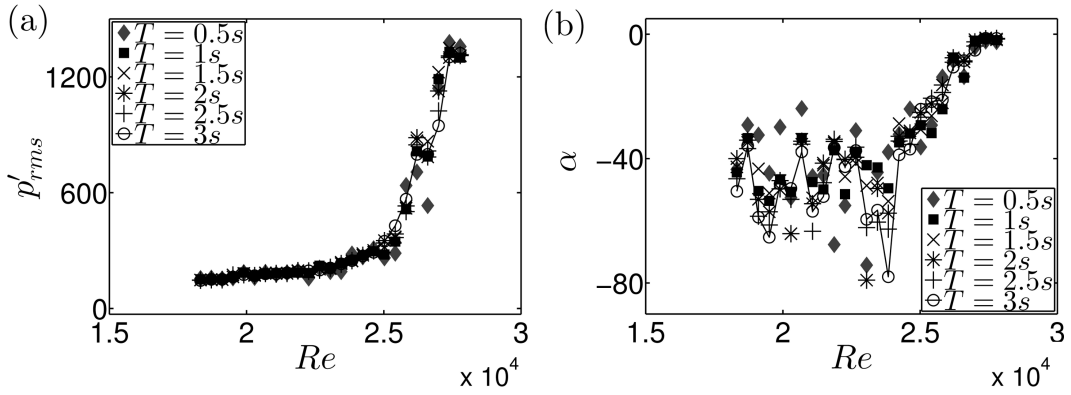

Figure 4.3: Variation of the sound levels in the combustor as measured by (a) the r.m.s. values of unsteady pressure signal (p'_{rms}) with Re ($\dot{m}_f = 0.59g/s$). (b) The variation of the precursor measure based on the effective damping rate of the autocorrelation of the pressure time traces.

Shown in Fig. 4.3(b) is the variation of the damping rate of the autocorrelation of the pressure time traces acquired for various values of flow Reynolds number starting from regimes of combustion noise towards combustion instability. The damping rate was computed for $0.04s$ (roughly 10 acoustic cycles at instability), by performing a linear regression. Unlike in Lieuwen (2005), a band pass filter was not applied to the input pressure signals. To compare the performance of this precursor measure, the variation of the r.m.s. values of the pressure time series for the various conditions are also shown in Fig. 4.3(a). To show the convergence of the measures, the damping rates and r.m.s. values computed for increasing intervals of data acquisition are also shown. The regression errors associated with the straight line fit for the damping rates have not been shown for the sake of clarity.

It is seen that the precursor based on damping rates perform satisfactorily and show linear dependencies only after the amplitude starts rising in the combustor. In other words, they were seen to have a performance comparable to the measure f used to construct the bifurcation diagrams. Further, it is seen that the decay rates fluctuate wildly and converge slowly, for regimes prior to the sharp amplitude rise. The precursor based on decay rates are thus seen to perform inadequately and show non-monotonic dependencies during regimes of combustion noise and the start of intermittency. This

is expected since an 'effective damping rate'—which is an average measure based on a linear analysis—cannot be defined for intermittent or chaotic signals that entail non-linear, time-localized dynamics. In the next subsection, we introduce measures that can characterize the intermittency in a measured signal and compare the capability of these measures with the traditional methods as precursors to combustion instability.

4.2 Recurrence quantification

4.2.1 Recurrence plots

The temporal features of the dynamics of a measured signal can be characterized by tracking the regularity of the trajectories using recurrence plots. Recurrence is a fundamental property of dynamical systems and recurrence plots allow one to visually identify the times at which the trajectory of the system visits roughly the same area in the phase space (Marwan *et al.*, 2007). The technique requires reconstruction of the mathematical phase space of evolution of the pressure fluctuations, the procedure for which is outlined in Chapter 3. In reconstructing an appropriate phase space, a knowledge of the appropriate embedding dimension d_0 and the optimum time lag τ_{opt} that is used to generate the delay vectors from the measured pressure time series (of length N_0) is necessary. A recurrence plot is constructed by computing the pairwise distances between points in the phase space. Then, a matrix of recurrences may be obtained as:

$$R_{ij} = \Theta(\epsilon - ||\boldsymbol{p'_i} - \boldsymbol{p'_j}||) \qquad i, j = 1, 2, ..., N_0 - d_0\tau_{opt} \tag{4.2}$$

where Θ is the Heaviside step function and ϵ is a threshold or the upper limit of the distance between a pair of points in the phase space to consider them as close or recurrent. The indices represent the various time instances when the distances are computed and the boldface represents the vector of coordinates in the phase space. The recurrence matrix is a symmetric matrix composed of zeros and ones and a recurrence plot is the 2D representation of this matrix as the trajectories evolve in time. The ones in the recurrence plot are marked with black points and represent those time instants when

the pairwise distances are less than the threshold ϵ. White points in the recurrence plot correspond to the zeros in the recurrence plot and correspond to those instants when the pairwise distances exceed the threshold.

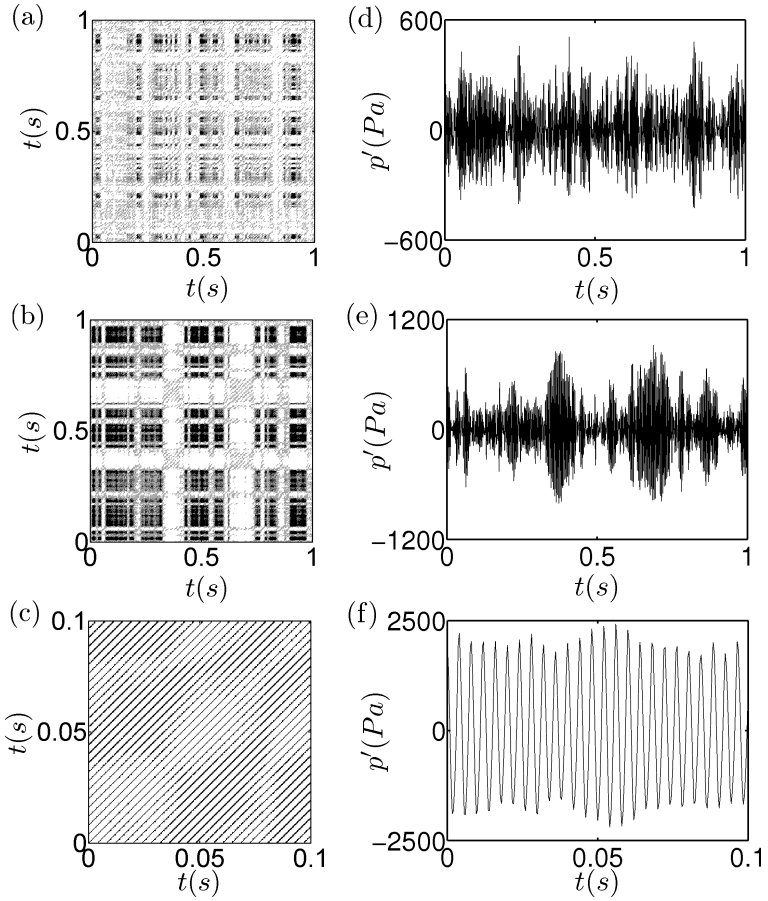

Figure 4.4: Recurrence plots and the corresponding unsteady pressure signals acquired during combustion noise (top row, $Re = 1.83 \times 10^4$), intermediate intermittent regime (middle row, $Re = 2.50 \times 10^4$) and combustion instability (bottom row, $Re = 2.78 \times 10^4$) from the bluff-body stabilized combustor. The threshold for the recurrence plot was chosen to be $\epsilon = \lambda/5$ where λ is the size of the attractor, defined as the maximum distance between pairs of points in the phase space. The black patches in the intermittent and chaotic oscillations correspond to regions of low amplitude pressure fluctuations relative to λ. The distance between the diagonal lines in (c) corresponds to the time period of oscillation during instability.

Figure 4.4 shows the recurrence plots drawn for the pressure signals acquired during (i) combustion noise, (ii) intermittent regime and (iii) combustion instability. The data was under-sampled to a frequency F_s of $2.5kHz$ and was embedded in a phase space of $d_0 = 10$ with an embedding delay $\tau_{opt} = 1ms$. The under-sampling was done to reduce the computational cost involved in obtaining the recurrence matrix. The recurrence plot for the chaotic combustion noise is seen to be grainy (Fig. 4.4(a)). This is to be expected since the dynamics is chaotic with little repeatability in the patterns. On

the other hand, the recurrence plot during combustion instability displays a pattern of diagonal lines indicating high repeatability (recurrence) in the dynamics (Fig. 4.4(c)). The time duration of the signal was chosen to be $0.1s$ to highlight the diagonal lines in the recurrence plot which would otherwise not be visible. The separation between the diagonal lines gives the fundamental time period of oscillation during combustion instability. The intermediate regime has a recurrence plot that consists of perforated black patches amidst white patches (Fig. 4.4(b)). The black patches represent the times when the system exhibits low amplitude chaotic oscillations and white patches represent the higher amplitude periodic bursts. This is a pattern typical of intermittent burst oscillations. The recurrence plots thus help visually identify the route to instability in turbulent combustors. The transition proceeds from chaos (combustion noise) to order (combustion instability) through an intermediate intermittent regime.

4.2.2 Precursors using recurrence quantification

Several statistical measures may be constructed through a recurrence quantification analysis of a measured signal that could serve as useful measures of intermittent oscillations. These measures can further be used as precursors to an impending instability because they vary in a smooth fashion as the operating conditions traverse the intermittent regime into conditions of combustion instability. By tracking the probability distribution of black points (or white points) in such plots, measures can be constructed that can distinguish amongst the dynamically different regimes of the combustor, the procedure for which is outlined in the next subsection.

In constructing the recurrence plots of Fig. 4.4, the threshold ϵ was a relative measure as it depended on the size of the attractor at that particular operating condition (Reynolds number). This enables one to understand the qualitative changes in the underlying dynamics in phase space. In order to obtain quantifiable precursors across different values of Reynolds number, the threshold needs to be held fixed at some suitable value. Fixing the threshold allows one to compare the values of the various statistical measures obtained using recurrence quantification as the control parameter is varied. In what follows, the fixed threshold value (say ϵ_0) was chosen to be slightly higher than the size of the attractor obtained at the lowest operational Reynolds number. It should be mentioned that the thresholds sizes are indicative of the Euclidean distances between

points in the phase space ($\sim \sqrt{d_0}|p'|$), and should not be confused with the amplitude levels in the combustor ($|p'|$).

A number of suitable markers that foretell an impending instability may be constructed by counting the number of black points in the recurrence plot. The density of black points in a recurrence plot measures the recurrence rate in the dynamics of the system and can be obtained as:

$$RR = \frac{1}{N_1^2} \sum_{i,j=1}^{N_1} R_{ij} \tag{4.3}$$

where $N_1 = N_0 - d_0 \tau_{opt} F_s$. R_{ij} is one for a black point and zero for a white point. The signal was sampled at a frequency F_s of $2.5kHz$ for $3s$ to give a value of N_0 of 7500 and was embedded in a phase space of $d_0 = 10$ with an embedding delay $\tau_{opt} = 1ms$. This density of points in the recurrence plot is seen to decrease on the approach of instability (Fig. 4.5(a)). This is expected since the number of black points in the recurrence plot would come down as instability is reached because the pairwise distances now exceed the threshold more often.

This decrease in the density of black points should then correspond to a decrease in the time spent by the system in aperiodic states which is measured by a quantity τ_0 (normalized with the time duration of evolution of the trajectory in phase space), defined as:

$$\tau_0 = \frac{1}{N_1} \frac{\sum_{v=1}^{N_1} vP(v)}{\sum_{v=1}^{N_1} P(v)} \tag{4.4}$$

with $P(v)$ being the frequency distribution of the vertical (horizontal) black lines of length v in the recurrence plot for a signal sampled at a frequency F_s. The quantity τ_0 also quantifies how long the system remains in a particular dynamical state (in this case, chaotic fluctuations). Hence we expect this quantity to tend towards 0 as the system transitions completely into periodic oscillations (see Fig. 4.5(b)). The value of τ_0 will be equal to one at conditions of combustion noise.

Finally, the Shannon entropy s of the signal can be obtained from the recurrence

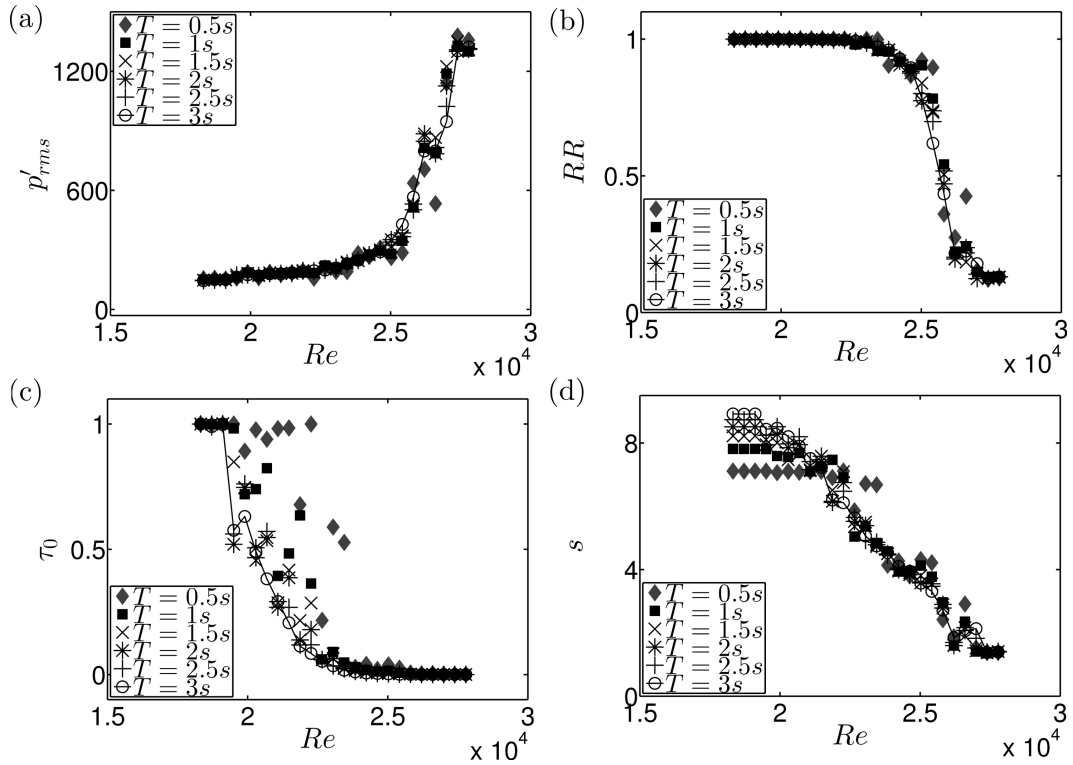

Figure 4.5: Performance of the statistical measures of intermittency obtained through recurrence quantification for pressure time traces sampled at $2.5kHz$ for $3s$. The measures plotted correspond to (a) the recurrence rate of dynamics (RR) which measure the density of points in the recurrence plot, (b) the average passage time spent by the dynamics in aperiodic fluctuations (τ_0), and (c) the entropy (s) of the diagonal length distribution. The threshold was chosen as $\epsilon_{0,bluff} = 1900Pa$ which are close to the size of the attractor ($\lambda_{bluff} = 1955.5Pa$) in the underlying phase space at the lowest measured Re.

plot using the expression:

$$s = \sum_{l=1}^{N_1} p(l) \log p(l) \tag{4.5}$$

where the probability that a diagonal line has length l, $p(l)$ is given by:

$$p(l) = \frac{P(l)}{\sum_{l=1}^{N_1} P(l)} \tag{4.6}$$

where $P(l)$ is the frequency distribution of the black diagonal lines of length l. Shannon entropy is a measure of the amount of order (disorder) in the system. We see that the Shannon entropy of the signal (s) tends towards zero at the onset of instability (Fig. 4.5(c)). A decrease in entropy indicates that the system is approaching a state of

regularity or there is an emergence of order out of chaos. This makes sense intuitively as we know that the recurrence plots for a periodic signal consists of black, parallel diagonal lines and that the oscillations correspond to an ordered state. Hence, we naturally expect the entropy to come down as operating conditions approach combustion instability.

The relative merits of these measures as early warning signals to instability were gauged by comparing their performance with the r.m.s. values of the pressure time series (Fig. 4.6(a)). The convergence of the measures with an increasing duration of data acquisition was also inspected to ensure that the precision of the measured quantities are increased. The converged measure represents its average value at the flow condition, as an ensemble average of the measure over many realizations should tend to an average measure obtained over large time durations. Since we do not have multiple realizations (pressure time traces) at the same operating condition, we have adopted this measure of convergence to infer that uncertainties in estimation of these average measures have been minimized.

The measure RR is seen to have inverse relationship with p'_{rms} and has good convergence as the time duration is increased from $T = 0.5s$ to $T = 3s$. However, we see that the variation in τ_0 and s starts much earlier than the regimes when amplitudes start rising in the combustor as indicated by p'_{rms}. These measures vary sooner as they quantify the time-localized statistics of the burst oscillation; for instance τ_0 measures the average duration between two successive bursts. The variability in the measures with the threshold size ϵ_0 is shown in Fig. 4.6. Among the precursor measures, τ_0 shows the largest variation as ϵ_0 is varied. However, the overall qualitative features are preserved even when the threshold is varied. These results indicate that a knowledge of the amplitude levels in the combustor during stable operation is desirable for the optimum performance of the precursors.

Although it is possible to define additional quantifiable precursors (see Marwan *et al.* (2002) for a detailed list of statistical measures constructed using recurrence plots), our purpose in this section was merely to illustrate the power of recurrence quantification in forewarning impending combustion instability. The reason why these precursors work is due to the presence of an intermittent regime of burst oscillations amidst chaotic combustion noise and ordered periodic oscillations. More generally, since these

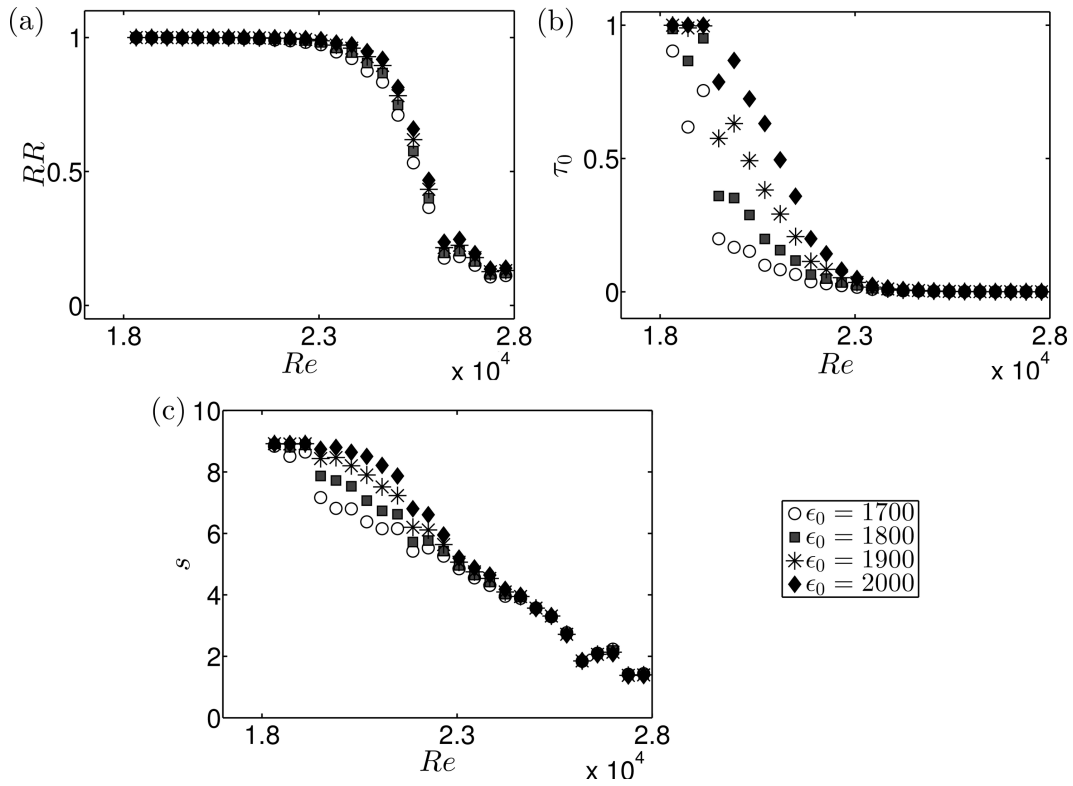

Figure 4.6: Variability in the statistical measures of intermittency for different threshold sizes ϵ_0 for the pressure time traces sampled at $2.5kHz$ for $3s$ at various Re. The measures plotted correspond to (a) the recurrence rate of dynamics (RR) which measure the density of points in the recurrence plot, (b) the average passage time spent by the dynamics in aperiodic fluctuations (τ_0), and (c) the entropy (s) of the diagonal length distribution.

measures only distinguish the passage of dynamics from a chaotic to an ordered state through intermittency, such precursors can possibly be used as early warning signals to an impending instability in a variety of turbulent flow systems encountering periodic oscillations.

4.3 Concluding remarks

The transition from combustion noise to combustion instability in turbulent combustors was always seen to be presaged by an intermittent regime composed of bursts of high-amplitude periodic pressure oscillations amidst regions of aperiodic, low-amplitude fluctuations. This gives an altogether different picture from what one would expect from a mean-field description of the phenomenon, wherein the transition happens from a fixed point to a limit cycle via a Hopf bifurcation. A mechanism was proposed which necessitates that on changing a system parameter, the transition to instability in com-

bustors must happen via the intermittent route, provided the underlying flow-field is turbulent.

A smooth and continuous measure to plot bifurcation diagrams for parameter variation in combustors with a turbulent flow-field can be obtained by counting the number of peaks in a measured signal above a predefined threshold. Hysteresis was observed for variations in the Reynolds number using this measure. Further, precursors to an impending instability can be obtained through recurrence quantification that can warn an operator of fielded systems sufficiently in advance, so that appropriate control action may be taken to prevent detrimental oscillations. These precursors are seen to detect and warn the onset of an oscillatory regime well in advance of other measures based on the sound levels in the combustor and effective damping rates. These measures act as effective precursors because they act as quantifiers of the intermittency in a measured signal.

It is quite possible that combustors in fielded systems can tolerate limit cycle oscillations, provided the amplitudes are within a reasonable range. The passive control methods available in the literature work by increasing the damping, or by modifying some design or flow features to suppress the instability amplitudes, and possibly improve stability margins. Hence, they fall under a different class of methods complementary to what is proposed herein. The methods described in this chapter warn the operator that oscillations are about to set in for further variations in an operating parameter. Armed with this knowledge, the decision lies with the operator whether to let the operating conditions cross over to regimes of limit cycle operation.

At present, there are no reliable measures to pre-determine the amplitudes of oscillation at the onset of instability in combustors. Employing passive control measures requires a knowledge of the amount of damping required to suppress the instability amplitudes when the oscillations set in whilst ensuring that the performance is not compromised. The technique presented here provide the operator with an alternative choice, one which is aimed at avoiding a region of unstable operation altogether.

In the next chapter, we shall discuss a simple phenomenological model that describes the intermittent features seen in experiments based on the proposed mechanism.

CHAPTER 5

A phenomenological model for intermittency

Based on the insights gained from the experiments, a phenomenological model is introduced in this chapter to describe the intermittency route to combustion instability. It is adapted from the vortex impingement model of Matveev and Culick (2003). Intermittency arises through a variability in the travel times of the vortices to reach and impact the bluff-body starting from the dump plane. The chapter ends with a qualitative comparison of the precursor measures obtained from the model with the experiments.

5.1 Inputs from experiments

Typically, for the kinds of flow-fields established in combustors, the instability becomes hydrodynamically coupled (Poinsot *et al.*, 1987; Yu *et al.*, 1991). The formation of large-scale coherent vortices at the onset of combustion instability has been reported by a number of authors in the literature (Parker *et al.*, 1979; Pitz and Daily, 1983; Hegde *et al.*, 1983; Poinsot *et al.*, 1987; Yu *et al.*, 1991). Shown in Fig. 5.1 are a sequence of line-of-sight integrated instantaneous flame images acquired during combustion instability. The image sequence shows a vortex forming in the dump plane of the combustor during the compression phase, growing as it convects downstream and impinging on the bluff-body; resulting in vigorous mixing and heat release (Schadow and Gutmark, 1992; Coats, 1996). The flame is then pushed back towards the dump plane in the rarefaction phase of the pressure signal and the cycle renews.

The spectra of pressure oscillations as well as that of the intensity signal as measured by a PMT during combustion instability reveal a sharp frequency at the subharmonic of the instability frequency (Fig. 5.2). The dominant frequency is at $f_a = 244.9Hz$ and the subharmonic is at $f_v = 123.1Hz$. The spectral bin size was $\Delta f = 0.12Hz$. The mean temperature of the gas near the wall as measured by a thermocouple located $50mm$ from the backward facing step was $T_0 = (1196 \pm 30)K$; which gives the quarter-wave mode at $(247.6 \pm 4)Hz$. The sub-harmonic frequency is thus probably hydrodynamic

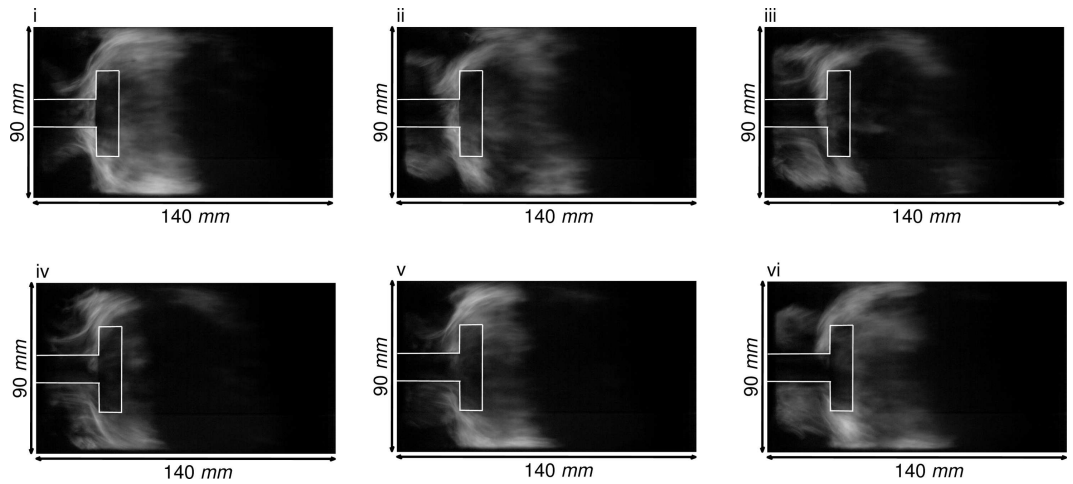

Figure 5.1: A sequence of line-of-sight integrated, instantaneous CH^* chemiluminescence acquired during combustion instability ($Re = 3.17 \times 10^4$,$\phi = 0.62$). The time delay between successive images is $1ms$. The outline of the bluff-body is provided for the ease of visualization.

and lies roughly at half the frequency corresponding to the quarter-wave mode at the operating condition ($Re = 3.17 \times 10^4$, $\phi = 0.62$).

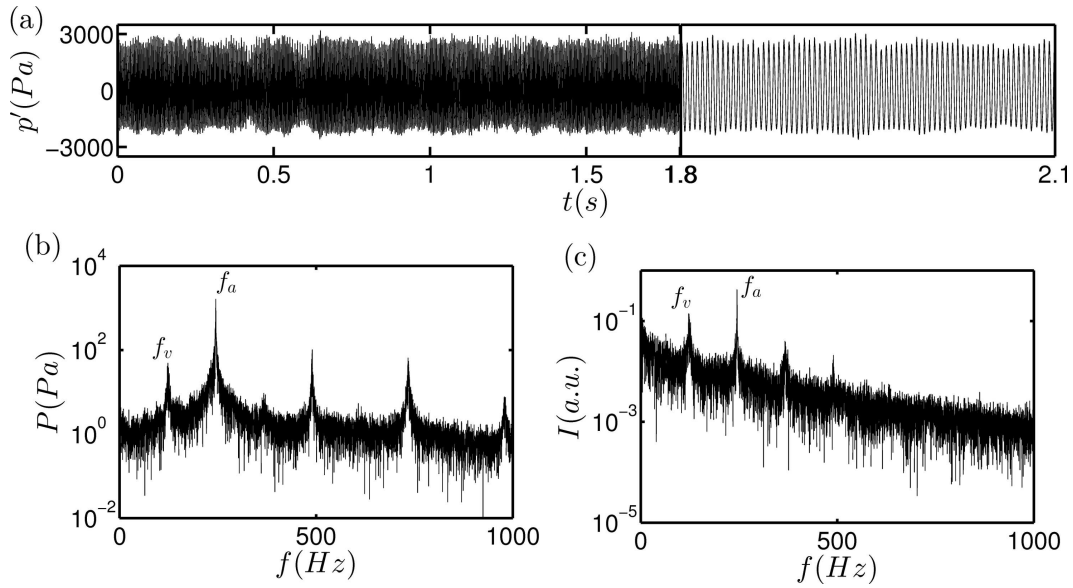

Figure 5.2: Evidence for sub-harmonic forcing during combustion instability. (a) The pressure signal and (b) the corresponding amplitude spectra obtained through a FFT ($Re = 3.17 \times 10^4$, $\phi = 0.62$). (c) The spectra of the CH^* chemiluminescence intensity at the same operating condition near the bluff-body.

If the mechanism proposed in Chapter 4 is correct, the presence of intermittent burst states are also a result of the coupling of the hydrodynamics with the acoustics. The model that we use to describe intermittency must therefore necessarily incorporate the coupled two-way interactions amongst the hydrodynamics and the acoustics of the

confinement.

5.2 Model description

We consider a bluff-body stabilized backward facing step combustor of length L operating at turbulent Reynolds numbers with an incoming flow velocity of U_0 (Fig. 5.3). Vortices are formed at the dump plane that carry the flame and convect downstream to impinge on the bluff-body located at a distance L_c from the backward facing step of step height d. This impingement leads to intense fine scale mixing and heat release. When the heat release rate by vortex impingement on the bluff-body happens in phase with the pressure fluctuations inside the combustion chamber, the pressure fluctuations are amplified. The acoustic field then in turn modifies the velocity at the dump plane resulting in a periodic heat release rate through vortex impingement. This creates a positive feedback loop between the hydrodynamics and the confinement acoustics and the oscillations become self-sustained, resulting in combustion instability.

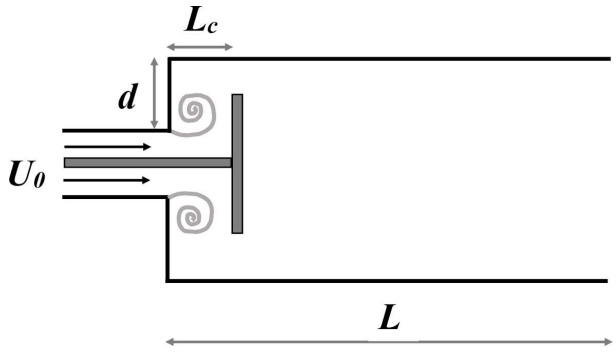

Figure 5.3: Schematic of the bluff-body stabilized combustor. The length of the combustor is L and L_c refers to the location of the bluff-body in the combustion chamber. The reactants flow into the combustor through the burner at a mean flow velocity U_0 and d is the height of the backward facing step.

The typical Mach numbers in combustion chambers are low due to the high temperatures. Hence, the contributions of mean flow velocity can safely be ignored in the governing equations for the acoustic oscillations which after neglecting temperature

gradients and viscous effects may be written as (Annaswamy *et al.*, 1997):

$$\frac{\partial u'}{\partial t} + \frac{1}{\rho_0}\frac{\partial p'}{\partial x} = 0, \tag{5.1a}$$

$$\frac{\partial p'}{\partial t} + \gamma p_0 \frac{\partial u'}{\partial x} = (\gamma - 1)\dot{Q} \tag{5.1b}$$

with the heat release rate $\dot{Q}$ modelled as in (Matveev and Culick, 2003):

$$\dot{Q} = \beta \sum_j \Gamma_j \delta(t - t_j)\delta(x - L_c) \tag{5.2}$$

Here t_j refers to the instance of impingement of the j^{th} vortex that has a circulation Γ_j. The term β is a suitable coefficient that relates the vortex impingement to the heat release rate. Since the wavelength of sound propagation is comparable to the combustion chamber length, the acoustic field can be treated as one-dimensional and the geometry is approximated as a closed-open duct.

The pressure and the velocity fluctuations inside the duct can then be formally expanded in terms of basis functions (Zinn and Lores, 1971) that satisfy the boundary conditions as follows:

$$p'(x,t) = -p_0 \sum_{n=1}^{N} \frac{\dot{\eta_n}(t)}{\omega_n} \cos k_n x, \tag{5.3a}$$

$$u'(x,t) = \frac{c_0}{\gamma} \sum_{n=1}^{N} \eta_n(t) \sin k_n x \tag{5.3b}$$

with $p_0 = \rho_0 c_0^2/\gamma$, $k_n = (2n-1)\pi/2L$ and $\omega_n = c_0 k_n$. These expansions satisfy Eq. (1) and the boundary conditions ($u'(x=0) = 0$ and $p'(x=L) = 0$) trivially. Substituting Eq. (4) into Eq. (2) and performing a projection over the basis functions (Balasubramanian and Sujith, 2008*b*) results in the following set of second-order ordinary differential equations.

$$\ddot{\eta_n} + \xi_n \dot{\eta_n} + \omega_n^2 \eta_n = c\omega_n \cos k_n L_c \sum_j \Gamma_j \delta(t - t_j) \tag{5.4}$$

where $c = -2(-1)\beta/Lp_0$. In the equation, the damping term $\xi_n \dot{\eta_n}$ was introduced to model the acoustic losses with the mode dependent damping defined as:

$$\frac{\xi_n}{\xi_1} = \frac{\omega_n}{\omega_1} = (2n-1)^2 \tag{5.5}$$

where ξ_1 is the damping rate of the combustion chamber which can be measured experimentally. The damping term ξ_n represents the end losses from the chamber (Sterling and Zukoski, 1991). The jump conditions are obtained by integrating Eq. (5) once and imposing continuity of the solution. These jump conditions for acoustics at the moment of vortex impingement may be written as:

$$\eta_n^{t_j^+} = \eta_n^{t_j^-}, \tag{5.6a}$$

$$\dot{\eta_n}^{t_j^+} = \dot{\eta_n}^{t_j^-} + c\Gamma_j \omega_n \cos k_n L_c \tag{5.6b}$$

The convection of the vortices from the dump plane are modelled as:

$$\frac{dx_j}{dt} = \alpha U_0 + u'(x,t) \tag{5.7}$$

Here, α is a coefficient that describes the fraction of the mean velocity (U_0) at which the vortices convect in the combustion chamber. To account for the variations in the size of the vortices and the accompanying differences in their convection velocities, a Gaussian distribution $\mathcal{N}(\alpha_0, \sigma_\alpha)$ is assigned to α centered around the fraction α_0 corresponding to the mean convection velocities in the following manner:

$$\alpha = \alpha_0 + \sigma_\alpha \phi \tag{5.8}$$

where $\phi = \mathcal{N}(0,1)$, and σ_α is the standard deviation. The choice of a Gaussian distribution is motivated by observations on turbulent velocity measurements. The distribution

of α thus represents a distribution of the vortex sizes or of the vortex convection velocities and can be thought of as modelling the broadband nature of turbulence. The presence of the damping term ensures that the contributions due to turbulence are more dominant at low frequencies as observed in turbulent velocity measurements. Following (Matveev and Culick, 2003) the variation in circulation at the dump plane is given by the expression:

$$\frac{d\Gamma}{dt} = \frac{u_{sep}^2}{2} \tag{5.9}$$

with $u_{sep} = U_0 + u'(0,t)$. When this value of circulation exceeds a critical value $\Gamma_{crit} = u_{sep}d/2St$, a new vortex is formed at the step (Matveev and Culick, 2003) which then convects downstream according to Eq. 5.7. Here, St is the Strouhal number for the backward facing step of step height d. It is assumed that the circulation is conserved as the vortex convects downstream and impinges on the bluff-body.

5.3 Preliminary results

Simulations were performed using the model to obtain a qualitative match with the phenomena obtained in combustors operating at turbulent flow conditions. The parameters, where possible, were chosen to match those corresponding to the experiments described in the previous chapters. The value of the parameter α was chosen as 0.2 with $\sigma_\alpha = 0.05$ which corresponds to a turbulent intensity of 5% at the dump plane. The Strouhal number St was chosen as 0.29 based on experimental observations in backward facing step geometries (Bhattacharjee *et al.*, 1986). The value of the jump coefficient c was chosen as 6×10^{-3} to obtain a qualitative match between the pressure amplitudes from the simulation and experiments. The damping coefficient $c_1 = 29s^{-1}$ was obtained by measuring the decay rates of pressure oscillations in the experiments when the fuel was cut-off. Equations were integrated using a 4^{th} order Runge-Kutta scheme with a time step $dt = 5 \times 10^{-5}$ for 100001 time steps and convergence was ensured by choosing $N = 10$ basis functions. The acoustic pressure was measured at $x = 0.09$ in line with the position of the transducer used in the experiments ($90mm$ from the backward facing step).

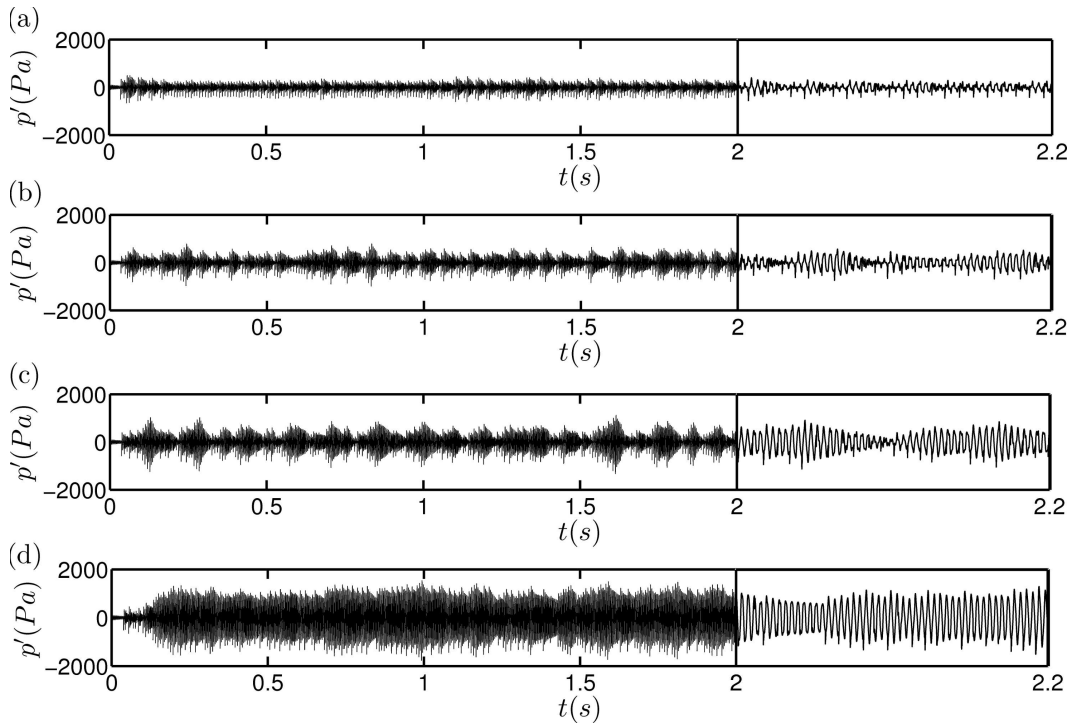

Figure 5.4: Results from the model for (a) $U_0 = 8.0m/s$, (b) $U_0 = 8.4m/s$, (c) $U_0 = 8.7m/s$ and (d) $U_0 = 9.0m/s$. As the flow velocity increases, the dynamics transition from intermittent regime towards self-sustained combustion instability. The duration of such intermittent bursts increase as the system approaches instability. The transient response is also visible in the signal. The values of the various parameters are $c_0 = 700m/s$, $\gamma = 1.4$, $L_c = 0.05$, $L = 0.7$, $d = 0.025$, $c_1 = 29s^{-1}$. The initial conditions correspond to $\eta_1 = 0.001$, $\eta_{i1} = 0$, $\dot{;}_i = 0$ with $N = 10$ basis functions.

The results from the model for various flow velocities leading up to combustion instability are shown in Fig. 5.4. As the flow velocity increases, the pressure signals start displaying intermittent bursts as seen in the experiments (Fig. 5.4(b,c)). The duration of these periodic bursts increases with increases in flow velocity until eventually the system transitions to large-amplitude oscillations. The results are in qualitative agreement with the experimental results. These bursts of periodic oscillations emerge from the background fluctuations in a near-random manner. This was seen to correspond directly to the parameter σ_α in the model. In other words, small variations in the size of the vortices lead to small variations in their convection velocities. Therefore, these vortices impinge on the bluff-body at slightly different times. It is this variation that results in the almost random appearance of these bursts in the pressure signals. The modulation in the amplitudes of pressure oscillations at combustion instability also results from the small variations in vortex impingement times.

The amplitude spectrum of the pressure oscillations obtained from the model prior

to instability is shown in Fig. 5.5(a). The spectrum reveals the presence of a frequency around $250Hz$. This is the acoustic frequency of the duct (f_a) as it remains invariant with flow velocities (see Fig. 5.5(b)). The spectra also show the presence of another dominant frequency (f_v) whose higher harmonic slowly approaches the acoustic frequency and finally locks-on to the acoustics. This sub-harmonic frequency corresponds to the frequency of vortex impingement on the bluff-body. Since the frequency of impingement varies linearly with flow velocity (Fig. 5.5b), when the flow velocity U_0 is such that the vortex impingement happens at the sub-harmonic frequency of the fundamental acoustic frequency, the oscillations become self-sustained and the amplitudes rise sharply. The presence of this sub-harmonic frequency due to hydrodynamics around $125Hz$ is clearly visible in the experimental data shown in Fig. 5.2(b,c). The peak seen at $500Hz$ in the experiments is absent in the simulation (Fig. 5.5(a)) as we have assumed a closed-open geometry for the combustor. However, the experimental mode shape obtained from the combustor using pressure transducers mounted along the length of the combustion chamber is close to a quarter-wave mode and hence we approximate the solution using quarter-wave modes.

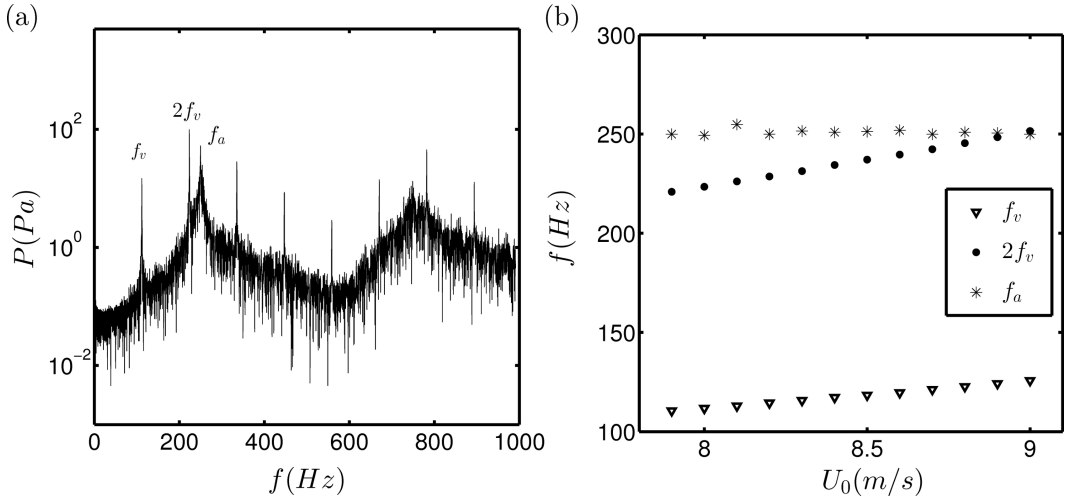

Figure 5.5: (a) Amplitude spectrum of the signals for $U_0 = 8.0m/s$. (b) As the mean flow velocity increases, the hydrodynamic frequency f_{2v} approach the fundamental acoustic frequency ($f_a \sim 250Hz$). At the onset of instability, the acoustic oscillator receives a forcing from the hydrodynamic oscillator at its sub-harmonic frequency ($f_v \sim 125Hz$) and there is a flow acoustic lock-on inside the combustor which results in large amplitude combustion instability.

The intermittent oscillations will not be observed if we set $\sigma_\alpha = 0$. In this case, the effects of vortex impingement are either stabilizing or destabilizing depending on the frequency of impingement. When the vortex convection velocities are distributed

($\sigma_\alpha \neq 0$), occasionally the convection velocity of a vortex is such that its impingement frequency is close to the sub-harmonic of the fundamental acoustic frequency. This results in a favourable phase relationship between the heat released through impingement and the acoustic pressure oscillations and leads to the formation of an intermittent burst in the signal. The distribution for α was chosen as a Gaussian to emulate the near-random appearance of bursts in experimental data. Such distributions of α may be refined using PIV measurements to obtain better quantitative comparisons. The intermittent feature in the dynamics was seen to be robust to different choices of the parameter α.

Systematic variation of operating conditions for experiments on bluff-body and backward-facing step combustors in turbulent flow-fields from stable to unstable operation indicate the presence of a lock-on phenomena between the vortex shedding and duct acoustics, resulting in the excitation of high-amplitude discrete tones at the onset of combustion instability (Chakravarthy *et al.*, 2007*b*,*a*). It is also known from measurements of the response of flames to flow disturbances, that flames are capable of driving the subharmonics of the fundamental acoustic frequency—in addition to the fundamental (B. D. Bellows, 2006). Such subharmonic peaks were also observed in the spectra of the CH^* emissions measured by a photomultiplier (Fig. 5.2). The model thus introduces a simple approach to interpreting the dynamics observed in combustors operating in a turbulent flow-field.

5.4 Precursors to combustion instability

In the previous chapter, several precursors to an impending combustion instability were defined by quantifying the intermittency in experimental pressure measurements. One of these precursors involved tracking repeating patterns or recurrences in the dynamics of pressure oscillations. These recurrences are quantified using binary distance matrices depending on whether the distances between pairs of points in the reconstructed phase space (of dimension d and embedding delay τ) exceed a fixed threshold (Marwan *et al.*, 2007). A plot of this matrix $R_{ij(N\times N)}$ on a 2D plane is called a recurrence plot (Fig. 5.6) wherein the black points correspond to those time instants when the distances fall below the threshold. Precursors are constructed by defining measures based on the statistical

properties of the black points in the recurrence plots.

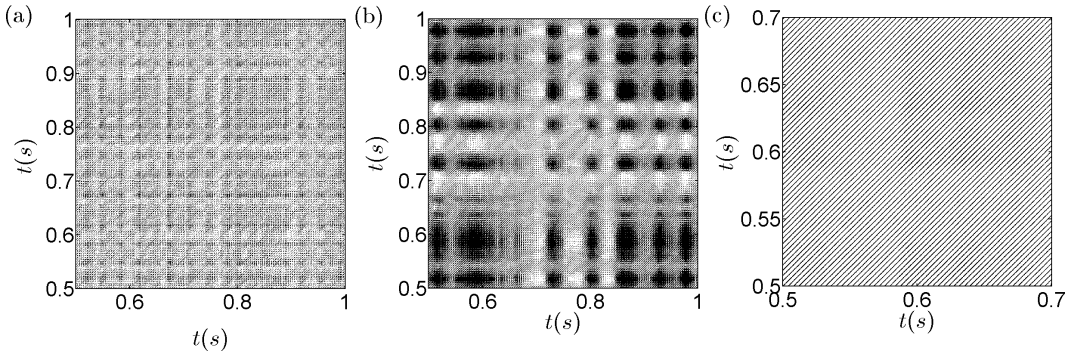

Figure 5.6: Recurrence plots from the model for the pressure signals at (a) $U_0 = 7.9m/s$, (b) $U_0 = 8.4m/s$, and (c) $U_0 = 9.0m/s$. The threshold was defined as $\epsilon = \lambda/5$ where λ is the size of the underlying attractor in phase space defined as the maximum distance between pairs of points in phase space at the flow condition. The signal was embedded in a dimension $d_0 = 8$ with embedding delay $\tau_{opt} = 1ms$.

Shown in Fig. 5.6 are the recurrence plots obtained from the model corresponding to chaotic, intermittent and periodic dynamics respectively. The recurrence plot during the chaotic regime is grainy whereas during instability they are composed of parallel diagonal lines as expected and observed in experiments. The recurrence plot during intermittency also compares well with the experiments and consists of black rectangular patches that appear in a near-random fashion. The precursors defined earlier were computed for the various flow velocities from stable operation leading to combustion instability and the results are shown in Fig. 5.7. They are seen to forewarn the transition to instability well before the amplitudes start to rise (Fig. 5.7(a)) just as in experiments.

An alternate way of quantifying the intermittency is by measuring the loss of chaos in the measured pressure signals. Shown in Fig. 5.8 are the results from the model on applying the 0-1 test for chaos (Gottwald and Melbourne, 2004) on pressure signals obtained for various inlet flow velocities. The model shows that the no lock-in regime is chaotic and that there is a gradual loss of this chaos as operating conditions approach instability. The results obtained from the model compare well with the observed trend in experiments which show that the regime of stable operation classified as combustion noise is deterministic and chaotic. The model is thus seen to capture the mechanisms of onset of combustion instability; intermittency presages combustion instability in a combustor with a turbulent flow-field and quantifying this intermittency enables precursors to be constructed that forewarn instability.

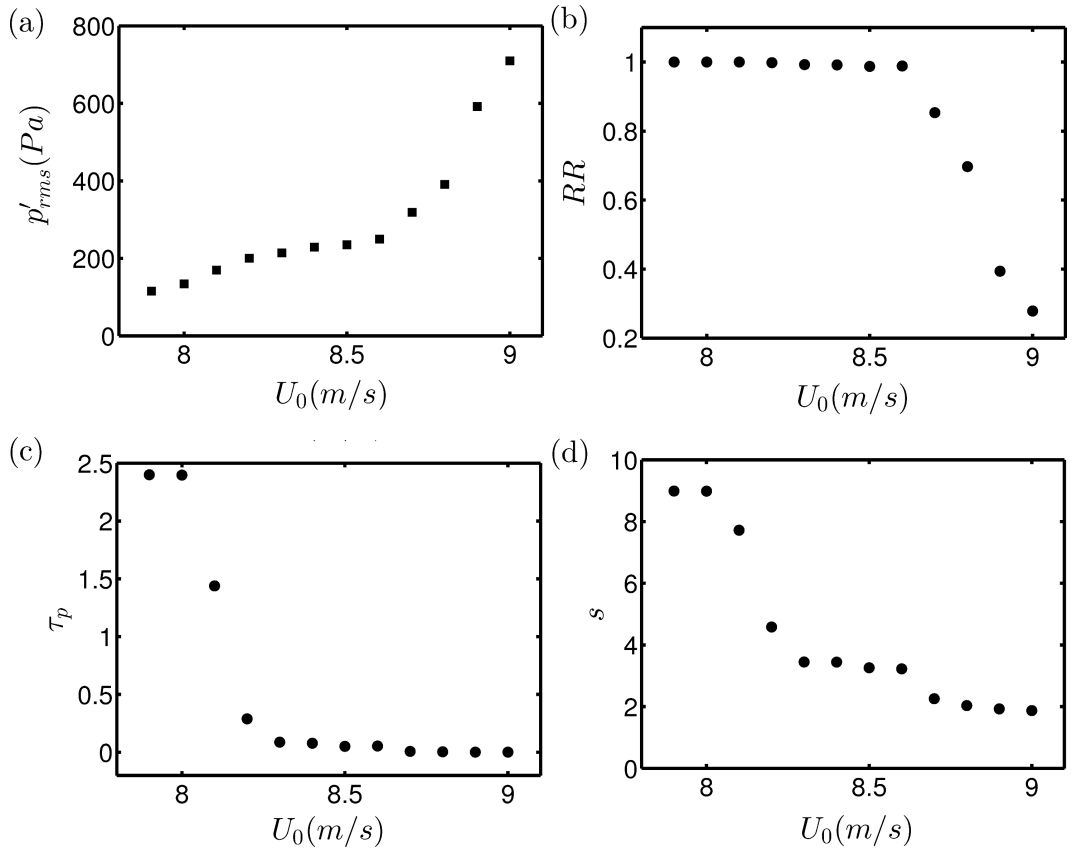

Figure 5.7: Variation of (a) the pressure amplitude levels (p_{rms}) and precursors to combustion instability obtained from the model through statistical recurrence quantification: (b) The recurrence rate RR, (c) entropy s and, (d) average passage time τ_p. These precursors fall at independent rates well in advance of the actual transition to instability. The threshold was kept fixed at a value $\epsilon = 3000$. The behaviour of these precursors are comparable to those obtained from the experimental data from the bluff-body combustor.

5.5 Concluding remarks

A simple phenomenological model was described to understand the onset of instability in combustors operating in a turbulent flow environment. The phenomenon of intermittent burst oscillations observed in such combustors and the subsequent transition to combustion instability was qualitatively reproduced using the model. The instability can be understood as a lock-on mechanism or synchronization between the acoustic oscillator and the hydrodynamic oscillator. Comparison of the spectra obtained from the experiments and the model shows that a subharmonic forcing of the acoustic field in the combustion chamber by the hydrodynamics is responsible for combustion instability.

The various techniques that forewarn combustion instability from experimental measurements were applied to the model to understand the effectiveness of the model in

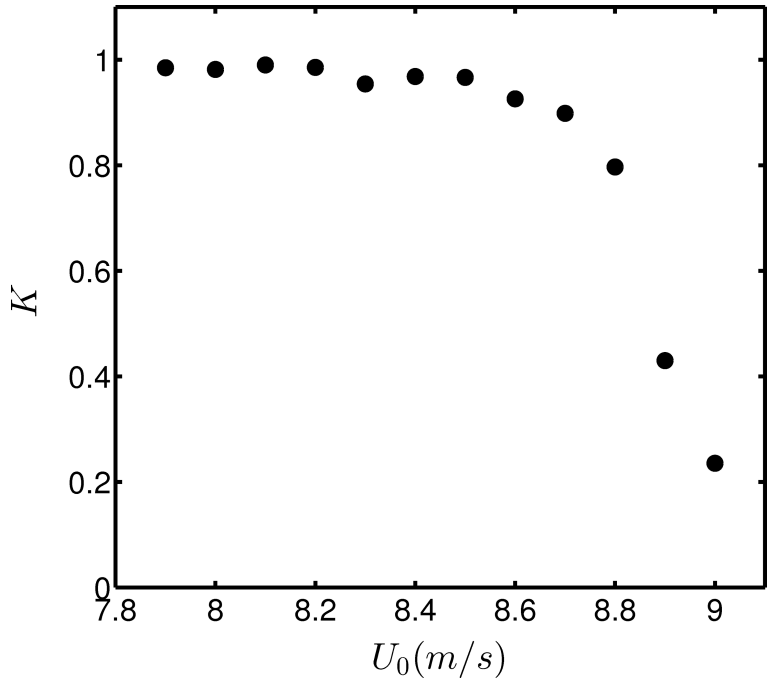

Figure 5.8: Variation of the measure based on the 0-1 test for chaos (K) when applied to pressure fluctuations from the model, as the mean flow velocities are increased ($7.9 - 9.0m/s$) towards combustion instability. The results are comparable with the experimental data.

describing the physics of precursors. It was seen that the time signals obtained from the model show the loss of chaos seen in experiments and by quantifying intermittency is able to warn the onset of combustion instability well in advance.

CHAPTER 6

Instability as a loss of multifractality

As we have seen so far, the dynamic processes happening inside a combustion chamber involve the coupled nonlinear processes which cannot be described by simple linear techniques. In this chapter, we shall introduce the framework of fractals and multifractals in order to tackle this complexity. Using a technique known as multifractal detrended fluctuation analysis, the deviations of the central moments of measured fluctuations with time are computed, which can directly be related to the fractal dimension of the time signal. It is shown that combustion noise is multifractal and that the onset of combustion instability results in a loss of this multifractality. The rate of variation of central moments decrease gradually towards zero as instability is approached, which can be used as yet another early warning signal to impending combustion instability.

6.1 Background

The term ‘fractal’ is used to describe objects that have a fractional dimension (Mandelbrot 1982). Whereas classical Euclidean geometry deals with smooth objects that have integer dimensions, structures in nature often tend to be fractals because they are wrinkly at all levels of magnification. Measures such as length, area or volume cannot be defined for such objects since they depend on the scale of measurement. For instance, the length of a fractal curve increases when the ruler is made smaller because additional details are now revealed. A logarithmic plot of the measured length of the curve against the length of the ruler for such a curve would then show an inverse power-law; i.e., a straight line with a negative slope. This slope, which is a number between one and two, is referred to as the ‘fractal dimension’ of the curve. Thus, we see that such curves occupy more space than a straight line which scales as the length of the ruler, but less space than a square which scales as the square of the length of the ruler.

The concept of fractals can also be used to describe complex dynamics that results in fluctuations spread over multiple orders of temporal magnitude. A fractal process is

characterized by a broad-band power spectrum with an inverse power-law, known more popularly as the $1/f$ spectrum (Montroll and Schlesinger, 1982; Schlesinger, 1987) since there is here an inverse relationship between frequency and power. Similar to a fractal curve, a fractal time signal also has a dimension between one and two. A fractal time series also displays a property known as 'scale invariance', which means that features of the signal look the same on many different scales of observation (seconds, minutes etc.). Mathematically, for a fractal time signal, $p(ct) = p(t)/c^H$ for some scaling c and a constant H. Scale invariance thus relates the time series across multiple time scales. Such a dependence on multiple time scales results in a broad profile of responses in the amplitude spectrum representative of details that are present at these time scales. On the contrary, if the process can adequately be represented in terms of one or a few discrete time scales, then the signal would have an amplitude spectrum with discrete, narrow peaks. In the next subsection, we will show how the presence of fractality is related to the memory of a time signal.

6.1.1 Statistical description of a time signal

Statistical analysis of time signals involve obtaining the distribution of their fluctuations (Gaussian, Poisson, Levy etc.) or representing this distribution in terms of representative measures computed around the most likely measurement value (central moments). Fluctuations that are fractals, but appear noise-like, differ from noise in that they do not satisfy the statistics of classical random variables. Whereas the central moments of a random variable are bounded in time, the central moments of a fractal signal diverge with time at least over a short range (Mandelbrot 1974). This can happen—for instance—when the measurement values represent variations both in time and space, which makes the signal non-stationary. A signal is non-stationary, if the central moments vary with time, or in other words, there is a variation in the underlying distribution of data values. As an example, unsteady pressure values acquired during confined combustion in a convecting flow-field are non-stationary, since the pressure measurement at any location at a given instant depends not only on pressure values at previous instants, but also on the pressure values at other locations in the flow-field.

In the description of non-stationary time signals, classical measures such as mean or variance are not very useful since they vary with time Instead, they are character-

ized by examining how the moments depend on the time interval over which they are evaluated. For instance, the dependency of the standard deviation of the time signal on time interval is encapsulated in a parameter called the Hurst exponent H (Hurst 1951). It measures the amount of correlation or the memory in a time series and is related to the fractal dimension D of the time series as $D = 2 - H$ (Basingthwaighte *et al.*, 1994). The concept of structure functions introduced by Kolmogorov (Kolmogorov, 1941; Frisch, 1995) is a generalized version of this idea, which explores scaling relationships between the variations in the moments of measured fluctuations and the time interval of measurement.

A time series is called persistent (anti-correlated) if a large value is typically (i.e., with high statistical preference) followed by a large value and a small value is followed by a small value (Kantelhardt, 2011). In other words, the signal retains a memory of what happened in the previous time step and has an increased probability of the next step being in the same direction—such signals have a trend. For a persistent signal, the Hurst exponent H lies between 0.5 and 1 and the strength of the trend increases as H approaches one. An anti-persistent (correlated) time series, on the other hand, is one in which a large value is typically followed by a small value, and a small value is followed by a large value. Such signals have a tendency to revert to its mean value. For anti-persistent signals, values of H lie between 0 and 0.5. The strength of mean reversion increases as H approaches zero. For time signals that are persistent or anti-persistent, fractal scaling law holds in at least a limited range of scales (Kantelhardt, 2011). For an uncorrelated time series, the Hurst exponent is 0.5. This is expected, since the variance of fluctuations in a memory-less diffusion process should scale linearly with time.

The Hurst exponent also determines the scaling properties of the fractal time series. If $p(t)$ is a fractal time signal with Hurst exponent H, then $p(ct) = p(t)/c^H$ is another fractal signal with the same statistics (West *et al.*, 2003). Algorithms that compute the Hurst exponent are mostly based on this scaling property. This scaling behaviour typically has an upper and a lower cut-off that is dependent on the system dynamics. Detrended fluctuation analysis (DFA) (Peng *et al.*, 1994) provides an easy approach to characterize fractality in a given time series data. Through an evaluation of the structure functions, correlations in the data are sought for by computing the Hurst exponent which can then be related to the fractal dimension of the time series.

6.1.2 Multifractality and multiplicative processes

Many time signals exhibit a complex scaling behaviour that cannot be accounted for by a single fractal dimension. A full description of the scaling in such signals involves multiple generalized Hurst exponents, resulting in interwoven subsets of varying fractal dimension (varying Hurst exponents) producing what is termed a 'multifractal' behaviour (Frisch and Parisi, 1985). In other words, fluctuations in a time signal that have different amplitudes follow different scaling rules. The method of DFA can be expanded to explore multifractality in a time signal and the technique is called multifractal detrended fluctuation analysis (Kantelhardt *et al.*, 2001, 2002). The procedure involves computing generalized Hurst exponents that describe the scaling of central moments for various negative as well as positive orders of the moments (q) that have been appropriately scaled. For instance, standard deviation has an order of two and its scaling with time interval gives the Hurst exponent. For a multifractal signal, the generalized Hurst exponents would have different values for different orders of the moments. Through a Legendre transform, this variation in generalized Hurst exponents at different orders can alternately be represented as a spectrum of singularities $f(\alpha)$, in terms of the new variable α which is conjugate to q. A plot of $f(\alpha)$ for various values of α is termed the multifractal spectrum, the width of which provides a measure of the multifractality in the signal (see Appendix B for details on implementation). An excellent description of multifractal processes may be found in Paladin and Vulpiani (1987).

The presence of multifractality is an indication that there are multiplicative processes involved in the transfer of energy across various time scales (Sreenivasan, 1991). Provided one accepts Taylor's frozen flow hypothesis (Taylor, 1938), the argument can be extended to hold for energy transfer across various spatial scales as well. The energy transfer at turbulent flow conditions involve a multiplicative Richardson's cascade (Richardson, 1922) in the inertial subrange from the integral scale down to Kolmogorov scale. As a consequence of this cascade, we should expect the multifractality to persist even in the presence of heat addition. However, the onset of combustion instability transforms the dynamics from one characterized by a multiplicity of scales to one dominated by a few discrete time scales associated with the formation of large-scale coherent structures in the flow field. It remains an interesting problem to identify how the interaction of turbulence with the acoustic field of a confinement (augmented by

heat release) transforms such an energy transfer across multiple time-scales to transfers that are dominated by a few time-scales. This can happen—for instance—through an inverse cascade (Kraichnan, 1967), wherein the energy of the smaller scales gets transferred to progressively larger scales. The formation of large-scale coherent structures during combustion instability possibly hints at the presence of such an inverse cascade co-existing simultaneously with the usual direct cascade that dissipates energy at Kolmogorov scales.

6.2 Results

The pressure measurements acquired from the combustor during stable operation and after the onset of combustion instability are shown in Fig. 6.1. The fluctuations prior to instability (Fig. 6.1(a)) are seemingly random and display an amplitude spectrum which is boradband (Fig. 6.1(c)). This has traditionally been classified as combustion noise in the literature. After the onset, the amplitude spectrum has sharp, discrete peaks (Fig. 6.1(d)) distinctive of combustion instability. The amplitudes of these oscillations are fairly high compared to combustion noise suggesting an underlying lock-in mechanism. Such a lock-in may happen for instance between the hydrodynamic fluctuations associated with periodic vortex formation and the fluctuations of the acoustics in the confinement. It should be mentioned that although the spectrum of the signal prior to instability appears to have a shallow peak near the instability frequency, no information can be gleaned as to how close the operating conditions are to combustion instability, or which of the many frequencies that have comparable peaks in the spectrum would be the dominant frequency at instability. Therefore, the fractal properties of signals are sought to obtain precursors to combustion instability, by computing the Hurst exponents.

In order to demonstrate the utility of Hurst exponent in identifying the dynamics, a comparison is made of three different time series data; (i) Gaussian white noise, (ii) combustion noise acquired from a bluff-body stabilized configuration ($\phi = 1.1$, $Re = 1.83 \times 10^4$), and (iii) synthetic periodic data. Synthetic periodic data along with Gaussian white noise represent the limiting cases on the values of Hurst exponent for an anti-persistent (correlated) signal. The instability frequency for the data presented at combustion instability (Fig. 6.1(b)) was $249Hz$. Hence, the time scales for the compu-

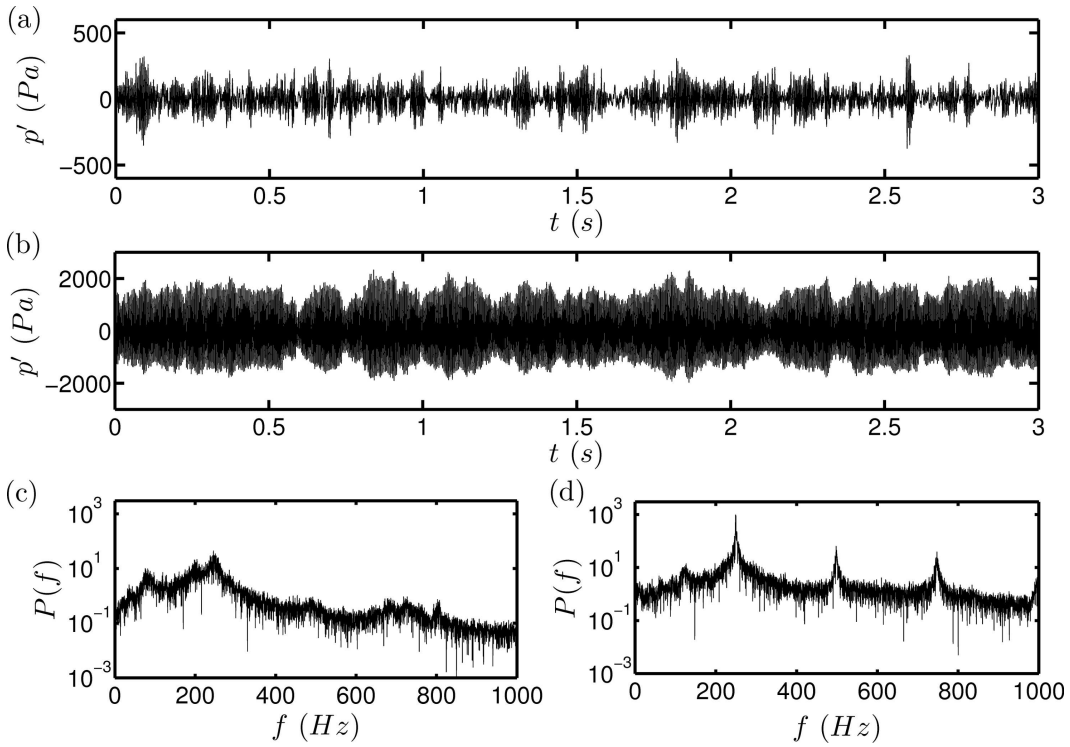

Figure 6.1: Unsteady pressure signals acquired from the bluff-body stabilized configuration: (a) $\phi = 1.1$, $Re = 1.8 \times 10^4$, (b) $\phi = 0.7$,$Re = 2.8 \times 10^4$, showing transition from combustion noise to combustion instability. Low amplitude, aperiodic pressure fluctuations get transformed to high amplitude, coherent oscillations on increasing Re. There is a transition in the frequency spectrum from (c) a broad profile with shallow peaks to (d) a spectrum with sharp peaks. The bin size of frequency in calculating the FFT was $0.3Hz$.

tation of Hurst exponent was varied between $8-16ms$ which correspond approximately to 2-4 cycles of oscillations at combustion instability. For the sake of comparison, the frequency of the synthetic periodic data was chosen as $250Hz$ so as to be in the vicinity of the dominant frequency of the data presented at combustion instability.

The Hurst exponents were estimated for the four time signals from the variation of the structure functions (F_w^q) at different time scales of measurement (w) (shown in Fig. 6.2). White noise has a Hurst exponent of 0.5, characteristic of a diffusive Brownian process. This is because the variance scales linearly with time for white noise. Hence, the variation of the standard deviation with time, which is also the Hurst exponent, would have a slope of 0.5 when plotted on a logarithmic scale. The periodic data has a slope close to zero because the variance of the fluctuations must necessarily be bounded and remain constant over a time period. The slope of the combustion noise data however, lies between the two limiting conditions for a persistent time signal. Combustion noise thus represents an anti-persistent (correlated) process since the

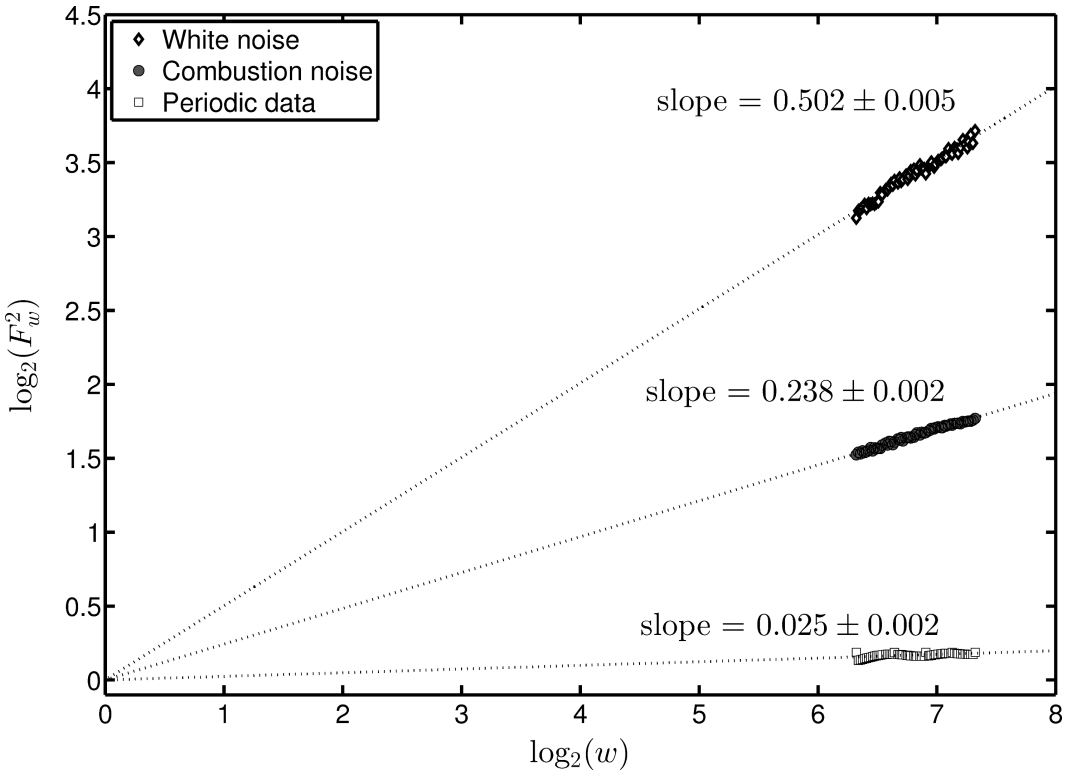

Figure 6.2: Illustration of fractal features of combustion noise through Hurst exponent. The combustion noise data presented in Fig. 6.1 are seen to lie amidst those corresponding to Gaussian white noise and periodic oscillations. The intercepts have been removed from the abscissae and dotted lines are provided to guide the eye. Uncertainties reported correspond to standard errors in slope estimation.

Hurst exponent is between 0 and 0.5. The fractal dimension D for such a process lies between 1.5 and 2. The Hurst exponent obtained for the pressure signals at combustion instability (Fig. 6.2(b)) was 0.029 and is not shown in the plot for the sake of clarity.

The multifractality of the three signals presented in Fig. 6.2 was investigated by computing the generalized Hurst exponents, the results of which are shown in Fig. 6.3:I (a-c). The high and low amplitude fluctuations in different time intervals (w) are preferentially selected by varying the order of the structure function (q). Whereas a positive order ($q > 0$) selects high amplitude fluctuations, a negative order ($q < 0$) would select low amplitude fluctuations. We see that the structure functions (F_w^q) remain parallel for Gaussian white noise. This invariance of the slope means that the fluctuations are uncorrelated at all amplitudes, and that F_w^q has an identical linear variation with time interval at all orders. For the periodic data, the values of the Hurst exponent lie fairly close to zero at different orders because there is just a single time scale associated with the fluctuations, thereby making the structure functions bounded in time.

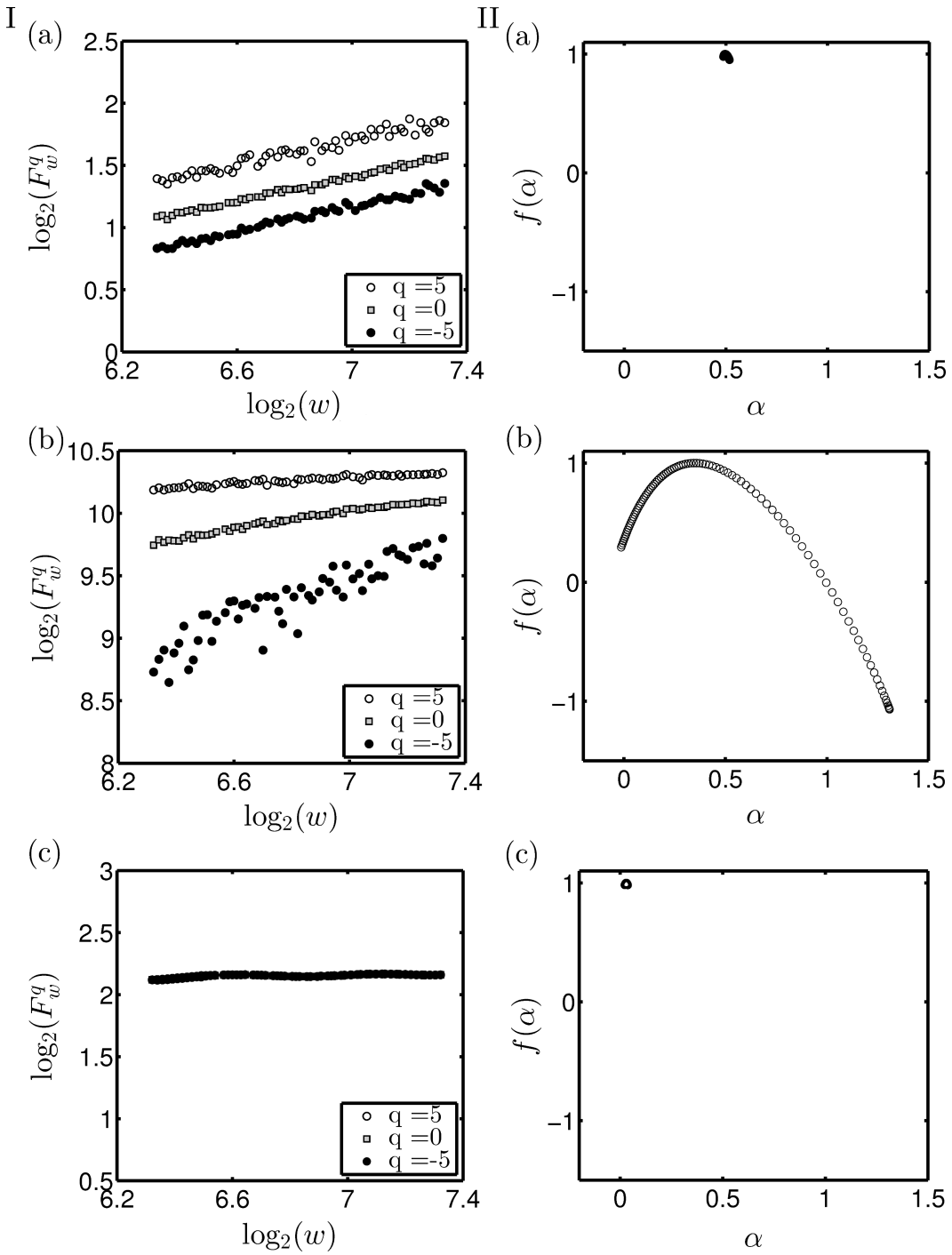

Figure 6.3: I. The variation in structure functions F_w^q at different orders q as the time interval w is increased (marked as hollow circles ($\circ$) for $q = 5$, squares ($\Box$) for $q = 0$, and filled circles ($\bullet$) for $q = -5$). The ordinates are shown on the same scale to represent the variations more clearly. II. Multifractal analysis of different signals wherein the singularity spectrum $f(\alpha)$ is plotted as a function of the singularity strength α which is comparable to the Hurst exponent. The data presented correspond to (a) monofractal time series, (b) Gaussian white noise, (c) combustion noise ($\phi = 1.1$,$Re = 1.8 \times 10^4$), and (d) periodic data ($f = 250Hz$).

Now if combustion noise were monofractal; i.e., characterized by just a single fractal dimension, the time series should show a behaviour similar to that of white noise

with the same value for all the generalized Hurst exponents, albeit with a slope different from 0.5. However, for combustion noise, we see a difference in the slopes of measured fluctuations at different values of the exponents (Fig. 6.3:I(b)). This variation in the Hurst exponents with q is a direct consequence of the multifractal nature of the time series (Kantelhardt, 2011). The high- and low-amplitude fluctuations present in the time series scale differently, which results in different values of H^q at different orders q. The multifractal spectrum of these signals is shown in Fig. 6.3:II (a-c). The spectrum is broad for combustion noise whereas it is clustered around a point for the white noise and periodic data. For white noise, we see that the spectrum is concentrated around a value of 0.5 as expected. The clustering is around zero for the periodic data which indicates the absence of scale invariance for periodic time signals, because fluctuations happen only at one time scale.

Multifractality in a time series can come about in two ways, (i) due to a broad probability distribution of the data points, e.g., a Levy distribution, and (ii) due to different long-term correlations of the small- and large-scale fluctuations (Kantelhardt *et al.*, 2002). An easy way to identify the presence of correlations in a time signal is to randomly shuffle its data values (West, 2006). Whereas multifractality due to correlations are removed by randomly shuffling the series, it persists in the former case even after shuffling. It is interesting to note that even when the multifractality arises due to long-term correlations, the probability density function of the time signal over a finite, fixed sampling duration can be a regular distribution with finite moments (for instance, a Gaussian). It is only when the sampling duration is varied that one observes the non-stationarity of the signal and divergence in central moments.

The source of multifractality in the data acquired during combustion noise was explored by randomly shuffling the acquired data as per the procedure suggested by West (2006). The original and the randomly shuffled surrogate pressure time-series from the combustor are shown in Fig. 6.4(a,b). A zoomed in view of the first 500 points in the series is shown in the inset. Whereas weak correlations are visible in combustion noise data, any such correlations are lost on randomly shuffling the data, making it memory-less. The distribution of the combustion noise data and the surrogate data from the bluff-body stabilized combustor is shown as a histogram in Fig. 6.4(c). It was verified to conform to a Gaussian distribution using the Kolmogorov-Smirnov test for normality (Massey, 1951), with the null hypothesis for non-Gaussianity rejected at 5%

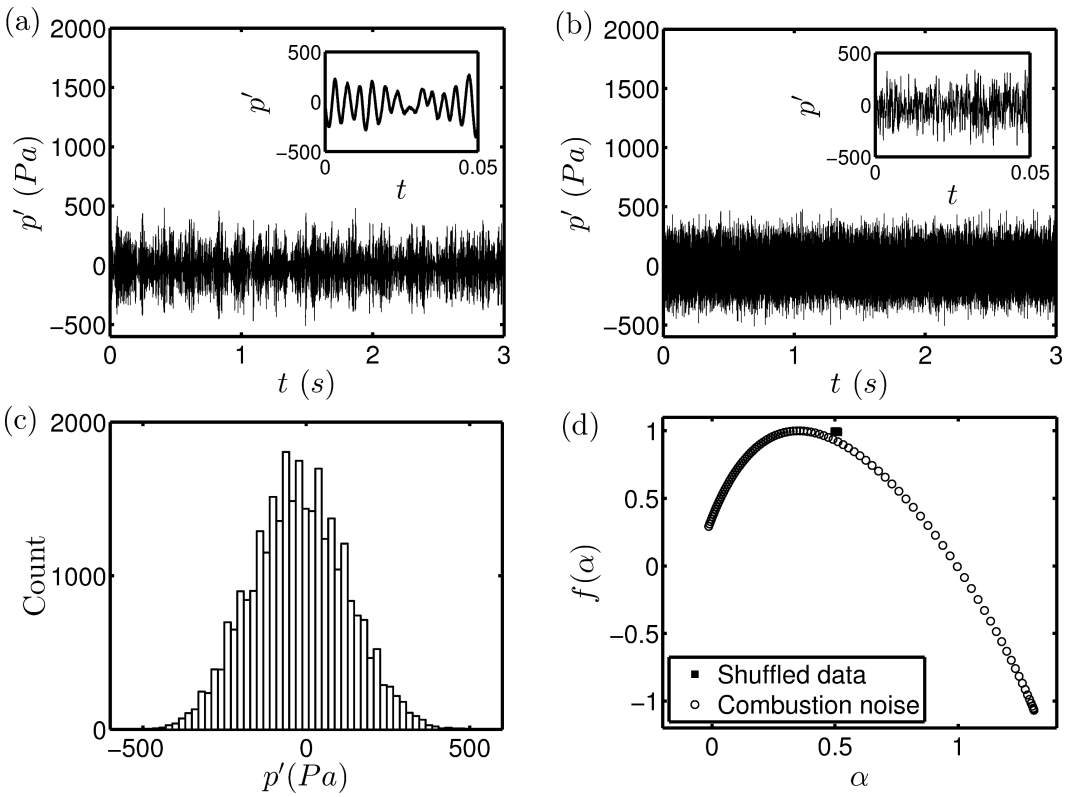

Figure 6.4: Effects of random shuffling on combustion noise data. Time signals of (a) the original combustion noise data and (b) the randomly shuffled data. The first 500 points in both data sets are shown in the inset. Whereas data corresponding to combustion noise display correlations with weak periodicity, the shuffled data is truly random with no memory. (c) Histogram showing the distribution of the data points (N) in the two signals over $3s$. It has a Gaussian profile. Hence, we see that although the data has a Gaussian distribution, it can arise out of deterministic dynamics. (d) An illustration of the presence of long-term correlations in the combustion noise data. There is a loss of multifractality on randomly shuffling the data corresponding to combustion noise because of a loss of memory among the data points in the signal. This shows that the multifractality is due to correlations in the signal and not merely a result of a broad profile in the probability density function for the values in the time signal. Such a loss of correlation strength is referred to as a loss of complexity of the system.

significance. Hence, even when the distribution of the acquired samples is a Gaussian, the dynamics can be complex and multifractal. The mere presence of correlations in the measured data suggests that it is incorrect to term the associated phenomena as 'combustion noise'. Further, as we have shown in the previous chapters, fluctuations termed combustion noise are the result of deterministic dynamics of the global system comprising flow, combustion and the chamber acoustics. In other words, combustion noise is deterministic chaos. It is probably the random appearance and the Gaussian distribution of the measured pressure fluctuations that prompted researchers to adopt a signal plus

noise paradigm in analyzing the phenomena.

Therefore, we feel that a more suitable term to describe the phenomena is to term it combustion chaos rather than combustion noise. In studying combustion noise and its transition to combustion instability, it may hence be imprudent to adopt the traditional signal plus noise paradigm, which currently is often implicitly assumed. To illustrate this point more clearly, the multifractal spectrum of the combustion noise and the shuffled series is shown in Fig. 6.4(d). Whereas the generalized Hurst exponents show variation at different orders as illustrated by the broad spectrum, they are clustered around 0.5 for the shuffled data, indicating that it has degenerated into a noise-like data. Thus, although techniques such as computation of the FFT or obtaining the probability density function may suggest a noise-like behaviour, a deeper analysis using nonlinear fractal analysis can show signs of determinism, if present.

According to a conjecture by Kraichnan (1967), if energy is injected into the flow at a constant rate at some intermediate scale, an inverse cascade will take place until the largest scales available are attained. The process of combustion instability involves a periodic heat release rate, wherein the fluctuations in heat release rate are in proper phase relationship with the perturbations in the acoustic pressure field inside the confinement, thereby satisfying Rayleigh's criterion (Rayleigh, 1878) which is a necessary condition for self-sustained pressure oscillations. The shear layer in a turbulent flow is characterized by several instability frequencies corresponding to the different sizes of vortices (Winant and Browand, 1974). On the interaction of acoustic waves with the shear layer, the vortex size can be stabilized when the frequency of these waves match the shear layer instability frequencies (Schadow and Gutmark, 1992). Hence, we suspect that the formation of large-scale coherent vortices at the onset of combustion instability as reported in the literature (Rogers and Marble (1956); Parker *et al.* (1979); Pitz and Daily (1983); Smith and Zukoski (1985); Hegde *et al.* (1983); Poinsot *et al.* (1987); Yu *et al.* (1991) to name a few) is due to the establishment of an inverse cascade with the energy being injected into the flow through combustion at scales defined by matching of the acoustics with shear layer instability frequencies. Further, a theoretical analysis of nearly incompressible flows in the presence of heat addition (Zank and Matthaeus, 1990) indicate the possibility of such an inverse cascade, wherein energy can get transported to the long-wavelength acoustic modes from smaller scales, provided the Mach numbers are low.

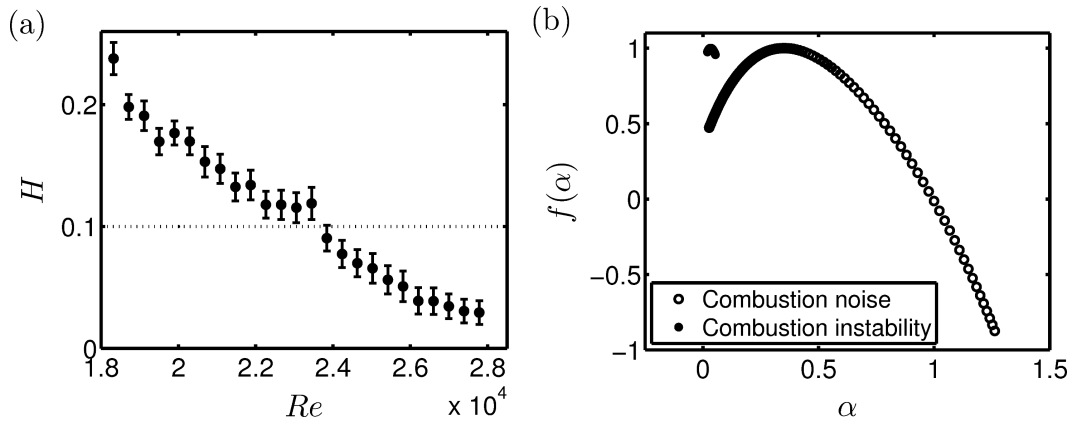

Figure 6.5: (a) Variation of the Hurst exponent H with Re. The Hurst exponents drop well before the amplitudes start rising in the combustors (Fig. 4.3(a)). The error bars correspond to the 6-σ intervals on the computed values. Threshold values (shown as horizontal dotted lines) are nominally set to 0.1 to indicate the transition. This threshold is user-defined and is independent of the geometry of system or the fuel composition unlike the amplitude measurements. (b) The loss of multifractality at the onset of combustion instability where the spectrum was plotted for the initial and final points in (a). The time series from which the spectrum was obtained is the same as that shown in Fig. 6.1(a,b).

It has been possible to successfully predict and prevent combustion instability in the two combustor configurations using the Hurst exponent as an early warning measure; the results from the studies without control are shown in Fig. 6.5. As Re is increased, there is smooth decrease in the value of Hurst exponent towards zero. This decrease happens well before the amplitude starts rising in the combustor (see Fig. 4.3). Hence, by defining a suitable threshold for the Hurst exponent sufficiently distant from zero (say, 0.1), we can track the proximity of the system to instability and take suitable control measures. The results present the average value of Hurst exponent computed over segments ranging from roughly 2 to 4 acoustic cycles of the unsteady pressure data ($8 - 16ms$) acquired over $3s$ at a sampling rate of $10kHz$. However, it is possible to obtain comparable results even with shorter time signals. Also, the threshold is independent of the system configuration since it merely is an indicator of the proximity of the system to an oscillatory regime.

The loss of multifractality in the signals at the onset of combustion instability is illustrated in Fig. 6.5(b). The plot clearly shows the spectrum diminishing to a point at the onset of combustion instability. This loss of multifractality is due to the predominance of a single time scale that dominates the dynamics. For a fractal signal, such a loss of variability in scales observed as narrowing of the frequency spectrum is termed

a ‘loss of spectral reserve’ (West and Goldberger, 1987). In a combustor, since this loss of spectral reserve happens in a gradual manner when the parameters are varied, it can serve as an early warning signal to an impending combustion instability.

It should be noted that the flow is still turbulent after the combustor becomes unstable. The power spectrum (Fig. 6.1(d)) also shows that the contributions from time scales other than the instability frequencies and their multiples, though small, are still present. The effect of turbulence can also be seen in the modulation of the amplitude of pressure fluctuations at instability. It is this turbulence that results in a small range of α in the multifractal spectrum during combustion instability. However, the range of α is reduced significantly when compared to regimes of combustion noise and is clustered around zero for the instability dominated signals. This collapse of scales leads to a loss of multifractality. A signal is multifractal when contributions of different time scales cannot be ignored without missing out on significant details of the phenomena. During combustion instability, it is entirely acceptable to consider the dynamics as a single time-scale problem. However, in the regions prior to instability, the contributions of other time-scales cannot be ignored without missing key aspects of the dynamics. Also, ignoring the contributions of these time scales—as we have seen—results in the loss of predictability of an impending instability.

6.3 Concluding remarks

Traditional analysis and modeling of combustion noise as well as its transition to high amplitude combustion instability often neglects or averages out the unsteady irregular fluctuations observed in the measured data, or treat them as a stochastic background. A detailed analysis of the irregular fluctuations can provide information that is of diagnostic as well as prognostic value. Combustion noise is deterministic chaos and results from the coupled nonlinear interaction amongst turbulence, combustion and the chamber acoustics. Hence, the use of the term noise to describe the pressure fluctuations inside a combustor during stable operation requires careful consideration as the measurements do not display features one would expect from a stochastic random process. Moreover, these fluctuations contain useful information that can help forewarn an impending instability.

The pressure fluctuations during combustion noise display multifractality which shows that multiple spatial/temporal scales are involved in the energy transfer. This further draws attention to the possibility of an inverse energy cascade in the inertial subrange. There is a gradual loss of multifractalilty for increases in Reynolds number towards combustion instability. Such a loss of spectral reserve can act as an early warning signal that predicts combustion instability well before the amplitudes start to rise in the combustor, in other words, well before the actual stability margins are reached. Moreover, the superiority of the method is clear on realizing that techniques such as FFT that rely on a frequency-domain analysis often cannot predict the proximity of the operating conditions to combustion instability.

CHAPTER 7

Dynamics of intermittency

In this chapter, we will see that intermittent burst oscillations are also observed in the combustor on increasing the Reynolds number further past conditions of combustion instability towards the lean blowout limit. Intermittent dynamics is thus a typical feature in the dynamics of turbulent combustors—even more so than limit cycle oscillations. The chapter aims to establish that such intermittent bursts arise naturally in systems composed of two attractors through the formation of homoclinic orbits in the phase space of the global system dynamics. It also aims, through analyzing the recurrence properties of these intermittent states, to provide a systematic way to inspect the presence of such homoclinic orbits from a measured time signal. Finally, the flame dynamics of the intermittent states observed prior to lean blowout will be investigated using high-speed CH^* chemiluminescence imaging.

7.1 Background

The phenomenon of intermittency has received a lot of attention in the description of deterministic dynamics arising from pattern forming complex systems. Through a study of simple dissipative dynamical systems, Pomeau and Manneville (1980) presented three models of intermittency classified as type I-III to describe the routes of transition from a stable periodic behaviour to chaos. Even more varieties of intermittency were discovered later on such as chaos-chaos intermittency (Richardson, 1993) (eg: on-off intermittency (Ott and Sommerer, 1994) and in-out intermittency (Covas *et al.*, 2001), crisis-induced intermittency (Grebogi *et al.*, 1987), type-X intermittency (Price and Mullin, 1991) or type-V intermittency (Bauer *et al.*, 1992). There has also been a number of experimental observations (Hammer *et al.*, 1994; Argoul *et al.*, 1993) of intermittent dynamics in the literature.

As we have seen so far, interaction of sound with a reacting turbulent flow provides us with yet another dynamical system where intermittency is observed—seen

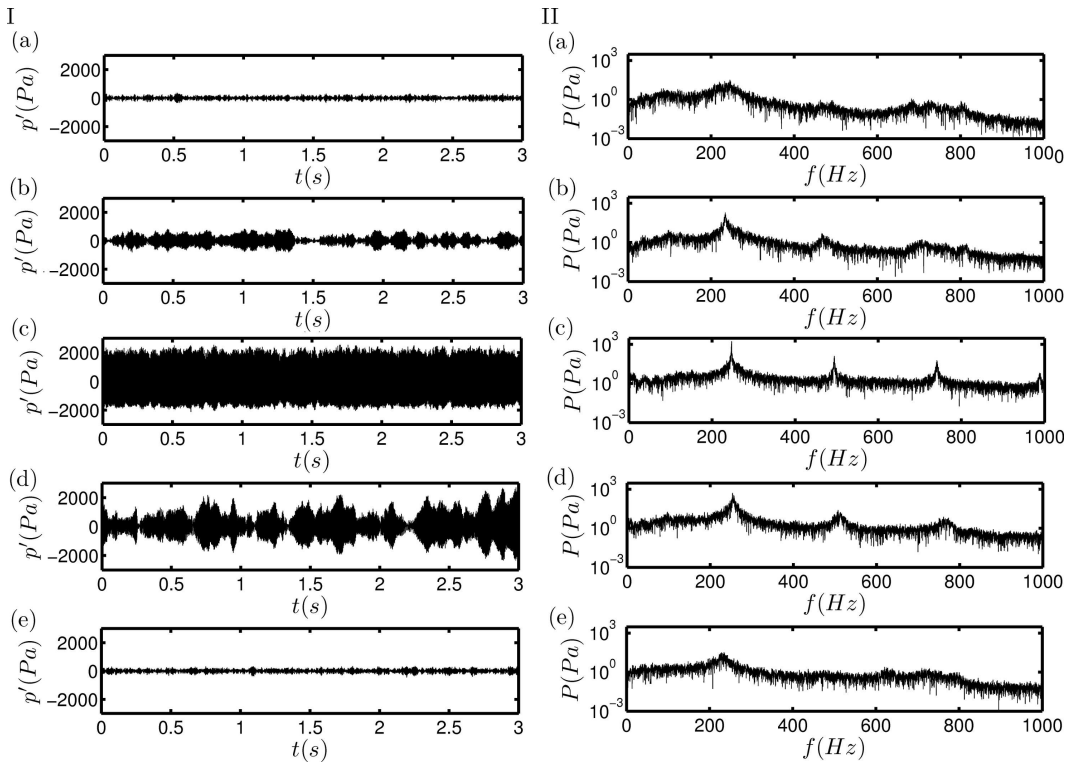

Figure 7.1: (I) Typical unsteady pressure measurements and (II) corresponding amplitude spectra acquired during the dynamically different flow regimes from the combustor. (a) Combustion noise ($Re = 2.19 \times 10^4$, $\phi = 0.93$), (b) intermittency prior to combustion instability ($Re = 2.42 \times 10^4$, $\phi = 0.83$), (c) combustion instability ($Re = 2.74 \times 10^4$, $\phi = 0.72$), (d) intermittency prior to lean blowout ($Re = 4.95 \times 10^4$, $\phi = 0.39$) and (e) near lean blowout ($Re = 6.92 \times 10^4$, $\phi = 0.27$).

as intermittent bursts of pressure oscillations that emerge from a chaotic background. Shown in Fig. 7.1 are the various qualitatively different stages observed in the unsteady pressure measurements from the combustor at progressively increasing flow Reynolds numbers (decreasing equivalence ratios). Observe the wide variation in amplitudes in the pressure signals shown in Fig. 7.1:I(b,d). We see that the dynamic transition from low-amplitude fluctuations (Fig. 7.1:I(a)) to high-amplitude combustion instability (Fig. 7.1:I(c)) happens via such a regime of intermittent oscillations where the pressure fluctuations rise in bursts of periodic, high-amplitude oscillations from a background of low-amplitude, aperiodic fluctuations. Correspondingly, the spectra of the pressure signals show a gradual emergence of peaks as the dynamics approaches combustion instability (Figs. 7.1:II(a-c)).

Further increases in Reynolds number after the onset of combustion instability leads to the occurrence of intermittent oscillations again (Fig. 7.1:I(d)) suggesting yet another transition in the combustor dynamics. These intermittent oscillations persist for a range

of Reynolds number until the pressure signals eventually transform to low-amplitude fluctuations (Fig. 7.1:I(e)) before the flame eventually blows out. The strength of the peaks in the pressure spectra also start diminishing as the dynamics transitions towards intermittency and lean blowout (Figs. 7.1:II(d,e).

From the figure, it is clear that intermittency represents a transition regime in the dynamics of combustors prior to large-amplitude combustion instability as well as lean blowout. Also, it is evident from the pressure spectra (Fig. 7.1:II(a-e)) that the dynamics of these intermittent oscillations involve time scales other than those of the confinement acoustics. For instance, although it is a reasonably good approximation to consider combustion instability as dynamics happening over a single time scale (and its multiples), at least one additional time scale is required to describe the modulation of the pressure amplitudes from high to low values and back to low values observed during regimes of intermittency.

Recently, Kabiraj and Sujith (2012) showed that intermittency is possible in simple thermoacoustic systems prior to lean blowout of the flame. The flame was seen to be highly unsteady and wrinkled during such intermittent regimes with irregular lift-off and reattachment. Further, the intermittent signal was characterized by high-amplitude chaotic oscillations that emerged from a quiet background. In the case of combustors in a turbulent flow field, we observe that the signals display what is termed an intermittent bursting phenomenon—bursts of periodic oscillations that appear in a near-random fashion amidst aperiodic irregular fluctuations. As has been shown in previous chapters, the dynamics of such systems can be thought of as being composed of two subsystems or attractors that operate on different time scales; acoustics which is characterized by the local speed of sound and hydrodynamics which operates over a broader range of time scales defined by the local flow speeds. In what follows, we shall probe deeper into the dynamic aspects of such intermittent burst oscillations.

7.2 Intermittency and homoclinic orbits

A homoclinic orbit is one in which the unstable manifold of a hyperbolic equilibrium state of the system merges with its own stable manifold. Although a close association between homoclinicity and intermittency has been shown experimentally in the

literature (Richetti *et al.*, 1986; Herzel *et al.*, 1991; Parthimos *et al.*), identification of homoclinic orbits from a measured time series has proved a difficult task. In Fig. 7.2, the evolution in phase space of an intermittent burst is shown for the pressure signal acquired prior to lean blowout. The trajectory is seen to spiral out of the center to the unstable orbit and then spirals back in through the plane of oscillations, which could possibly represent a homoclinic orbit. However, the existence of such orbits cannot be concluded by a mere visual inspection of the phase space. Therefore, we propose a new technique to infer the presence of homoclinic orbits in the phase space of the global attractor.

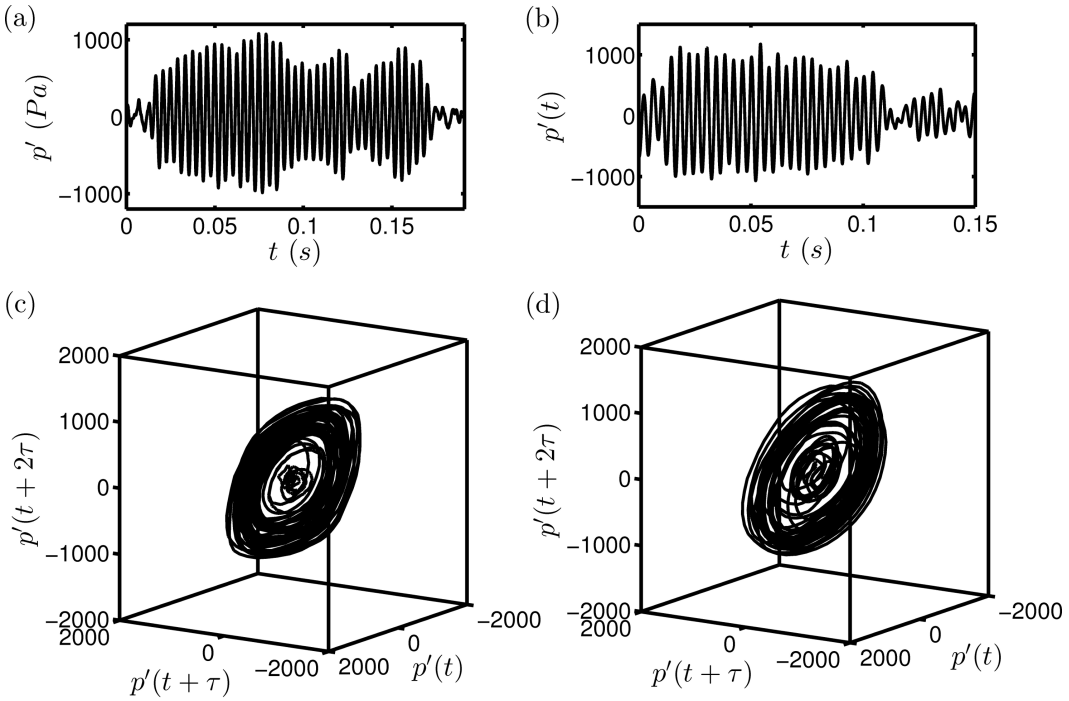

Figure 7.2: A portion of the burst signal of (a) the intermittent signals prior to combustion instability ($Re = 2.57 \times 10^4$,$\phi = 0.89$) and (b) the intermittent signals prior to lean blowout ($Re = 5.14 \times 10^4$,$\phi = 0.37$). The corresponding phase portraits (in 3D) are shown in (c) and (d) respectively. The embedding dimension was chosen to be $d_0 = 10$ with $\tau_{opt} = 1.0ms$ for both the signals. The evolution of burst oscillations in phase space results in the aperiodic oscillations spiraling out into high amplitude oscillations and then again spirals back into the low amplitude aperiodic dynamics.

The circulation time of trajectories in phase space for homoclinic orbits are dominated by their passage time near the saddle fixed point. This time is highly sensitive to external perturbations and the distribution of passage times for a given initial distribution of points near the saddle point is given by the expression (Holmes, 1990):

$$P(T) = \frac{2\lambda\Delta(T)\mathrm{e}^{-\Delta^2(T)}}{\sqrt{\pi}(1-\mathrm{e}^{-2\lambda T})} \tag{7.1}$$

where $\Delta(T) = \delta\left[\left(\frac{\alpha^2}{\lambda}\right)(\mathrm{e}^{2\lambda T}-1)\right]^{-1/2}$, λ is the unstable eigenvalue of the saddle point, α is the noise level rms, δ is the size of the neighbourhood influenced by noise. $P(T)$ is a skewed distribution with its peak value different from the mean and has an exponential tail (Holmes, 1990) as $T \to \infty$ ($P(T) \approx \frac{2\delta}{\sqrt{\pi\alpha}}\lambda^{3/2}\mathrm{e}^{-\lambda T}$). This behaviour is independent of the details of the initial distribution (Stone and Holmes, 1991). It is known that the distribution of the laminar phases (quiet, aperiodic regimes) for both type-II and type-III intermittencies have an exponential tail (Klimaszewska and Zebrowski, 2009). Inspection of the recurrence plots of the combustor pressure signal acquired during intermittency is inconclusive; however, the detected features correspond to type-II or type-III intermittency. As the analysis described above illustrates, systems exhibiting type-II or type-III intermittency are characterized by homoclinic orbits in the underlying phase space.

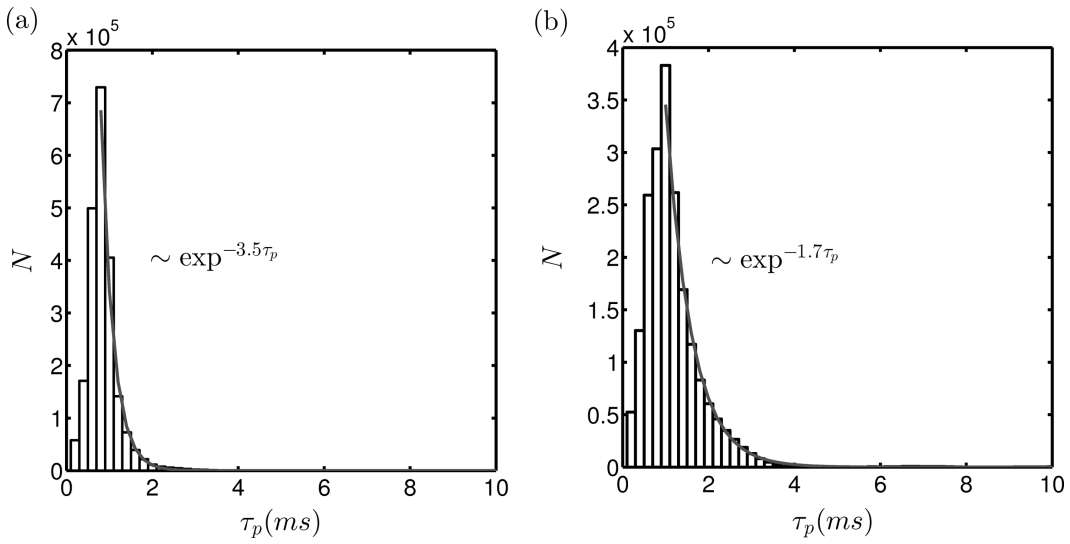

Figure 7.3: Histograms of the number of visits and the duration of time spent trapped in the low amplitude aperiodic regimes for (a) the intermittent signals prior to combustion instability ($Re = 2.57 \times 10^4$,$\phi = 0.89$) and (b) the intermittent signals prior to lean blowout ($Re = 5.14 \times 10^4$,$\phi = 0.37$). The data sets correspond to pressure signals acquired for a duration of $1.5s$ at a frequency of $5kHz$. A skewed distribution with an exponential fall-off is visible in both the histograms which is a distinctive feature of systems that have homoclinic orbits in the phase space of dynamics. An exponential fit to the tail is shown as gray lines over the histogram.

The distribution of the passage time of the dynamics in low amplitude regimes can

be estimated from a recurrence plot as the frequency distribution of the vertical lines (or horizontal lines since the matrix is symmetric) in the recurrence plot. Histograms of this vertical length frequency distribution for the two signals were plotted in Fig. 7.3 to understand the variation of the frequency of visits as a function of the trapping time. The histogram reveals a skewed distribution with its peak off the mean and has an exponentially decaying tail.

The presence of such an exponential tail is thus indicative of homoclinic orbits in the system (Stone *et al.*, 1996). The trajectory of such a homoclinic orbit is repeatedly injected near the stable manifold of a saddle node as a result of the perturbations in the turbulent base flow. Thus, recurrence quantification serves as an efficient tool for the inspection of homoclinic orbits in the phase space of the system dynamics. In the next subsection, we will revisit our current understanding of the flame dynamics near lean blowout and analyze them in terms of the observed intermittency.

7.3 Intermittent flame dynamics near lean blowout

In a comprehensive review of bluff-body stabilized flames, Shanbhogue *et al.* (2009) showed that spatially and temporally localized extinction events—manifested as holes in the flame sheet—occur sporadically near lean blowout. The frequency of such events increase as lean blowout is approached. Increased presence of time-localized and intermittent events in the acoustic data near lean blowout was also reported by Nair and Lieuwen (2005) for three combustors with pilot, swirl and bluff-body stabilized flames respectively.

We have seen that intermittent dynamics corresponds to time-localized behaviour of pressure oscillations with high-amplitude bursts of oscillations appearing in a measured pressure signal in a near-random manner. In order to understand how the measured intermittency translates to unsteady flame dynamics in the combustor, high speed images with CH^* filter were acquired simultaneously with pressure measurements at an operating condition within the intermittent regime observed prior to lean blowout (Fig. 7.4). The amplitudes vary over a wide range from high to low amplitudes (Fig. 7.4(a)) and the zoomed portion of the time signal clearly displays the periodic and the aperiodic regimes in the signal (Fig. 7.4(b)). The instantaneous images show the flame gradually

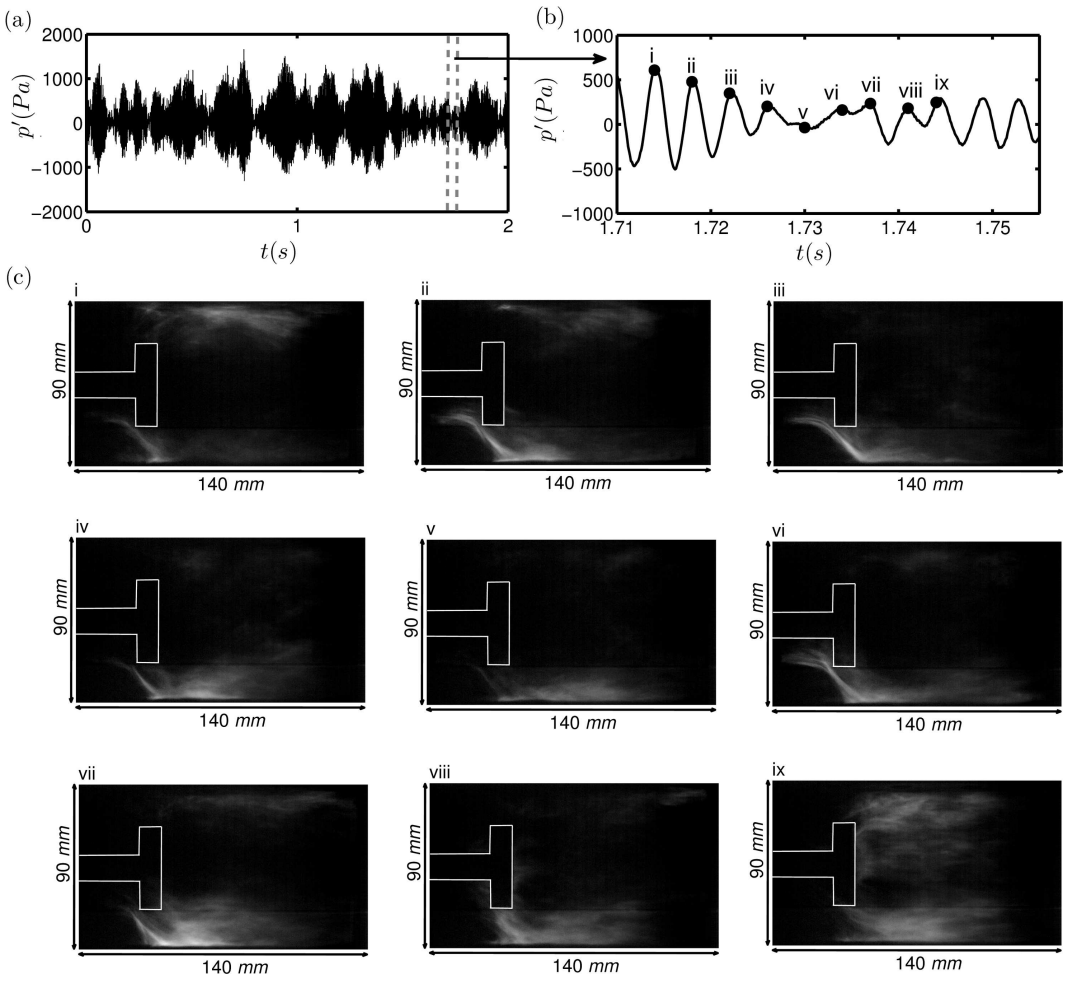

Figure 7.4: (a) Unsteady pressure signal and a sequence of line-of-sight integrated instantaneous flame images acquired at the intermittent state prior to lean blowout in the combustor ($Re = 5.14 \times 10^4$,$\phi = 0.37$). (b) A zoomed portion of the signal reveals aperiodic segments amidst periodic dynamics. (c) The corresponding high speed images show aperiodic detachment of the flame from the upper lip of the bluff-body and subsequent reattachment. As a result of this detachment, there is a decrease in the heat released and the pressure signal loses its periodicity and the amplitudes decrease. The signal eventually gains amplitude and periodicity upon flame reattachment. This appearance of bursts of periodic oscillations in a near-random manner is a dynamical state termed intermittency. The outline of the bluff-body is shown for the ease of visualization.

disappearing (Fig. 7.4(c): i-iii) from the upper portion of the bluff-body, remains in the same state for a short time (Fig. 7.4(c): iv-vi) and eventually reestablishes itself on the upper portion of the bluff-body (Fig. 7.4(c):vii-ix). When the flame detaches from the upper portion of the bluff-body, the corresponding pressure signal loses its periodicity and becomes aperiodic due to the lack of sufficient, sustained energy release to acoustics from the unsteady heat release. The signal is seen to regain periodicity when the flame reattaches which further corroborates that it is the unsteady heat release that

sustains the periodic oscillations.

The state of intermittency in the pressure oscillations can thus directly be linked to aperiodic detachment of the flame from the flame holder resulting in an insufficient driving of the oscillations in the combustor. This insufficient driving can be envisaged to result from the flame detachment or extinction or even due to the presence of holes in the flame sheet due to high turbulent strain rates. The characterization of the intermittency in the measured signals hence allows for an indirect characterization of the unsteady flame dynamics near lean blowout reported widely in the literature and can therefore be utilized to provide precursors that forewarn an impending blowout in the combustor.

7.4 Concluding remarks

Intermittent bursts characterized by periodic high amplitude oscillations amidst irregular low amplitude chaotic fluctuations are produced when a turbulent flow interacts with the acoustics of a confinement forming dynamic objects known as homoclinic orbits in phase space. Recurrence plots provide a convenient and quantitative descriptive tool to inspect and identify the presence of a homoclinic orbits in the phase space by measuring the amount of time the system lingers around the low amplitude fluctuations. A skewed distribution of passage times with an exponential tail is a distinctive signature of systems with a homoclinic orbit; i.e., the trajectory is repeatedly injected near the stable manifold of a saddle in the presence of small perturbations. Observing the flame images close to lean blowout identifies the aperiodic detachment of flame from the bluff-body as the source of intermittent burst oscillations. This intermittent detachment reduces the driving of the acoustics by the unsteady heat release as a result of which the pressure oscillations lose their periodicity and amplitude comes down resulting in turbulent aperiodic fluctuations.

CHAPTER 8

Is combustion necessary for intermittency?

In this chapter, we show that intermittent burst oscillations are a typical feature of turbulent flow-sound interaction, even in the absence of combustion.The onset of self-sustained oscillations in a turbulent pipe flow across an orifice is investigated in a whistling apparatus. Analysis of measured pressure fluctuations reveals that this emergence of order from turbulence happens through an intermediate intermittent regime characterized by bursts of periodic oscillations that appear in a near-random fashion amidst the background chaotic fluctuations. The interesting feature is that these intermittent bursts correspond to a frequency distinct from the final oscillatory state as the boundary condition at the orifice exit undergoes a transition at the onset of whistling.

8.1 Introduction

Pressure fluctuations in unsteady flows are classified as sound or pseudo-sound depending on whether the underlying pressure field is propagating or non-propagating (**?**). The pressure variations p' in a sound field (acoustic waves) are dependent on the local speed of sound c_0 via $p' \sim \mathcal{O}(\rho_0 c_0 u)$, where ρ_0 is the mean flow density and u refers to the typical magnitude of the local flow velocity. On the other hand, the local variations in pressure due to a pseudo-sound field vary as $p' \sim \mathcal{O}(\rho_0 u^2)$, thus independent of the sound speed. When an unsteady flow passes through a confinement, both forms of pressure fluctuations are induced and these fluctuations are characterized by a multiplicity of time scales associated with local unsteadiness and acoustic wave propagation. When one of the local hydrodynamic time scales matches an acoustic time scale, self-sustained periodic oscillations, which are difficult to control in practice, are established. Screech in jets with shocks, edge tones, howling of ejectors, cavity noise, whistling in pipes (pipe tones) are some such examples of flow-induced oscillations (**?**).

In this chapter, the mechanism underlying the transition from a turbulence-dominated state to a state dominated by periodic dynamics in a system without combustion will be

illustrated through experiments and theoretical arguments. This emergence of order (periodic dynamics) from turbulence is contrary to the transitions often encountered in hydrodynamic flow-fields where an increase in the Reynolds number results in a transition from periodic oscillations to turbulence (**?**).

8.2 Experiments

Motivated by the pioneering work on pipe tones by Anderson (**??**), we investigate the multi-scale temporal dynamics of turbulent flow-sound interaction in an experimental setup consisting of a pipe of length $L = 600$mm and diameter $D = 50$mm terminated by a circular orifice of diameter $d_o = 15$mm and thickness $t = 5$mm (Fig. 8.1). Such a configuration is present, for instance, in automobile exhaust pipes (**?**), segmented solid rocket motors (SRMs) (**?**) and gas transport systems (**??**). The pressure-driven flow, after passing through a moisture separator and a rotameter (used to measure the incoming flow rates), enters the pipe through an upstream cylindrical chamber of length $L_c = 300$mm and diameter $d_c = 300$mm.

A region of strong velocity gradients (shear layer) forms at the leading edge of the orifice and rolls up into a vortex sheet that convects downstream. It has previosuly been conjectured that the separated shear flow produces fluctuations in the effective aerodynamic orifice area due to the growth and periodic shedding of vortices from the orifice side walls (**?**). These area fluctuations in turn produce variations in the pressure drop across the orifice (**?**). When the frequency of these variations matches one of the acoustic modes of the pipe-orifice combination, self-sustained pipe tones or whistling is established. Later studies have further proposed that whistling is established when the separation streamline from the leading edge of the orifice impinges on the trailing edge (**?**).

Experimental measurements were performed by systematically increasing $\dot{m}$ from $0.60g/s$ to $0.92g/s$ in steps of $0.02g/s$ and then decreasing back to $0.60g/s$, where $\dot{m}$ is the mass flow rate of air through the duct-orifice system. The Reynolds number, which serves as the non-dimensional control parameter, is defined as $Re = 4\dot{m}/(\pi d_o \mu)$, where $\mu = 1.85 \times 10^{-5} Pa.s$ is the dynamic viscosity of air at the ambient condition of $26\,^{\circ}\mathrm{C}$ and $1atm$. The variation in Re was in the range $2.75 \times 10^3 - 4.22 \times 10^3$ with

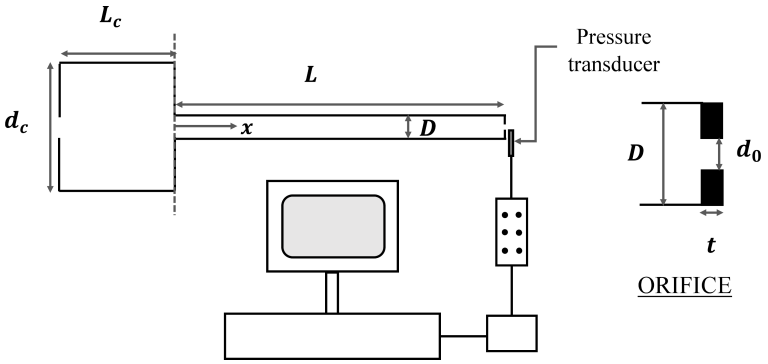

Figure 8.1: Schematic of the experimental setup used in the present study. The pipe has a length $L = 600$mm and diameter $D = 50$mm terminated by a circular orifice of diameter $d_o = 15$mm and thickness $t = 5$mm. Air enters the upstream cylindrical chamber, of length $L_c = 300$mm and diameter $d_c = 300$mm, through the opening in the left.

a measurement uncertainty of 2.7%. The pressure fluctuations generated by turbulence (pseudo-sound) decays much faster than the radiated sound field downstream of the orifice (**??**). Hence, pressure measurements were acquired with a transducer located $2mm$ to the right of the trailing edge of the orifice, a location where the levels of the turbulent pressure field were above the noise threshold of the transducer (Fig. 8.1). A total of 33 pressure measurements were performed; each pressure measurement corresponds to an acquisition for a duration of $10s$ at a sampling frequency F_s of $10kHz$ using a free-field microphone. Though the microphone has a resolution of $200\mu Pa$, measuring the electrical noise prior to the experiments revealed that pressure fluctuations below $\sim 0.09Pa$ are not well resolved. To obtain the amplitude of pressure P at various frequencies f, a Fast Fourier Transform (FFT) was performed on the pressure time series with a spectral bin size of $\Delta f = 0.08Hz$.

8.3 Results

Figure 8.2 presents the results from an experiment in which the Reynolds number was increased from $Re_1 = 2.75 \times 10^3$ to $Re_2 = 4.22 \times 10^3$ in steps of $\Delta Re = 0.09 \times 10^3$. At each Re, the flow was allowed to settle for $5s$ before pressure measurements were made. The frequency content of the 14 signals obtained for $Re < 4.04 \times 10^3$ (Fig. 8.2(a)) reveal the presence of a broad peak centered around a dominant frequency f_1 that remains almost invariant ($f_1 = 537Hz$ with a variation within $1Hz$) on increasing Re. The invariance suggests that f_1 is one of the natural acoustic frequencies of the duct-

orifice system rather than a flow frequency. The broad profiles of the spectra shown in Fig. 8.2(a) indicate a pressure signal dominated by turbulence, and a typical time signal acquired at $Re = 2.75 \times 10^3$ (Fig. 8.3(a)) does display an aperiodic behaviour. A secondary shallow peak centered around $f_2 = 217Hz$ is also visible in the spectra for $Re < 4.04 \times 10^3$ and it gradually bifurcates into two as Re is increased (Fig. 8.2(a)). Such pairs of peaks in the spectra have previously been shown to signify the proximity of the operating conditions to a period doubling bifurcation (**?**).

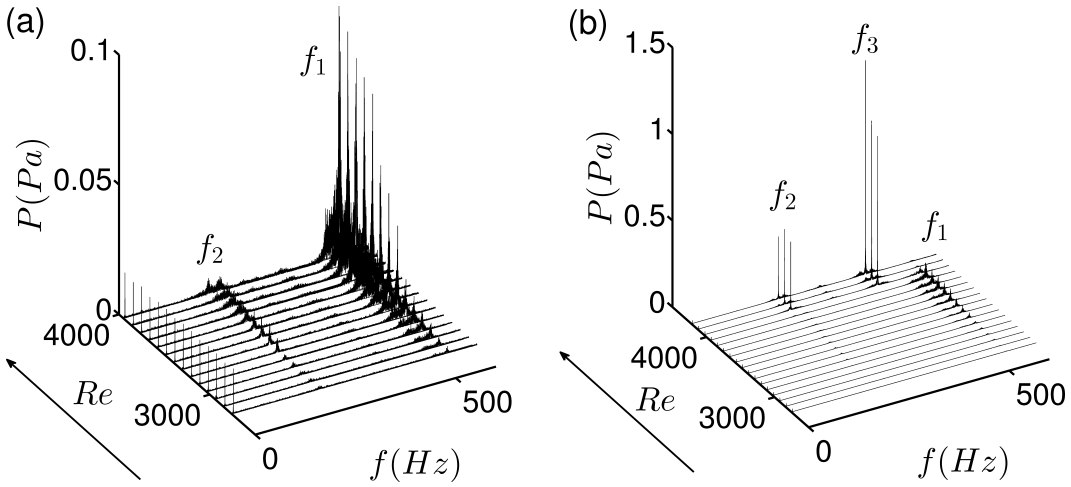

Figure 8.2: (a) Plots of the spectra (P vs. f) computed from the pressure time series for various Re prior to the onset of whistling ($Re < 4.04 \times 10^3$). (b) Plots of the spectra for $Re \in [2.75 - 4.22] \times 10^3$. The arrows indicate the direction of change of Re in the experiment.

For relatively large Re ($Re = 3.85 \times 10^3$, for example), the pressure time series displays bursts of periodic oscillations (of frequency f_1) that appear in an almost random manner amidst aperiodic fluctuations (Fig. 8.3(b)). The average duration of these periodic bursts increases with an increase in Re, leading to the increased spectral content at f_1 as seen in Fig. 8.2(a). Spatially localized puffs of turbulence with a finite lifetime are often observed in pipe flows prior to the critical transition to turbulence (**??**). In our experiments, we observe the converse scenario, with intermittent puffs of time-localized periodic oscillations forming in a background of turbulent fluctuations.

Figure 8.2(b) shows the amplitude spectra for all the 17 pressure measurements, spanning $Re_1 = 2.75 \times 10^3$ to $Re_2 = 4.22 \times 10^3$. While the spectra for $Re < 4.04 \times 10^3$ contain broad peaks around f_1 and f_2, the pressure fluctuations for $Re \geq 4.04 \times 10^3$ are more coherent with sharp peaks of significantly higher amplitudes in the spectra (termed tones); a typical times series obtained at $Re = 4.22 \times 10^3$ is shown in Fig. 8.3(d). This transition in the spectra occurs at $Re = 4.04 \times 10^3$, wherein the dynamics undergoes a

bifurcation from a low-amplitude intermittent regime to high amplitude self-sustained periodic oscillations (Fig. 8.3(c)). The sudden rise in amplitudes and the sharpening of the spectra signify the onset of whistling, with the two dominant frequencies during whistling related by $f_3 = 2f_2 = 434Hz$, resulting in period-2 oscillations. In the whistling regime, while the spectral content at f_1 is very small, the dominant frequencies f_2 and f_3 increase linearly with Re. We further note that the flow is still turbulent during whistling although the dynamics is dominated by periodic pressure fluctuations.

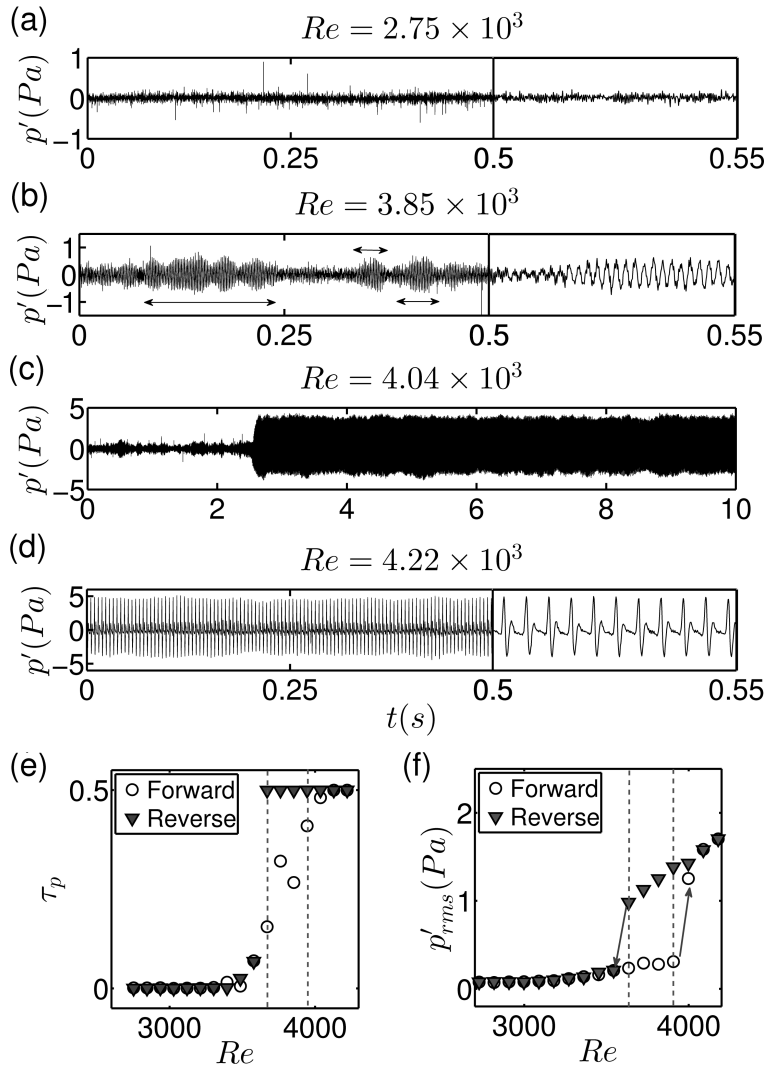

Figure 8.3: Dynamics of the transition for increasing Reynolds number (Re): (a) aperiodic fluctuations ($Re = 2.75 \times 10^3$), (b) intermittent bursts ($Re = 3.85 \times 10^3$), (c) transition to periodic oscillations ($Re = 4.04 \times 10^3$), and (d) ordered period-2 oscillations ($Re = 4.22 \times 10^3$). (e) τ_p, the time spent by the dynamics in the periodic state over a 0.5s duration, plotted as a function of Re along the forward and reverse paths. (f) The r.m.s. value of pressure fluctuations (p'_{rms}) plotted as a function of Re along the forward and reverse paths. The bistable regime in Re lies between the two vertical dashed lines. Three bursts of varying duration are shown using horizontal arrows in (b).

For a fixed Re, the time spent by the dynamics in the periodic regime was computed

by tracking the repeating patterns in the pressure fluctuations after delay embedding the data onto a suitable mathematical phase space (of dimension $d_0 = 8$ and embedding delay $\tau_{opt} = 0.4ms$) (Marwan *et al.*, 2007; Abarbanel *et al.*, 1993). The first 9 seconds of the signals were divided into segments of $T_s = 0.5s$ duration and two points in the phase space are treated as recurrent when the distance between them is less than a fixed threshold $\epsilon_0 = 2.5Pa$, which roughly corresponds to a pressure amplitude $|p'|$ of $\epsilon_0/\sqrt{n} \approx 0.9Pa$ when the signal is embedded in eight dimensions. This thresholding generates a binary recurrence matrix R_{ij} which has a value of one when the distance between points i and j in the phase space exceeds ϵ_0 and a value of zero otherwise. The time span $T = 0.5s$ is much higher than the largest dominant time period of oscillations during whistling ($T_0 \sim 4.6ms$). The average duration of the time spent in the periodic state in a segment i is then computed as:

$$\tau_p^i = \frac{1}{F_s} \frac{\Sigma_{v=1}^{N} v P(v)}{\Sigma_{v=1}^{N} P(v)}, \quad i = 1, 2, ..., 18. \tag{8.1}$$

where $P(v)$ is the probability distribution of strings v of consecutive $1s$ in the recurrence matrix R_{ij}, for a time series comprising $N = 5000$ data points sampled at a frequency F_s. The mean time spent in the periodic state τ_p is then computed as the average of τ_p^i over 18 such segments. A value of $\tau_p = 0.5s$ corresponds to the dynamics spending all the time in the periodic state. As Re is increased, i.e. along the forward path, the trajectory in phase space repeats itself more often and consequently the duration of time spent in the periodic state increases from $0s$ to $0.5s$ (Fig. 8.3(e)), as the duration of an individual periodic burst increases on the average.

The periodic oscillations represent a state of hydrodynamic-acoustic lock-in. Shown in Fig. 8.3(f) is the variation of the r.m.s. value p'_{rms} of the pressure time series (obtained over 10s) as a function of Re from the two experiments in which Re was varied from $Re_1 = 2.75 \times 10^3$ to $Re_2 = 4.22 \times 10^3$ (forward path) and then back from $Re_2 = 4.22 \times 10^3$ to $Re_1 = 2.75 \times 10^3$ (reverse path), respectively. The transition to self-sustained whistling is subcritical: as shown in Fig. 8.3(f), along the reverse path, the periodic oscillations (whistling) persist until $Re = 3.67 \times 10^3$, for which we observed intermittent fluctuations along the forward path. The upper branch in the bistable regime of Fig. 8.3(f) corresponds to the periodic states with frequencies f_3 and f_2 in the spectra and the lower branch corresponds to the intermittent burst states with a domi-

nant frequency f_1 in the spectra. The hysteresis is also visible in the plot of τ_p vs. Re (Fig. 8.3(e)).

A theoretical model based on 1D linear acoustics is constructed by linking the plenum, duct and the orifice as three network elements separated by junctions that satisfy the interface conditions (pressure continuity and mass flow conservation) (**?**). Both the plenum left end and the orifice right end are acoustically open. The effects of mean flow and mean density variations are negligible as the maximum mean flow velocity ($u_0 = 4.4m/s$) is much smaller than the speed of sound ($c_0 = 346.6m/s$) in air at the operating conditions. Assuming a harmonic variation for the acoustic pressure perturbations, the acoustic pressure and velocity fluctuations may be represented as:

$$p' = \Re[\mathrm{e}^{i\omega t}(A\mathrm{e}^{ikx} + Be^{-ikx})], \tag{8.2}$$

$$u' = \Re\left[\mathrm{e}^{i\omega t}\left(A\mathrm{e}^{ikx} - B\mathrm{e}^{-ikx}\right)/\rho_0 c_0\right], \tag{8.3}$$

where $k = \omega/c_0$ is the wavenumber and $\Re$ denotes the real part. With the origin of the coordinate system ($x = 0$) fixed at the duct-plenum junction, and taking the direction of mean flow to be the positive x-axis, the boundary conditions may be expressed in matrix form as:

$$\begin{bmatrix} 1 & 1 & -1 & -1 & 0 & 0 \\ S_p & -S_p & -S_d & S_d & 0 & 0 \\ \mathrm{e}^{-ikL_c} & \mathrm{e}^{ikL_c} & 0 & 0 & 0 & 0 \\ 0 & 0 & \mathrm{e}^{ikL} & \mathrm{e}{-ikL} & -\mathrm{e}^{-ikL} & -\mathrm{e}^{-ikL} \\ 0 & 0 & S_d\mathrm{e}^{ikL} & -S_d\mathrm{e}^{-ikL} & -S_o\mathrm{e}^{-ikL} & S_o\mathrm{e}^{-ikL} \\ 0 & 0 & 0 & 0 & \mathrm{e}^{ik(L+t)} & \mathrm{e}^{-ik(L+t)} \end{bmatrix} \begin{pmatrix} A_p \\ B_p \\ A_d \\ B_d \\ A_o \\ B_o \end{pmatrix} = 0 \tag{8.4}$$

where the subscripts p, d and o refer to the plenum, duct and orifice respectively, and S_p, S_d and S_o are the corresponding areas of cross-section. By setting the determinant of the matrix equal to zero, a non-trivial solution is found at $f = 533Hz$ which compares well with the frequency f_1 observed prior to the transition to whistling. The frequency

f_1 arises due to the presence of the plenum, as removing the plenum element from the theoretical analysis removed the frequency f_1. No solution, however, was found near f_2 or f_3 with this arrangement.

Based on the mechanism conjectured in **?**, instability is established when the shear layer reattaches at the trailing edge of the orifice. This should produce a recirculating vortex bubble on the orifice with a circulation time given to first order by $T_c = 2t/u_0$, where u_0 is the mean flow velocity through the orifice. The value of the frequency associated with this circulation at the transition Re ($= 4.13 \times 10^3$) is $f_c = 1/T_c = 428.6Hz$, which is in good agreement with the frequency f_3 obtained from experiments. The transition Re is defined as the Re at and above which low amplitude pressure fluctuations are not possible in the forward path experiment.

The mechanism also provides further insight on why the frequencies f_2 and f_3 are absent in the linear acoustic analysis prior to whistling. Formation of the vortex bubble at the orifice can acoustically close the right end of the orifice boundary since the effective area for the flow to pass through is reduced. Imposing a closed boundary condition at the orifice exit and performing the linear acoustic analysis, a non-trivial solution is obtained at $f = 435Hz$ which is close to the dominant frequency f_3 observed during whistling. This also explains why the frequency f_1 is not obtained once whistling is established. Increasing the Re (or u_0) further would require temporal adjustment of the boundary conditions (acoustic pressure drop across the orifice) such that the flow-acoustic lock-in is maintained. Flow visualization experiments performed by **??** have revealed vortex coalescence downstream of the orifice for various orifice parameters. The subharmonic frequency f_2, and the observation of period-2 oscillations at whistling hence occur when two vortices with frequencies f_3 coalesce downstream of the orifice, forming a bigger vortex with an associated frequency $f_2 = f_3/2$.

The multifractal spectrum which was broad prior to transition collapses to a growth rate near 0 after the transition (Fig. 8.4(a)). In other words, the relevant time scales that dictate the physics of the problem become fewer in number. The loss of multifractality can also be used as a precursor to an impending instability. Shown in Fig. 8.4(b) is the variation of Hurst exponent H (or H_2) of the pressure fluctuations over a range of Reynolds number varying from conditions far from whistling to conditions of self-sustained oscillations. The Hurst exponent drops smoothly across this

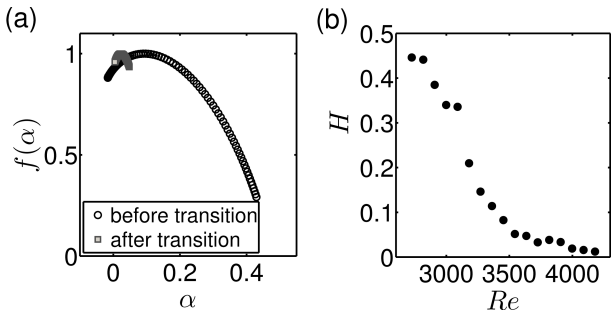

Figure 8.4: Characterizing the onset of self-sustained oscillations. (a) The multifractal spectrum acquired for the first 2s of the data overlaid on the spectrum estimated for the data from $4 - 10$s after the onset. (b) Variation of Hurst exponent H with Re along the forward path.

range of Reynolds number. This smooth decline in the divergence rates is due to the presence of a regime of Reynolds number characterized by intermittent bursts in the signal. The density of such periodic 'puffs' in the signal for a fixed time period of measurement increases as the mean flow velocities approach conditions of whistling and the Hurst exponents are an alternate measure of this density.

8.4 Concluding remarks

The results from this chapter show that intermittency is a universal feature that presages self-sustained flow-induced oscillations in a number of systems, and not just in pressure measurements of turbulent flow through combustors with unsteady heat release. The nature of the problem requires that the effects of flow turbulence be incorporated appropriately in models of flow-sound interaction and not just ignored as background perturbations to the underlying dynamics, as is currently often done. Finally, the study shows that quantities like the Hurst exponent are universal indicators of the proximity of a system to self-sustained oscillations no matter what the source of the underlying dynamics is.

CHAPTER 9

Conclusions and outlook

The present thesis focussed on characterizing the various dynamical states underlying the transitions observed in a laboratory-scale combustor operating in a turbulent flow-field from regimes of stable operation towards large amplitude combustion instability. It was identified that combustion noise is deterministic chaos and that the transition towards combustion instability is preceded by a regime of intermittent bursts composed of large-amplitude pressure oscillations that emerge in a near-random manner from the background of low-amplitude, chaotic pressure fluctuations.

A mechanism was proposed, which necessitates the existence of such an intermittent regime prior to the onset of combustion instability, provided the underlying flow-field is turbulent. A phenomenological model was described using this mechanism which was able to qualitatively reproduce the intermittency observed in experiments. Further, a host of precursors were also obtained by quantifying these intermittent states that can act as early warning signals to combustion instability in fielded combustors.

Traditional linear techniques that rely on a ‘signal plus noise’ paradigm was found to be insufficient to characterize the intermittent and chaotic states observed in the combustor, or predict the onset of an instability. The complexity of the dynamics requires that one employ fractal measures to describe the scaling of these irregular pressure fluctuations. It was found that combustion noise is multifractal, with different scaling properties for different amplitudes. Further, the onset of instability results in a loss of this multifractality, which in turn can be utilized as yet another early warning measure to combustion instability.

It is shown that the intermittency is due to the establishment of homoclinic orbits in the phase space of the underlying attractor. Such orbits connect the periodic and aperiodic portions in phase space resulting in burst oscillations. The intermittent regime was also found to be a characteristic of the pressure signals prior to lean blowout. Analysis of the high speed flame images reveal aperiodic detachment and reattachment of the

flame from the bluff-body lip. The detachment leads to a drop in the pressure amplitude and aperiodicity and reattachment results in the er-establishment of periodicity.

Intermittency was seen to be a characteristic feature in confined turbulent flow-fields, even in the absence of combustion. Measured pressure fluctuations of an unsteady flow-field through a pipe across an orifice reveals the formation of intermittent burst oscillations prior to the transition to pipe tones (whistling). The mechanism was identified as the closing of the boundary condition resulting in the formation of period-2 oscillations at the onset of whistling.

Precursors could be defined only because there was a regime of intermittent burst oscillations that presaged an instability. It would, therefore be interesting to explore the validity of the proposed mechanism for a variety of fluid systems and machines that operate in a turbulent flow-field. It would also be interesting to test whether such intermittent states can be observed in systems with a laminar flow-field; for instance, in ducted laminar premixed or diffusion flames and electrical Rijke tubes with a laminar flow-field. A possible study could then further entail proposing precursors in such laminar systems and identifying universal features underlying a transition to combustion instability.

APPENDIX A

Validation of phase space reconstruction

In this chapter, a simple three dimensional model is introduced, that displays chaotic behaviour for certain parameter values and initial conditions. The techniques that are used to reconstruct the phase space and determine the presence of chaos in the combustor time trace are then applied to the time traces obtained from this model to illustrate and validate the applicability of the techniques.

A.1 Lorenz system

The Lorenz system comprises a set of three nonlinear ordinary differential equations that were developed by Edward Lorenz as a simple model for atmospheric convection. The equations describe fluid circulation in a shallow layer which is heated from below and cooled above and in its simplest form may be written as:

$$\dot{x} = \sigma(y - z), \tag{A.1a}$$

$$\dot{y} = -xz + rx - y, \tag{A.1b}$$

$$\dot{z} = xy - bz \tag{A.1c}$$

where σ, r and b are three constant parameters. Shown in Fig. A.1 is the time variation of the 3 variables and the evolution of the variables in a three dimensional phase space for the following choice of the parameters: $\sigma = 10$, $r = 28$ and $b = 8/3$. It is seen that the fluctuations in the three dynamical variables display highly erratic behaviour with no apparent periodicity. The evolution in phase space shows a pattern which consists of two loops formed by the evolution of the trajectory around two fixed points. The trajectory remains bounded as variations in x, y and z remain within certain fixed limits determined by the constant parameters. The boundedness and the aperiodicity satisfy

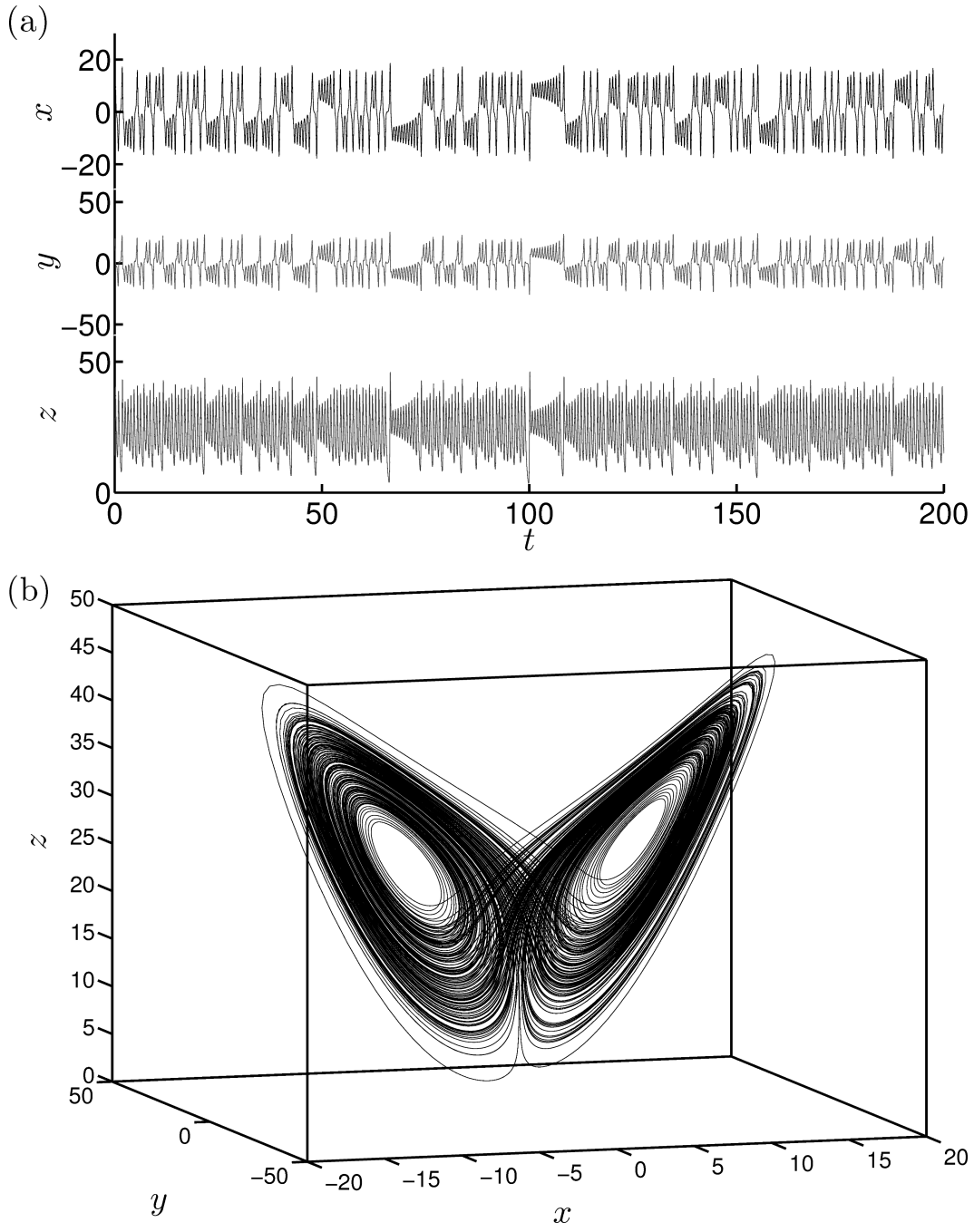

Figure A.1: (a) The evolution of the variables x, y and z of the Lorenz system. The parameter values are $\sigma = 10$, $r = 28$ and $b = 8/3$ with the initial condition chosen as $x_0 = 0.1$, $y_0 = 0$, and $z_0 = 0$. (b) The evolution of the trajectory starting at the prescribed initial condition in a phase space consisting of the three variables. It has a characteristic shape more popularly known as the 'Lorenz butterfly'.

two out of the three requirements which the trajectory of the variables must satisfy in order to be termed chaotic.

A third additional requirement for chaos is the sensitive dependence of the trajectories on the initial conditions. For a chaotic system, nearby trajectories diverge exponen-

tially even when they are separated by an infinitesimal separation initially. Figure A.2 shows the evolution of the variable x as describe by the Lorenz system starting from two slightly different initial conditions: $x_{0,1} = 0.1$, $x_{0,1} = 0.100001$.

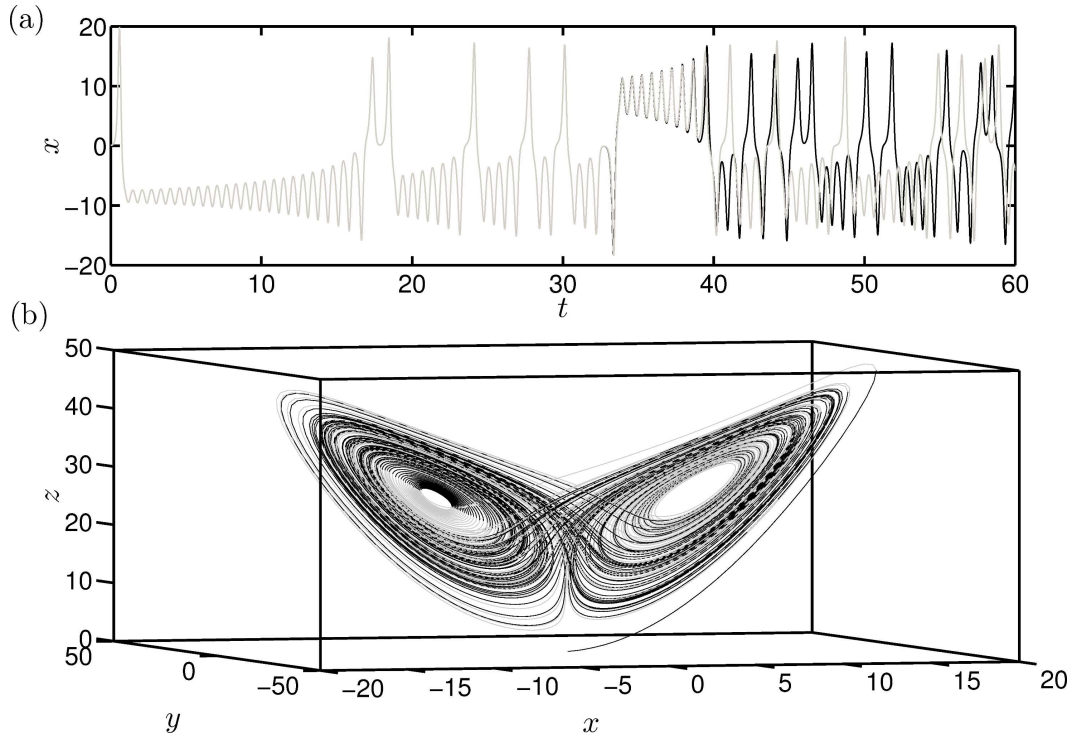

Figure A.2: An illustration of the sensitive dependence of the trajectory on the initial condition. (a) The evolution of the dynamical variable x starting from two slightly different initial conditions, $x_{0,1} = 0.1$ (black), $x_{0,1} = 0.100001$ (gray). (b)The corresponding trajectories in phase space.

As in evident from Fig. A.2, the trajectories are indistinguishable initially; however, they gradually diverge and two separate signals are visible in the time evolution. Correspondingly, two separate trajectories are visible in the phase space.

A.2 Results on phase space reconstruction

The technique of phase space reconstruction outlined in chapter 3 was applied to the time series data of x obtained from the Lorenz attractor with the following initial condition $x_0 = 0.1$, $y_0 = 0$, $z_0 = 0$. The time step was chosen as $\Delta t = 0.01$ and data was acquired for 25000 time steps. The first 5000 points were removed from the analysis to account for the transients. Shown in Fig. **??**(a, b) are the average mutual information I_τ and the variable E_1 for the x variable. Based on the saturation of E_1, we can conclude that the data comes out of a three dimensional system and that the optimal time delay is

$\tau_{opt} = 18$ time steps. The reconstructed phase space is shown in Fig. **??**(c). We see that the topological features of the original attractor such as the double loop are reproduced in the reconstructed phase space as well. This validates the proposed methodology to reconstruct the attractor of combustion dynamics from a single measured pressure time trace.

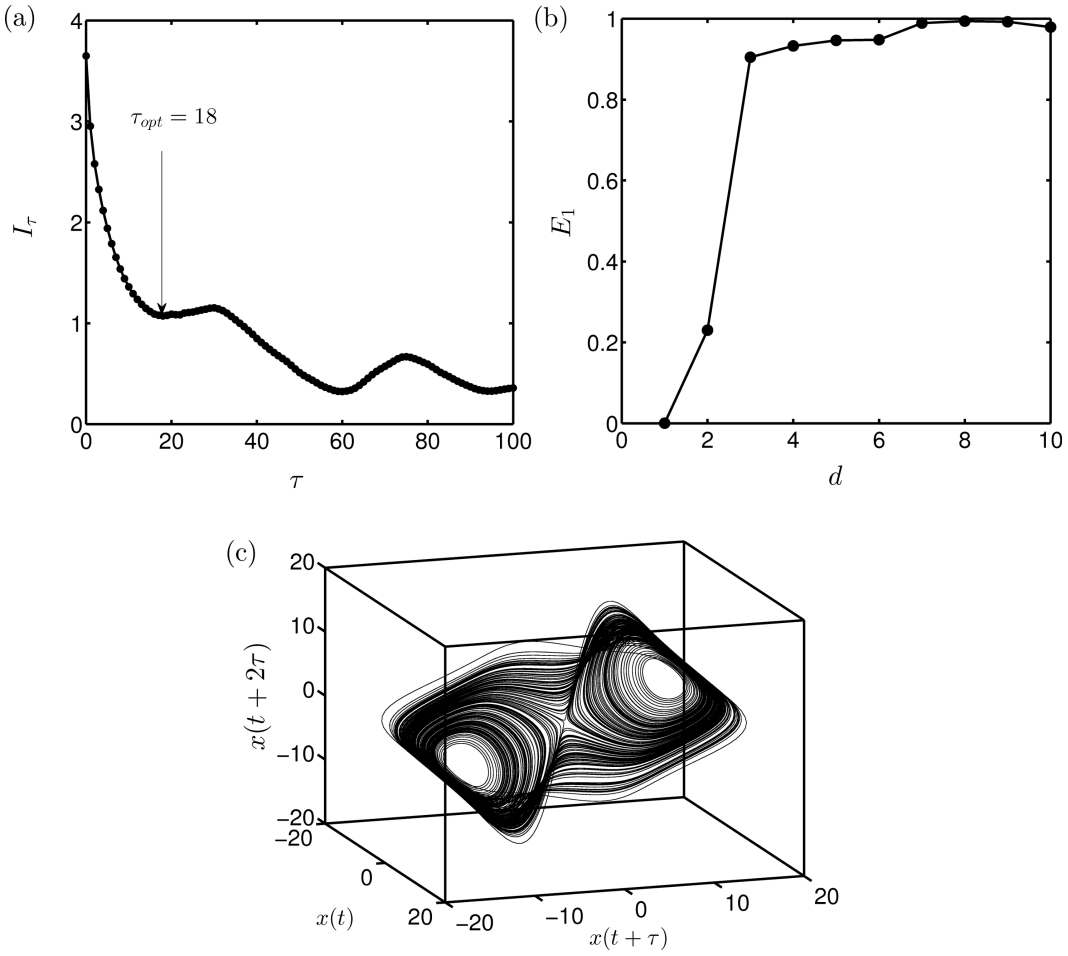

Figure A.3: (a) The variation of the average mutual information with the number of time steps τ. (b) The variation of the measure E_1 with the dimension of the attractor. (c) The phase space reconstructed using the dynamic variable x through delay embedding.

APPENDIX B

Evaluation of Hurst exponents and the multifractal spectrum

To estimate the Hurst exponent using detrended fluctuation analysis (DFA), the time signal $p(t)$ of length N is first mean-adjusted and then a cumulative deviate series y_k (see Fig. B.1)is obtained as:

$$y_k = \sum_{t=1}^{k} (p(t) - m) \tag{B.1}$$

where

$$m = \frac{1}{N} \sum_{t=1}^{N} p(t) \tag{B.2}$$

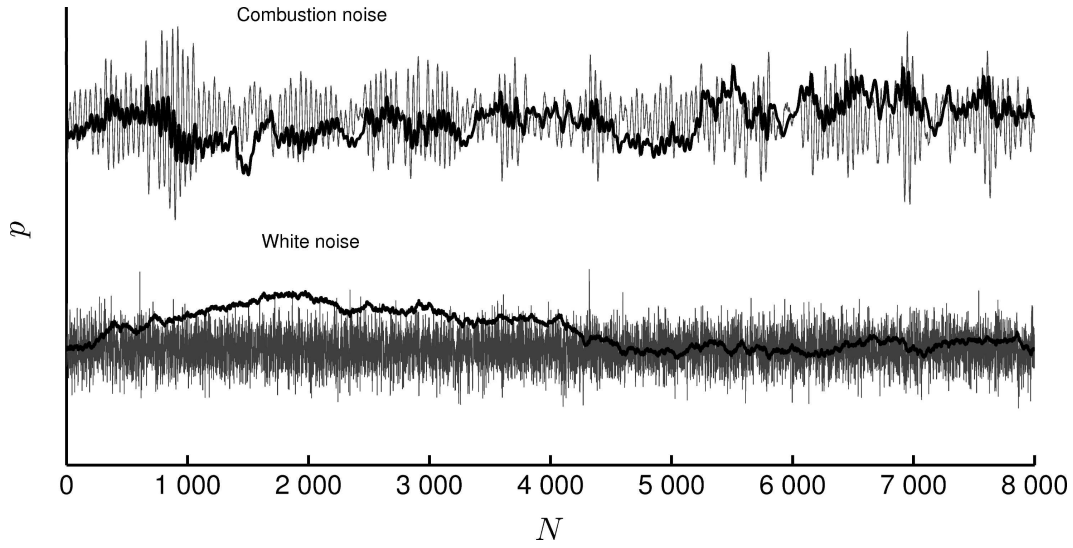

Figure B.1: A portion of the time signal (gray) and its cumulate deviate series (black) for (a) combustion noise and (b) a monofractal time series, and (c) Gaussian white noise. The monoftactal time series is persistent with a noticeable trend whereas combustion noise is anti-persistent with tendency towards mean reversion.

The deviate series is then divided into a number n_w of non-overlapping segments ($y_i(t), \quad i = 1, ..., n_w$) of equal span w. Shown in Fig. B.2 is a part of the combustion

noise signal which has been split into non-overlapping bins. In order to remove the trends in these segments, a local linear fit $\overline{y_i}$ is made separately to each of the sections of the deviate series y_i. These linear fits are shown as dashed lines in Fig. B.2. The detrended fluctuations are then obtained by subtracting the polynomial fit from the deviate series.

The structure function of order q and span w, F_w^q can be obtained from the detrended fluctuations as:

$$F_w^q = \left(\frac{1}{n_w} \sum_{i=1}^{n_w} \left(\sqrt{\frac{1}{w} \sum_{t=1}^{w} (y_i(t) - \overline{y_i})^2} \right)^q \right)^{1/q} \tag{B.3}$$

The Hurst exponent H^2 is then obtained from the slope of the linear regime in a log-log plot of F_w^2 for various span sizes w. For $q = 0$, the structure function is defined as (**?**):

$$F_w^0 = \exp\left(\frac{1}{2n_w} \sum_{i=1}^{n_w} \log\left(\frac{1}{w} \sum_{t=1}^{w} (y_i(t) - \overline{y_i})^2 \right) \right) \tag{B.4}$$

The generalized Hurst exponents H^q are the slopes of the straight lines in a log-log plot of the structure functions for various order exponents q for variations in the segment width (time interval), w. The information contained in H^q for different q can alternatively be represented as a spectrum of singularities $f(\alpha)$ that are related to the slopes of the generalized Hurst exponents via a Legendre transform as follows:

$$\tau_q = qH^q - 1, \tag{B.5a}$$

$$\alpha = \frac{\partial \tau_q}{\partial q}, \tag{B.5b}$$

$$f(\alpha) = q\alpha - \tau_q \tag{B.5c}$$

This spectrum, represented as a plot of $f(\alpha)$ against α, is known as the multifractal spectrum (also called the Hölder spectrum) and provides information on varying nature of the fractal dimension in the data.

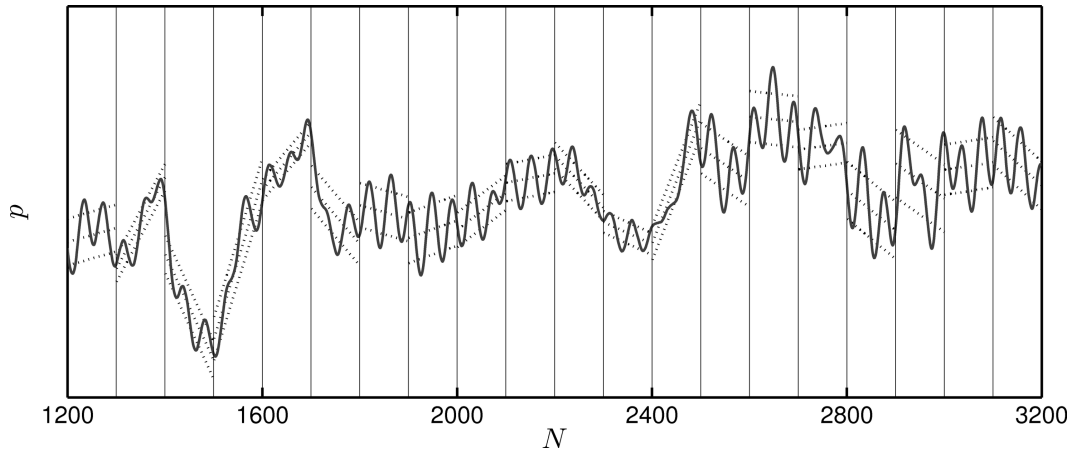

Figure B.2: The cumulative deviate series and its linear fit in 20 segments from a portion of the combustion noise signal. The deviate series $y_i(t)$ is shown in gray and the linear fit $\overline{y_i}$ and its local standard deviation are shown as black dashed lines.

REFERENCES

1. **Abarbanel, H. D. I.**, **R. Brown**, **J. J. Sidorowich**, and **L. Tsimring** (1993). The analysis of observed chaotic data in physical systems. *Rev. Mod. Phys.*, **65**, 1331–1392.

2. **Ananthkrishnan, N.**, **S. Deo**, and **F. E. C. Culick** (2005). Reduced-order modeling and dynamics of nonlinear acoustic waves in a combustion chamber. *Combust. Sci. Tech.*, **177**, 221–247.

3. **Annaswamy, A. M.**, **M. Fleifil**, **J. P. Hathout**, and **A. F. Ghoneim** (1997). Impact of linear coupling on the design of active controllers for the thermoacoustic instability. *Combust. Sci. Tech.*, **128**, 131–180.

4. **Argoul, F.**, **J. Huth**, **P. Merzeau**, **A. Arneodo**, and **H. L. Swinney** (1993). Experimental evidence for homoclinic chaos in an electrochemical growth process. *Physica D*, **62**, 170–185.

5. **Arndt, C. M.**, **A. M. Steinberg**, **I. G. Boxx**, **W. Meier**, **M. Aigner**, and **C. D. Carter** (2010). Flow-field and flame dynamics of a gas turbine model combustor during transition between thermo-acoustically stable and unstable states. *Proceedings of the ASME Turbo Expo, GT2010-22830*, 677–687.

6. **B. D. Bellows, T. L., Y. Neumeier** (2006). Forced response of a swirling, premixed flame to flow disturbances. *J. Propul. Power*, **22**, 1075–1084.

7. **Balachandran, R.** (2005). *Experimental Investigation of the Response of Turbulent Premixed Flames to Acoustic Oscillations*. Ph.D. thesis, University of Cambridge, Cambridge, U. K.

8. **Balasubramanian, K.** and **R. I. Sujith** (2008*a*). Non-normality and nonlinearity in combustion acoustic interactions in diffusion flames. *J. Fluid Mech.*, **592**, 29–57.

9. **Balasubramanian, K.** and **R. I. Sujith** (2008*b*). Thermoacoustic instability in a rijke tube: Non-normality and nonlinearity. *Phys. Fluids*, **20**, 044103.

10. **Basingthwaighte, J. B.**, **L. S. Liebovitch**, and **B. J. West**, *Fractal Physiology*. Oxford University Press, Oxford, UK, 1994.

11. **Bauer, M.**, **S. Habip**, **D. R. He**, and **W. Martienssen** (1992). New type of intermittency in discontinuous maps. *Phys. Rev. Lett.*, **68**, 1625–1628.

12. **Bhattacharjee, S.**, **B. Sheelke**, and **T. R. Troutt** (1986). Modification of vortex interactions in a reattaching separated flow. *AIAA J.*, **24**, 623–629.

13. **Burnley, V. S.** (1996). *Nonlinear combustion instabilities and stochastic sources*. Ph.D. thesis, California Institute of Technology, Pasadena.

14. **Burnley, V. S.** and **F. E. C. Culick** (2000). Influence of random excitations on acoustic instabilities in combustion chambers. *AIAA J.*, **38**, 1403–1410.

15. **Candel, S.** (2002). Combustion dynamics and control: Progress and challenges. *Proc. Comb. Inst.*, **29**, 1–28.

16. **Candel, S.**, **D. Durox**, **S. Ducruix**, **A. L. Birbaud**, **N. Noiray**, and **T. Schuller** (2009). Flame dynamics and combustion noise: progress and challenges. *Int. J. Aeroacoustics*, **8**, 1–56.

17. **Cao, L.** (1997). Practical method for determining the minimum embedding dimension of a scalar time series. *Physica D*, **110**, 43–50.

18. **Chakravarthy, S. R.**, **O. J. Shreenivasan**, **B. Boehm**, **A. Dreizler**, and **J. Janicka** (2007*a*). Experimental characterization of onset of acoustic instability in a nonpremixed half-dump combustor. *J. Acoust. Soc. Am.*, **122**, 120–127.

19. **Chakravarthy, S. R.**, **R. Sivakumar**, and **O. J. Shreenivasan** (2007*b*). Vortex-acoustic lock-on in bluff-body and backward-facing step combustors. *Sadhana*, **32**, 145–154.

20. **Clavin, P.**, **J. S. Kim**, and **F. A. Williams** (1994). Turbulence-induced noise effects on high-frequency combustion instabilities. *Combust. Sci. Tech.*, **96**, 61–84.

21. **Coats, C. M.** (1996). Coherent structures in combustion. *Prog. Energy Combust. Sci.*, **22**, 427–509.

22. **Covas, E.**, **R. Tavakol**, **P. Ashwin**, **A. Tworkowski**, and **J. Brooke** (2001). InâĂŞout intermittency in partial differential equation and ordinary differential equation models. *Chaos*, **11**, 404–409.

23. **Culick, F. E. C.** (1970). Stability of longitudinal oscillations with pressure and velocity couping in a solid propellant rocket. *Combustion Science and Technology*, **2**, 179–201.

24. **Culick, F. E. C.** (1976a). Nonlinear behavior of acoustic waves in combustion chambers-i. *ACTA Astronautica*, **3**, 715–734.

25. **Culick, F. E. C.** (1976b). Nonlinear behavior of acoustic waves in combustion chambers-ii. *ACTA Astronautica*, **3**, 735–757.

26. **Culick, F. E. C.**, Combustion instabilities in liquid-fueled propulsion systems: an overview. *In AGARD Conference for Combustion Instabilities in Liquid Propulsion Systems, NATO*. Seuille-Sur-Seine, France, 1988.

27. **Culick, F. E. C.** (1994). Some recent results for nonlinear acoustics in combustion chambers. *AIAA Journal*, **34**, 146–169.

28. **Culick, F. E. C.**, *Unsteady motions in combustion chambers for propulsion systems.*, volume AG-AVT-039. RTOAGARDograph, 2006.

29. **Dowling, A. P.** (1997). Nonlinear self-excited oscillations of a ducted flame. *Journal of Fluid Mechanics*, **346**, 271–290.

30. **ed: T. C. Lieuwen** and **V. Yang**, *Combustion Instabilities in Gas Turbine Engines: Operational Experience, Fundamental Mechanisms, and Modeling.*, volume 210. Progress in Astronautics and Aeronautics, AIAA Inc, 2005.

31. **Fichera, A.**, **C. Losenno**, and **A. Pagano** (2001). Experimental analysis of thermo-acoustic combustion instability. *Applied Energy*, **70**, 179–191.

32. **Frisch, U.**, *Turbulence: The legacy of A. N. Kolmogorov*. Cambridge University Press, Cambridge, UK, 1995.

33. **Frisch, U.** and **G. Parisi**, On the singularity structure of fully developed turbulence. *In* **R. B. M. Gil.** and **G. Parisi** (eds.), *Turbulence and Predictability in Geophysical Fluid Dynamics*. North-Holland, 1985, 84–88.

34. **Gotoda, H.**, **M. Amano**, **T. Miyano**, **T. Ikawa**, **K. Maki**, and **S. Tachibana** (2012). Characterization of complexities in combustion instability in a lean premixed gas-turbine model combustor. *Chaos*, **22**, 043128.

35. **Gotoda, H.**, **H. Nikimoto**, **T. Miyano**, and **S. Tachibana** (2011). Dynamic properties of combustion instability in a lean premixed gas-turbine combustor. *Chaos*, **21**, 013124.

36. **Gottwald, G. A.** and **I. Melbourne** (2004). A new test for chaos in deterministic systems. *Proc. R. Soc. Lond. A*, **460**, 603–611.

37. **Gouldin, F. C.** (1987). An application of fractals to modeling premixed turbulent flames. *Comb. Flame*, **68**, 249–266.

38. **Gouldin, F. C.**, **K. N. C. Bray**, and **J. Y. Chen** (1989*a*). Chemical closure model for fractal flamelets. *Comb. Flame*, **77**, 241–259.

39. **Gouldin, F. C.**, **S. M. Hilton**, and **T. Lamb** (1989*b*). Experimental evaluation of the fractal geometry of flamelets. *Symposium (International) on Combustion*, **22**(1), 541–550.

40. **Grebogi, C.**, **E. Ott**, **F. Romeiras**, and **J. A. Yorke** (1987). Critical exponents for crisis-induced intermittency. *Phys. Rev. A*, **36**, 5365–5380.

41. **Haken, H.**, *Laser light dynamics*, volume 2. North-Holland, 1985.

42. **Hammer, P. H.**, **N. Platt**, **S. M. Hammel**, **J. F. Heagy**, and **B. D. Lee** (1994). Experimental observation of on-off intermittency. *Phys. Rev. Lett.*, **73**, 1095–1098.

43. **Hegde, U. G.**, **D. Reuter**, **B. R. Daniel**, and **B. T. Zinn** (1983). Flame driving of longitudinal instabilities in dump type ramjet combustors. *Combust. Sci. Tech.*, **55**, 125–138.

44. **Herzel, H.**, **P. Plath**, and **P. Svensson** (1991). Experimental evidence of homoclinic chaos and type-ii intermittency during the oxidation of methanol. *Physica D*, **48**, 340–352.

45. **Hobson, D. E.**, **J. E. Fackrell**, and **G. Hewitt** (2000). Combustion instabilities in industrial gas turbines: Measurements on operating plant and thermoacoustic modeling. *J. Engg. Gas Turb. Power*, **122**, 420–428.

46. **Holmes, P.**, Can dynamical systems approach turbulence? *In* **J. Lumley** (ed.), *Whither Turbulence? Turbulence at the Crossroads*, volume 357. Springer, 1990, 195–249.

47. **Hong, J. G.**, **K. C. Oh**, **U. D. Lee**, and **H. D. Shin** (2008). Generation of low-frequency alternative flame behaviors in a lean premixed combustor. *Energy & Fuels*, **22**, 3016–3021.

48. **Hosseini, S. M. R.** and **C. J. Lawn**, Nonlinearities in the thermo-acoustic response of a premixed swirl burner. *In 12th International Congress on Sound and Vibration*. Lisbon, Portugal, 2005.

49. **Huber, A.** and **W. Polifke** (2009*a*). Dynamics of practical premix flames, part i: Model structure and identification. *International Journal of Spray and Combustion Dynamics*, **1**(2), 199–229.

50. **Huber, A.** and **W. Polifke** (2009*b*). Dynamics of practical premix flames, part ii: Identification and interpretation of cfd data. *International Journal of Spray and Combustion Dynamics*, **1**(2), 229–250.

51. **Jahnke, C. C.** and **F. E. C. Culick**, An application of dynamical systems theory to nonlinear combustion instabilities. *In AIAA Paper Number 93-0114, 31st Aerospace Science Meeting & Exhibit*. Reno, Nevada, 1993.

52. **Jahnke, C. C.** and **F. E. C. Culick** (1994). An application of dynamical systems theory to nonlinear combustion instabilities. *Journal of Propulsion and Power*, **10**, 508–517.

53. **Jegadeesan, V.** and **R. I. Sujtih** (2013). Experimental investigation of noise induced triggering in thermoacoustic systems. *Proc. Comb. Inst.*, **34**, 3175–3183.

54. **Johnson, C. E.**, **Y. Neumeier**, **T. C. Lieuwen**, and **B. T. Zinn** (2000). Determination of the stability margin of a combustor using exhaust flow and fuel injection rate modulation. *Proc. Comb. Inst.*, **28**, 757–763.

55. **Kabiraj, L.**, **A. Saurabh**, **P. Wahi**, and **R. I. Sujith**, Experimental study of thermoacoustic instability in ducted premixed flames: periodic, quasi-periodic and chaotic oscillations. *In Int'l Summer School & Workshop on Non-Normal and Nonlinear Effects in Aero- and Thermoacoustics*. Technische Universität München, Germany, 2010.

56. **Kabiraj, L.** and **R. I. Sujith**, Nonlinear self-excited oscillations in a thermoacoustic system. *In 4th International Symposium Bifurcations and Instabilities in Fluid Dynamics*. Barcelona, Spain, 2011.

57. **Kabiraj, L.** and **R. I. Sujith** (2012). Nonlinear self-excited thermoacoustic oscillations: intermittency and flame blowout. *J. Fluid Mech.*, **713**, 376–397.

58. **Kantelhardt, J. W.**, Fractal and multifractal time series. *In* **R. A. Meyers** (ed.), *Mathematics of Complexity and Dynamical Systems*. Springer, New York, 2011, 463–487.

59. **Kantelhardt, J. W.**, **E. Koscielny-Bunde**, **H. H. A. Rego**, **S. Havlin**, and **A. Bunde** (2001). Detecting long-range correlations with detrended fluctuation analysis. *Physica A*, **295**, 441–454.

60. **Kantelhardt, J. W.**, **S. A. Zschiegner**, **E. Koscielny-Bunde**, **S. Havlin**, **A. Bunde**, and **H. E. Stanley** (2002). Multifractal detrended fluctuation analysis of nonstationary time series. *Physica A*, **316**, 87–114.

61. **Kaplan, D. T.** (1993). Evaluating deterministic structure in maps deduced from discrete time measurements. *Int. J. Bifurcation Chaos*, **3**, 617–623.

62. **Kaplan, D. T.** and **L. Glass** (1992). Direct test for determinism in a time series. *Phys. Rev. Lett.*, **68**, 427–430.

63. **Kashinath, K.** (2013). *Nonlinear thermoacoustic oscillations of a ducted premixed laminar flame*. Ph.D. thesis, University of Cambridge, Cambridge, UK.

64. **Klimaszewska, K.** and **J. J. Zebrowski** (2009). Detection of the type of intermittency using characteristic patterns in recurrence plots. *Phys. Rev. E*, **80**, 026214.

65. **Kolmogorov, A. N.** (1941). Dissipation of energy in the locally isotropic turbulence. *Dokl. Akad. Nauk SSSR*, **32**, 16–18.

66. **Komarek, T.** and **W. Polifke** (2012). Impact of swirl fluctuations on the flame response of a perfectly premixed swirl burner. *J. Eng. Gas Turb. Power*, **132**, 061503.

67. **Kraichnan, R. H.** (1967). Inertial ranges in two-dimensional turbulence. *Phys. Fluids*, **10**, 1417–1423.

68. **Lei, S.** and **A. Turan** (2009). Nonlinear/chaotic behaviour in thermoacoustic instability. *Combustion Theory and Modelling*, **13**, 541–557.

69. **Lieuwen, T.** (2005). Online combustor stability margin assessment using dynamic pressure data. *J. Eng. Gas Turbines Power*, **127**, 478–482.

70. **Lieuwen, T.** and **A. Banaszuk** (2005). Background noise effects on combustor stability. *Journal of Propulsion and Power*, **21**(1), 25–31.

71. **Lieuwen, T.**, **Y. Neumeier**, and **B. T. Zinn** (1998). The role of unmixedness and chemical kinetics in driving combustion instabilities in lean premixed combustors. *Combust. Sci. Tech.*, **135**, 193–211.

72. **Lieuwen, T. C.** (2001). Phase drift characteristics of self-excited, combustion-driven oscillations. *Journal of Sound and Vibration*, **242**, 893–905.

73. **Lieuwen, T. C.** (2002). Experimental investigation of limit-cycle oscillations in an unstable gas turbine combustor. *Journal of Propulsion and Power*, **18**(1).

74. **Lieuwen, T. C.** (2003). Statistical characteristics of pressure oscillations in a premixed combustor. *Journal of Sound and Vibration*, **260**, 3–17.

75. **Lieuwen, T. C.** (2004). Nonlinear kinematic response of premixed flames to harmonic velocity disturbances. *Proceedings of the Combustion Institute*, **30**, 1725–1732.

76. **Mariappan, S.**, **P. J. Schmid**, and **R. I. Sujith**, Role of transient growth in subcritical transition to thermoacoustic instability in a horizontal rijke tube. *In 16th AIAA/CEAS Aeroacoustics Conference*. Stockholm, Sweden, 2010.

77. **Mariappan, S.** and **R. I. Sujith** (2010). Thermoacoustic instability in solid rocket motor: non-normality and nonlinear instabilities. *Journal of Fluid Mechanics*, **65**, 1–33.

78. **Mariappan, S.**, **R. I. Sujith**, and **P. J. Schmid**, Non-normal and nonlinear dynamics of thermoacoustic instability in a horizontal rijke tube. *In Int'l Summer School & Workshop on Non-Normal and Nonlinear Effects in Aero- and Thermoacoustics*. Technische Universität München, Germany, May 17-21, 2010.

79. **Marwan, N.**, **M. C. Romano**, **M. Thiel**, and **J. Kurths** (2007). Recurrence plots for the analysis of complex systems. *Phys. Reports*, **438**, 237–329.

80. **Marwan, N.**, **N. Wessel**, **U. Meyerfeldt**, **A. Schirdewan**, and **J. Kurths** (2002). Recurrence-plot-based measures of complexity and their application to heart-rate-variability data. *Phys. Rev. E*, **66**, 026702.

81. **Massey, F. J.** (1951). The kolmogorov-smirnov test for goodness of fit. *J. Am. Stat. Ass.*, **46**, 68–78.

82. **Matveev, K.** and **F. E. C. Culick** (2003). A model for combustion instability involving vortex shedding. *Combust. Sci. Tech.*, **175**, 1059–1083.

83. **McManus, K. R.**, **T. Poinsot**, and **S. M. Candel** (1993). A review of active control of combustion instabilities. *Prog. Energy Combust. Sci.*, **19**, 1–29.

84. **Meneveau, C.** and **K. R. Sreenivasan** (1987). The multifractal spectrum of the dissipation field in turbulent flows. *Nucl. Phys. B (Proc. Suppl.)*, **2**, 49.

85. **Meneveau, C.** and **K. R. Sreenivasan** (1989). Measurement of $f(\alpha)$ from scaling of histograms and applications to dynamical systems and fully developed turbulence. *Phys. Lett. A*, **137**, 103–112.

86. **Meneveau, C.** and **K. R. Sreenivasan** (1991). The multifractal nature of turbulent energy dissipation. *J. Fluid Mech.*, **224**, 429–484.

87. **Montroll, E. W.** and **M. F. Schlesinger** (1982). On $1/f$ noise and other distributions with long tails. *Proc. Natl. Acad. Sci. USA*, **79**, 3380–3383.

88. **Nair, S.** and **T. Lieuwen** (2005). Acoustic detection of blowout in premixed flames. *J. Prop. Power*, **21**, 32–39.

89. **Noiray, N.**, **D. Durox**, **T. Schuller**, and **S. Candel** (2008). A unified framework for nonlinear combustion instability analysis based on the flame describing function. *Journal of Fluid Mechanics*, **615**, 139–167.

90. **Noiray, N.** and **B. Schuermans** (2013). Deterministic quantities characterizing noise driven hopf bifurcations in gas turbine combustors. *Int. J. Non-Lin. Mech.*, **50**, 152–163.

91. **Ott, E.** and **J. C. Sommerer** (1994). Blowout bifurcations: the occurrence of riddled basins and on-off intermittency. *Phys. Lett. A*, **188**, 39–47.

92. **Paladin, G.** and **A. Vulpiani** (1987). Anomalous scaling laws in multifractal objects. *Phys. Rep.*, **156**, 147–225.

93. **Parker, L. J.**, **R. F. Sawyer**, and **A. R. Ganji** (1979). Measurement of vortex frequencies in a lean, premixed prevaporized combustor. *Combust. Sci. Tech.*, **20**, 235–241.

94. **Parthimos, D.**, **D. H. Edwards**, and **T. M. Griffith** (). ShilâĂŹnikov homoclinic chaos is intimately related to type-iii intermittency in isolated rabbit arteries: Role of nitric oxide. *Phys. Rev. E*, **67**, 051922.

95. **Peng, C. K.**, **S. V. Buldyrev**, **S. Havlin**, **M. Simons**, **H. E. Stanley**, and **A. L. Goldberger** (1994). Mosaic organization of dna nucleotides. *Phys. Rev. E*, **49**, 1685–1689.

96. **Peracchio, A. A.** and **W. M. Proscia** (1999). Nonlinear heat-release/acoustic model for thermo-acoustic instability in lean premixed combustors. *Journal of Engineering for Gas Turbines and Power-Transactions of the ASME*, **121**, 415–421.

97. **Pikovsky, A.**, **M. Rosenblum**, and **J. Kurths**, *Synchronization: A Universal Concept in Nonlinear Sciences (Cambridge Nonlinear Science Series)*. Cambridge University Press, 2003.

98. **Pitz, R. W.** and **J. W. Daily** (1983). Combustion in a turbulent mixing layer formed at a rearward-facing step. *AIAA J.*, **21**, 1565–1570.

99. **Poinsot, T.**, **F. Lacas**, **J. Chambon**, **D. Veynante**, and **A. Trouve** (1992). Apparatus for active monitoring of combustion instability. *US patent (US 5145355 A)*.

100. **Poinsot, T. J.**, **A. C. Trouve**, **D. P. Veynante**, **S. M. Candel**, and **E. J. Esposito** (1987). Vortex-driven acoustically coupled combustion instabilities. *J. Fluid Mech.*, **177**, 265–292.

101. **Pomeau, Y.** and **P. Manneville** (1980). Intermittent transition to turbulence in dissipative dynamical systems. *Commun. Math. Phys.*, **74**, 189–197.

102. **Prasad, R. R.**, **C. Meneveau**, and **K. R. Sreenivasan** (1988). The multifractal nature of the dissipation field of passive scalars in fully turbulent flows. *Phys. Rev. Lett.*, **61**, 74–77.

103. **Preetham, S. H.** and **T. C. Lieuwen**, Nonlinear flame-flow transfer function calculations: Flow disturbance celerity effects. *In AIAA Paper Number 2004-4035, 40th AIAA / ASME / SAE / ASEE Joint Propulsion Conference and Exhibit*. Fort Lauderdale, Florida, 2004.

104. **Preetham, S. H.** and **T. C. Lieuwen**, Nonlinear flame-flow transfer function calculations: Flow disturbance celerity effects part 2. *In AIAA Paper Number 2005-0543, 43rd AIAA Aerospace Sciences Meeting and Exhibit*. Reno, Nevada, 2005.

105. **Price, T. J.** and **T. Mullin** (1991). An experimental observation of a new type of intermittency. *Physica D*, **48**, 29–52.

106. **Rayleigh, L.** (1878). The explanation of certain acoustical phenomenon. *Nature*, **18**, 319–321.

107. **Renard, P. H.**, **D. Thévenin**, **J. C. Rolon**, and **S. Candel** (2000). Dynamics of flame/vortex interactions. *Progress in Energy and Combustion Science*, **26**, 225–282.

108. **Richardson, L. F.**, *Weather Prediction by Numerical Process.*. Cambridge University Press, Cambridge, UK, 1922.

109. **Richardson, L. F.**, *Chaos in Dynamical Systems.*. Cambridge University Press, Cambridge, UK, 1993.

110. **Richetti, P.**, **F. Argoul**, and **A. Arneodo** (1986). Type-ii intermittency in a peroidically driven nonlinear oscillator. *Phys. Rev. A*, **34**, 726–729.

111. **Rogers, D. E.** and **F. E. Marble** (1956). A mechanism for high-frequency oscillation in ramjet combustors and afterburners. *Jet Propulsion*, **26**, 456–462.

112. **Schadow, K. C.** and **E. Gutmark** (1992). Combustion instability related to vortex shedding in dump combustors and their passive control. *Prog. Energy Combust. Sci.*, **18**, 117–132.

113. **Schlesinger, M. F.** (1987). Fractal time and $1/f$ noise in complex systems. *Ann. NY Acad. Sci.*, **504**, 214–228.

114. **Schwarz, A.** and **J. Janicka**, *Combustion noise*. Springer-Verlag, 2009.

115. **Shanbhogue, S. J.**, **S. Husain**, and **T. Lieuwen** (2009). Lean blowoff of bluff body stabilized flames: Scaling and dynamics. *Prog. Energy Combust. Sci.*, **35**, 98–120.

116. **Smith, D. A.** and **E. E. Zukoski**, Combustion instability sustained by unsteady vortex combustion. *In AIAA/SAE/ASME/ASEE 21st Joint Propulsion Conference.*. Monterey, California., 1985.

117. **Sreenivasan, K. R.** (1991). Fractals and multifractals in fluid turbulence. *Annu. Rev. Fluid Mech.*, **23**, 539–604.

118. **Sreenivasan, K. R.** and **C. Meneveau** (1986). The fractal facets of turbulence. *J. Fluid Mech.*, **173**, 357–386.

119. **Sreenivasan, K. R.** and **C. Meneveau** (1988). Singularities of the equations of fluid motion. *Phys.Rev. A*, **38**, 6287–6295.

120. **Sterling, J. D.** (1993). Nonlinear analysis and modeling of combustion instabilities in a laboratory combustor. *Combustion Science and Technology*, **89**, 167–179.

121. **Sterling, J. D.** and **E. E. Zukoski** (1991). Nonlinear dynamics of laboratory combustor pressure oscillations. *Combust. Sci. Tech.*, **77**, 225–238.

122. **Stone, E.**, **M. Gorman**, **M. el Hamdi**, and **K. A. Robbins** (1996). Identification of intermittent ordered patterns as heteroclinic connections. *Phys. Rev. Lett.*, **76**, 2061–2064.

123. **Stone, E.** and **P. Holmes** (1991). Unstable fixed points, heteroclinic cycles and exponential tails in turbulence production. *Phys. Lett. A*, **155**, 29–42.

124. **Strahle, W. C.** (1978). Combustion noise. *Prog. Energy Combust. Sci.*, **4**, 157–176.

125. **Strahle, W. C.** and **J. I. Jagoda** (1989). Fractal geometry applications in turbulent combustion data analysis. *Symposium (International) on Combustion*, **22**(1), 561–568.

126. **Strogatz, S. H.**, *Nonlinear Dynamics And Chaos: With Applications To Physics, Biology, Chemistry, And Engineering (Studies in Nonlinearity)*. Westview Press, 2001.

127. **Subramanian, P.** (2011). *Dynamical systems approach to the investigation of thermoacoustic instabilities*. Ph.D. thesis, Indian Institute of Technology Madras, Chennai, India.

128. **Surovyatkina, E.** (2005). Prebifurcation noise amplification and noise-dependent hysteresis as indicators of bifurcations in nonlinear geophysical systems. *Nonlin. proc. geophys.*, **12**(1).

129. **Takens, F.**, Detecting strange attractors in turbulence. *In* **R. David** and **L.-S. Young** (eds.), *Dynamical Systems and Turbulence: Lecture Notes in Mathematics*, volume 898. Springer, Warwick, 1985, 366–381.

130. **Taylor, G. I.** (1938). The spectrum of turbulence. *Proc. R. Soc. Lond. A*, **164**, 476–490.

131. **Theiler, J.**, **S. Eubank**, **A. Longtin**, **B. Galdrikian**, and **J. D. Farmer** (1992). Testing for nonlinearity in time series: the method of surrogate data. *Physica D*, **58**, 77–94.

132. **Trefethen, L. N.** and **M. Embree**, *Spectra and Pseudospectra: The Behavior of Nonnormal Matrices and Operators*. Princeton University Press, 2005.

133. **Tyagi, M.**, **S. R. Chakravarthy**, and **R. I. Sujith** (2007). Unsteady combustion response of a ducted non-premixed flame and acoustic coupling. *Combustion Theory and Modelling*, **11**, 1148–1158.

134. **West, B. J.**, *Where medicine went wrong: Rediscovering the path to complexity*. World Scientific, 2006.

135. **West, B. J.** and **A. L. Goldberger** (1987). Physiology in fractal dimensions. *Am. Sci.*, **75**, 354–365.

136. **West, B. J.**, **M. Latka**, **M. Glaubic-Latka**, and **D. Latka** (2003). Multifractality of cerebral blood flow. *Physica A*, **318**, 453–460.

137. **Wicker, J. M.**, **W. D. Greene**, **S. I. Kim**, and **V. Yang** (1996). Triggering of longitudinal combustion instabilities in rocket motors: Nonlinear combustion response. *Journal of Propulsion and Power*, **12**, 1148–1158.

138. **Wiesenfeld, K.** (1985). Noisy precursors of nonlinear instabilities. *J. Stat. Phys.*, **38**, 1071–1097.

139. **Wilke, C. R.** (1950). A viscosity equation for gas mixtures. *J. Chem. Phys.*, **18**, 517–519.

140. **Winant, C. D.** and **F. K. Browand** (1974). Vortex pairing: the mechanism of turbulent mixing-layer growth at moderate reynolds numbers. *J. Fluid Mech.*, **63**, 237–255.

141. **Yu, K. H.**, **A. Trouve**, and **J. W. Daily** (1991). Low-frequency pressure oscillations in a model ramjet combustor. *J. Fluid Mech.*, **232**, 47–72.

142. **Zank, G. P.** and **W. H. Matthaeus** (1990). Nearly incompressible hydrodynamics and heat conduction. *Phys. Rev. Lett.*, **64**, 1243–1246.

143. **Zinn, B. T.** and **T. C. Lieuwen**, Chapter 1: Combustion instabilities: Basic concepts. *In* **T. C. Lieuwen** and **V. Yang** (eds.), *Combustion Instabilities in Gas Turbine Engines: Operational Experience, Fundamental Mechanisms, and Modeling.*, volume 210. Progress in Astronautics and Aeronautics, AIAA Inc, 2005.

144. **Zinn, B. T.** and **M. E. Lores** (1971). Application of the galerkin method in the solution of non-linear axial combustion instability problems in liquid rockets. *Combust. Sci. Tech.*, **4**, 269–278.

LIST OF PAPERS BASED ON THESIS

Refereed Journals

1. **V. Nair** and G. Thampi and S. Karuppusamy and S. Gopalan and R. I. Sujith Multifractality in combustion noise: predicting an impending combustion instability. *Journal of Fluid Mechanics*, 747, 635-655 (2014).

2. **V. Nair** and R. I. Sujith Identifying homoclinic orbits in the dynamics of intermittent signals through recurrence quantification. *Chaos*, 23, 033136, (2013).

3. **V. Nair** and R. I. Sujith Loss of chaos in combustion noise as a precursor of impending combustion instability. *International Journal of Spray and Combustion Dynamics*, 5, 273-290, (2013).

Peer-reviewed conferences

1. **V. Nair** and R. I. Sujith A reduced-order model for the onset of combustion instability: Physical mechanisms for intermittency and precursors. *35th International Symposium on Combustion*, San Francisco, California, USA, August 3-8, 2014.

2. **V. Nair** and R. I. Sujith Intermittency in the Dynamics of Turbulent Combustors. *ASME Turbo Expo 2014 (GT2014-26018)*, D usseldorf, Germany, June 16-20, 2014.

3. **V. Nair** and G. Thampi and R. I. Sujith Engineering Precursors To Forewarn The Onset Of An Impending Combustion Instability. *ASME Turbo Expo 2014 (GT2014-26020)*, D usseldorf, Germany, June 16-20, 2014.

Abstract-reviewed conferences

1. **V. Nair** and G. Thampi and R. I. Sujith Intermittent Burst Presage the Onset of Combustion Instability in Turbulent Combustors. *n3l - Int'l Summer School and Workshop on Non-Normal and Nonlinear Effects in Aero- and Thermoacoustics*, Munich, Germany, June 18-21, 2013.